INTERACTIONS OF POLYMERS WITH SURFACES

By

BAL KUMARI KHATIWADA

Bachelor of Science in Chemistry
Tribhuvan University
Kathmandu, Nepal
2006

Master of Science in Chemistry
Tribhuvan University
Kathmandu, Nepal
2009

Submitted to the Faculty of the
Graduate College of the
Oklahoma State University
in partial fulfillment of
the requirements for
the Degree of
DOCTOR OF PHILOSOPHY
July, 2014

INTERACTIONS OF POLYMERS WITH SURFACES

Dissertation Approved:

Dr. Frank D. Blum
_____
Dissertation Adviser

Dr. Jeffery L. White
_____

Dr. Kevin D. Ausman
_____

Dr. Toby L. Nelson
_____

Dr. Donghua Zhou
_____

ACKNOWLEDGEMENTS

It gives me a great pleasure to express my gratitude to all those people who have supported me and had a contribution in making this thesis possible. First and foremost, I would like to thank my advisor, Frank D. Blum for all of his untiring guidance, support, motivation, and enthusiasm throughout my doctorate period. I am fascinated by his way of thinking and suggestions during my program. He always listened to me first, and then gave feedback, which made me feel I had the freedom to express my thoughts and explore myself more. I would like to thank my advisory committee members, Dr. Jeffery White, Dr. Kevin Ausman, Dr. Toby Nelson and Dr. Donghua Zhou, for their help and suggestions during my PhD. program. I would like to thank Dr. Brian Grady (University of Oklahoma) for taking small angle XRD for graphene oxide and poly(vinyl acetate)/graphene oxide samples.

Several friends and other colleagues also deserve a special recognition for their contributions to this thesis. In particular, my lab colleagues, Bhishma Sedai, Helanka Perera, Charmaine Munro, Tan Zhang, Hamid Mortazavian, Ugo Arua, and Madhu Madduma Arachchilage, for their contribution directly or indirectly in this thesis. I express a very special gratitude to Dr. Nitin V. Patil and Dr. Gaumani Gyawali for teaching me to use instruments and research facilities at the head start of my research.

One person that I truly admire is my husband, Dr. Kedar Nepal who was always willing to help me anytime I needed it. Without his help and support, this work would not have been completed. I would like to thank my parents, dad Mr. Bodh Prasad Khatiwada and mom Mrs. Radhadevi Khatiwada, for all the support that I got in my high school and undergraduate studies. I like to thank my elder brother Mr. Dharmananda Khatiwada for providing financial and emotional support when I needed it.

Last but not the least, I acknowledge the financial support of the National Science Foundation (USA) under Grant No. DMR-1005606. I thank Graduate College at Oklahoma State University for providing me an opportunity for this degree program. I also thank Department of Chemistry for providing the facilities and mentors throughout my entire time. I truly liked the administrative staff in Chemistry Department and appreciate their assistance.

Name: BAL KUMARI KHATIWADA

Date of Degree: JULY, 2014

Title of Study: INTERACTIONS OF POLYMERS WITH SURFACES

Major Field: CHEMISTRY

Abstract:

The glass transition behavior of poly(methyl methacrylate) (PMMA) adsorbed on silica (surface area = 200 m^2/g) was studied by temperature modulated differential scanning calorimetry (TMDSC). For small amounts of the polymer adsorbed on silica (1-2 mg of polymer/m^2 of silica), the glass transition temperature (T_g) of the polymer was significantly increased compared to that of the bulk polymer. The polymer with a higher T_g has been called tightly-bound polymer. Addition of more polymer on the surface resulted in the composites with some polymer that had glass transitions similar to that of the bulk polymer, and has been called loosely-bound polymer. TMDSC heat flow curves were used to estimate the amount of tightly-bound polymer using a bound-segment model, a model based on the polymers divided into loosely and tightly-bound polymers.

Heat capacities of the bulk PMMA, silica, and PMMA/silica composites were measured by quasi-isothermal heat capacity measurements. The heat capacities of the composites were significantly smaller than the ones predicted by a simple mixture model, where the heat capacities of the composites are additive based on the two components. Two-state, exponential, and transitional models have been used to fit the heat capacity of the polymer adsorbed on silica surface.

Deuterium (^{2}H) solid-state NMR and differential scanning calorimetry (DSC) were used to probe the interfacial interactions of poly(vinyl acetate) (PVAc-d_3) incorporated into graphene oxide (GO) surfaces. The glass transition behavior of the bulk and PVAc-d_3/GO composites was determined by temperature modulated DSC. Incorporation of the PVAc-d_3 into the GO significantly reduced the intensity of the glass transition. In fact, the glass transitions of the composites almost disappeared (very weak and broad glass transition) when the composition of the polymer was 50 % or less (w/w). ^{2}H NMR measurements were carried out to understand the dynamics of the polymer segments incorporated with the GO. In contrast to the behavior for the bulk polymer, the polymer segments incorporated with GO showed heterogeneous mobility. The Pake powder patterns of PVAc-d_3/GO samples had peaks from polymer segments that were more mobile and less mobile than the bulk polymer.

TABLE OF CONTENTS

LIST OF TABLES

CHAPTER 4

.

CHAPTER 1

INTRODUCTION

High molecular mass substances with one or more than one repeating unit of small molecules covalently linked together are called polymers. Examples of these are polyethylene, polystyrene, poly(methyl methacrylate), and poly(vinyl acetate). The repeating units are called monomers, for example, ethylene, styrene, methyl methacrylate, and vinyl acetate. Polymers with only one type of repeating unit are called homopolymers and polymers with two or more than two types of repeating units are called copolymers. Copolymers can be either random, or alternating, or block copolymers. In a random copolymer, no specific sequence of monomer units is present. Alternating copolymers, as the name implies, contain monomers in alternating sequences. Block copolymers contain blocks of monomers connected to other blocks. Polymers can be either linear or branched or cross-linked. Due to their diverse structures, different polymers can have different physical properties. They can be very soft materials to hard and brittle plastics. Some polymers are good conductors of heat and electricity, while others are insulators. Some are miscible in water (a polar solvent) and can be considered as hydrophilic polymers such as poly(vinyl alcohol), poly(ethylene glycol), poly(acrylic acid), poly(vinylpyrrolidone).

Hydrophobic polymers are prepared from monomers with less hydrophilic functionalities. Poly(tetrafluoroethylene), polystyrene, polyethylene, polybutadiene. are some examples of hydrophobic polymers.

A tremendous amount of work has been done in the field of polymer and polymer-based materials around the time of World War II. Before that time, the types of materials for construction were mainly steel, glass, wood, stone, and concrete materials, and cotton, wool, and jute provided the raw materials for cloths and fabric products. The emergence of research and development on polymer and polymer-based materials has allowed the replacement of various conventional materials. Synthetic polymeric materials have been used as plastic bags, milk cartons, paints and coatings, epoxy glue, Teflon™ coated cookware, styrofoam, polyurethane cushions, nylon fibers, rubbers, and synthetic body parts. An enormous use of polymeric materials has made this era the polymer era.

Polymers are used either in bulk or in composites; bulk polymers refer to pure polymers and composites are mixtures of different polymers or polymers with solid substrates. Composite materials are very popular and have wide applications as these materials often offer superior performance and have various advantages such as light weight, corrosion resistance, flexibility, cost reduction, productivity, and durability over conventional materials. Strong reinforcing materials are generally required to meet the demand of strength and stiffness of these materials for various applications such as aerospace, automotive, microelectronic, bullet proof materials, infrastructure and construction, and chemical industries. The properties of the composite materials are very much dependent on the interactions of polymers with the reinforcing materials, especially at the interfaces, where the materials come into contact with each other.

Polymer composites are prepared in various ways, such as simple blending, physisorption, chemisorption, grafting to (surfaces), grafting from (surfaces), and polymerization in the mixture. Among them, polymer adsorption processes (physisorption and chemisorption) are frequently used to make composites for various applications such as adhesion, surface protection, colloidal dispersion, reinforcement, drug delivery, and membrane-polymer interaction in biology, etc. In the physisorption process, polymers are physically adsorbed on surfaces due to H-bonding, or dipole-dipole interactions, or simple van der Waals interactions. Such interactions are crucial in a variety of applications, especially when those applications are based on interfacial properties.[1] Many studies have been conducted with the aim of understanding the properties of interfacial materials with a variety of solid substrates and polymers.[2-10]

In this study, our research was focused on understanding the motions of polymeric segments at different interfaces at a molecular level using temperature modulated differential scanning calorimetry (TMDSC) and ^{2}H NMR spectroscopy. TMDSC has been used to study the glass transition temperatures (T_g) and heat capacities of bulk and adsorbed polymers. Glass transition temperatures of bulk polymers have been compared with those of the adsorbed polymers. Moreover, a change in heat capacity (ΔC_p) at the glass transitions of adsorbed polymers has been used to calculate the amount of tightly bound polymers using a two-state model, based on a loosely bound polymer (with a T_g similar to bulk) and a tightly-bound polymer (with a T_g higher than that of the loosely bound polymer). In addition to T_g measurements, the absolute heat capacities of the bulk and the adsorbed polymers have been used to measure the change in the heat capacity at T_g, using TMDSC. The heat capacity values have been fitted with a bound segment model, where polymers segments close to the

surfaces were tightly bound and those far from the surfaces were loosely bound, to estimate the amount of bound polymers on the surfaces.

In addition to thermal studies, solid-state deuterium (^{2}H) NMR spectroscopy has become a successful tool to probe interfacial polymers.[11-20] Bulk and adsorbed polymers can be labeled with deuterium and analysis can be done based on the ^{2}H powder pattern obtained from a solid sample put in a NMR tube. For specifically labeled compounds, the interference from naturally occurring deuterium is very minimal because of its low natural abundance. The shape of the spectrum and its intensity can provide valuable information regarding the segmental motion of the bulk polymer and polymer segments at different interfaces such as surface-polymer interfaces, polymer-polymer interfaces, and polymer-air interfaces in adsorbed polymers.[12,14,21] In this study, we have used ^{2}H NMR to study the interactions of graphene and graphene oxide with poly(vinyl acetate) (PVAc-d_3). The deuterium power patterns for the bulk PVAc-d_3 and the surface adsorbed polymers (PVAc-d_3 on graphene and graphene oxide) have been investigated.

REFERENCES

(1) Fleer, G. J.; Cohen-Stuart, M. A.; Scheutjens, J. M. H. M.; Cosgrove, T.; Vincent, B. *Polymers at Interfaces;* Chapman & Hall: London, **1993**.

(2) Alcoutlabi, M.; McKenna, G. B. *J. Phys.: Condens. Matter* **2005**, *17*, R461-R524.

3) Paul, D. R.; Robeson, L. M. *Polymer* **2008**, *49*, 3187-3204.

(4) Arrighi, V.; McEwen, I. J.; Qian, H.; Prieto, M. B. S. *Polymer* **2003**, *44*, 6259-6266.

(5) Winey, K. I.; Vaia, R. A. *MRS Bull.* **2007**, *32*, 314-319.

(6) Madathingal, R. R.; Wunder, S. L. *Langmuir* **2010**, *26*, 5077-5087.

(7) Porter, C. E.; Blum, F. D. *Macromolecules* **2000**, *33*, 7016-7020.

(8) Moniruzzaman, M.; Winey, K. I. *Macromolecules* **2006**, *39*, 5194-5205.

(9) Ramanathan, T.; Abdala, A. A.; Stankovich, S.; Dikin, D. A.; Herrera-Alonso, M.; Piner, R. D.; Adamson, D. H.; Schniepp, H. C.; Chen, X.; Ruoff, R. S.; Nguyen, S. T.; Aksay, I. A.; Prud'homme, R. K.; Brinson, L. C. *Nat. Nanotechnol.* **2008**, *3*, 327-331.

(10) Keddie, J. L.; Jones, R. A. L.; Cory, R. A. *Faraday Discuss.* **1994**, *98*, 219-230.

(11) Lin, W.-Y.; Blum, F. D. *Macromolecules* **1997**, *30*, 5331-5338.

(12) Lin, W.-Y.; Blum, F. D. *J. Am. Chem. Soc.* **2001**, *123*, 2032-2037.

(13) Metin, B.; Blum, F. D. *J. Chem. Phys.* **2006**, *125*, 054707 (1-9).

(14) Blum, F. D.; Krisanangkura, P. *Thermochim. Acta* **2009**, *492*, 55-60.

(15) Fernandez, V. L.; Reimer, J. A.; Denn, M. M. *J. Am. Chem. Soc.* **1992**, *114*, 9634-9642.

(16) Jelinski, L. W. *Annu. Rev. Mater. Sci.* **1985**, *15*, 359-377.

(17) Blum, F. D. *Coll. Surf.* **1990**, *45*, 361-376.

(18) Cosgrove, T., Griffiths, P. *Adv. Colloid Interface Sci.* **1992**, *42*, 175-204.

(19) Reichert, D. *NMR Studies of Dynamic Processes in Organic Solids*. In: "Annual Reports on NMR Spectroscopy", Webb, G. A., Ed. Academic Press: **2005**; Vol. Volume 55, pp 159-203.

(20) deAzevedo, E. R.; Bonagamba, T. J.; Reichert, D. *Prog. Nucl. Magn. Reson. Spectrosc.* **2005**, *47*, 137-164.

(21) Blum, F. D.; Xu, G.; Liang, M.; Wade, C. G. *Macromolecules* **1996**, *29*, 8740-8745.

CHAPTER 2

BACKGROUND

2.1. ADSORPTION OF POLYMERS ON SURFACES

      Polymer adsorption on solid substrates is generally carried out by the solution

processing, in which a polymer is dissolved in a solvent, mixed with a solid substrate and

allowed to equilibrate. In an adsorption process, any adsorbing polymer must diffuse

from the solution to reach a surface and attach to a surface adsorption site. Polymeric

chains also have to change their conformation to minimize the free energy of the

adsorption. At the same time, adsorption causes a decrease in entropy of the polymer

chains. The interactions between the polymer and surface must be strong enough to

compensate the entropy loss in an adsorption process.

      In an adsorption process, the concentration of polymers at polymer-surface

interfaces is generally greater than that of the polymer-solution interfaces.[1] Several

factors influence adsorption of polymers on surfaces such as molecular mass,[2-4]

polydispersity,[5-8] solvent, nature of surfaces,[9,10] concentration,[4,11] and temperature.[12-

15] The adsorbed amounts increase with an increase in molar mass of polymers, however,

these approach a limit where adsorption no longer depends on molar mass in the larger

molar-mass regime.[16] Since adsorption is more favored in the larger molar mass regime for randomly adsorbed polymers, larger molar mass polymers are adsorbed preferentially over smaller ones in a polydisperse sample. The effect is more pronounced when the concentration of polymers in solution is relatively low for a randomly adsorbing polymer.[17]

A number of studies have been undertaken to understand the effects of solvent on adsorption of polymer on surfaces.[18-20] It has been found that the adsorption is more favored in thermodynamically poor solvents for the polymers. This is because the energy of polymer-surface interactions, often estimated by an interaction parameter (χ_s), can easily overcome the energy interactions characterized by the polymer-solvent interaction parameter, (χ) between solvents and polymers in a thermodynamically poor solvent. Thus, adsorbed amounts decrease gradually with the adsorption of polymers from thermodynamically good solvents.[1] This is true for the adsorption of non-polar hydrocarbon polymers on non-porous and non-polar surfaces.[17,21] Effects of solvents become more complex for polar (or ionic) polymer adsorption on polar (or ionic) surfaces. The adsorbed amounts also depend on the nature of the surfaces and interactions between polymers and surfaces. Polymers with polar functional groups like polyacrylated can have stronger affinity with polar surfaces (silica surfaces), while weaker affinity with nonpolar surfaces (silane treated silica surfaces).[22-24] The amount of adsorbed polymers per unit surface area increases progressively with the concentration of the polymer solution and reaches a plateau value where it no longer depends on the solution concentration. This behavior can be easily observed in an adsorption isotherm.

The Langmuir adsorption isotherm, even though developed to describe adsorption of gases in non-porous surfaces, can be plausibly applied for adsorption of polymers from solution onto a solid surface. According to Langmuir, the surface of the adsorbent has a specific number of sites where the adsorbates are attached and the adsorption results in monolayer coverage. If the total number of adsorption sites is represented by S, and the sites that are occupied and unoccupied are represented by S_1 and S_0 respectively:

$$S_0 = S - S_1 \tag{1.1}$$

The adsorption is directly proportional to the number of sites unoccupied (S_0) and concentration (C) of adsorbate in the solution. The rate of desorption is proportional to number of sites occupied. At equilibrium, the rate of adsorption and desorption becomes equal:

$$K_1 S_1 = K_2 C S_0 \tag{1.2}$$

where K_1 and K_2 are rate constants for desorption and adsorption, respectively.

The fraction of sites covered, θ, can be written as S_1/S, and b can be used to represent the ratio of rate constants, K_2/K_1. The rearrangement of equation (1.2) leads to the equation (1.3), which is known as Langmuir equation,[25]

$$\theta = \frac{bC}{1+bC} \tag{1.3}$$

For the adsorption of polymers on surfaces, the fraction of the surface covered can be expressed in terms of mg of polymer adsorbed per m^2 of the surface. The fraction of the polymer adsorbed can be determined using thermogravimetric analysis (TGA). If the surface area is known, this adsorbed amount can be expressed as the mass of polymer adsorbed per surface area, mg/m^2 or:

$$AA = \frac{\Delta W}{(1 - \Delta W) \times A} \tag{1.4}$$

where AA (adsorbed amount) is the amount of polymers adsorbed that is expressed in

mg/m^2, ΔW is the fraction of polymer in the sample, and A is the specific surface area

(m^2/g) of the substrate. Similar to the other systems, the adsorbed amount is expected to

increase with increased concentration of polymer in solution, reach a maximum value and

remain constant with increases in solution concentration. A graphical plot of a Langmuir

adsorption isotherm is shown in Figure 1.
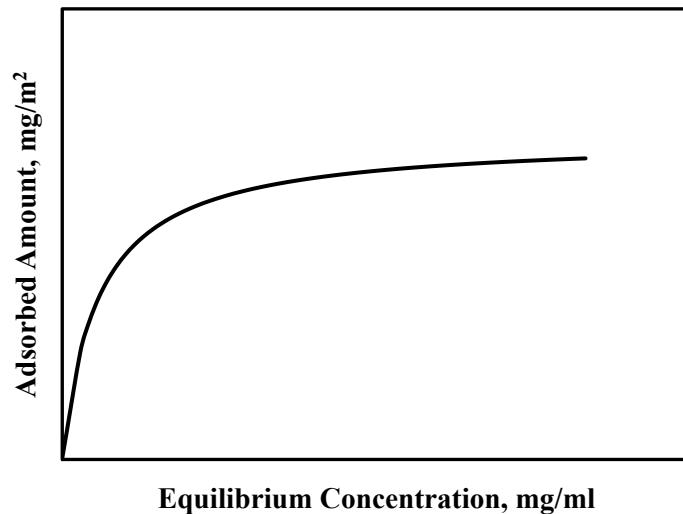
Figure 1. An idealized graphical representation of a Langmuir adsorption isotherm

adsorption of polymers on surfaces.

2.2. STRUCTURE OF POLYMERS ON SURFACE

The important feature relevant to this thesis of adsorbed polymers are their

conformations, interfacial structures, and adsorbed amounts on the surface. In an

adsorption process, the concentration of polymers at the polymer-surface interfaces is

often higher than in the solution, especially when there is a strong interaction between the

polymer and the surface. The excess concentration on the surface can be determined from the adsorbed amount and expressed either in terms of weight fraction of polymer or mass of polymers in mg per m^2 of surface. The adsorption is assisted by covalent or ionic bonds, polar (dipole dipole or H-bonding), or van der Waals forces. These forces are affective over a very short ranges, and thus, only a few segments that are directly bonded to the surface are affected very much. However, segments that are near to the attached segments are also affected due to the restriction in segmental motions caused by attached segments, and the effect becomes weaker for segments a few nanometers (nm) away from the surface segments.

Polymers adsorbed on surfaces can have various structures. For simplicity, two different modes of adsorbed structures, random or end-attached polymer structures are discussed. Homopolymers and random copolymers generally attach on surfaces in random fashion. However, introduction of selective functionality into the polymer chains can alter its surface configuration. For instance, in the case of random copolymers, one type of monomer segments can be preferentially adsorbed over the others on the surface. In this case, we can design a copolymers with different compositions of monomers with different fuctionalities for selective adsorption. For block copolymers, polymers can attach to the surface via one chain end. In either case, adsorption of large molecules means that only fractions of segments will be in direct contact with surface with rest of the segments attached indirectly.

For randomly adsorbed polymers, the structure of polymers can be described in terms of trains (segments that are directly attached to the surface), loops (segments in between trains), and tails (free chain ends) as suggested by Jenkel and Rumbach[26] as

shown in Figure 2a. The mobility of these segments can be different; trains are expected to have reduced mobility as compared to loops and tails for polymers strongly attached to the surface.

For block copolymers, the structure of polymers on surfaces can be rather different. These polymers can be attached with one end of the block via ionic or polar fuctional groups. In this case, one block of polymer segments may be adsorbed on the surface whereas the other block extends away from the surface in the form of either a mushroom or brush structures depending on a number of variables such as the molecularmass of each segment, solvent, etc. as shown in Figure 2b.[27]
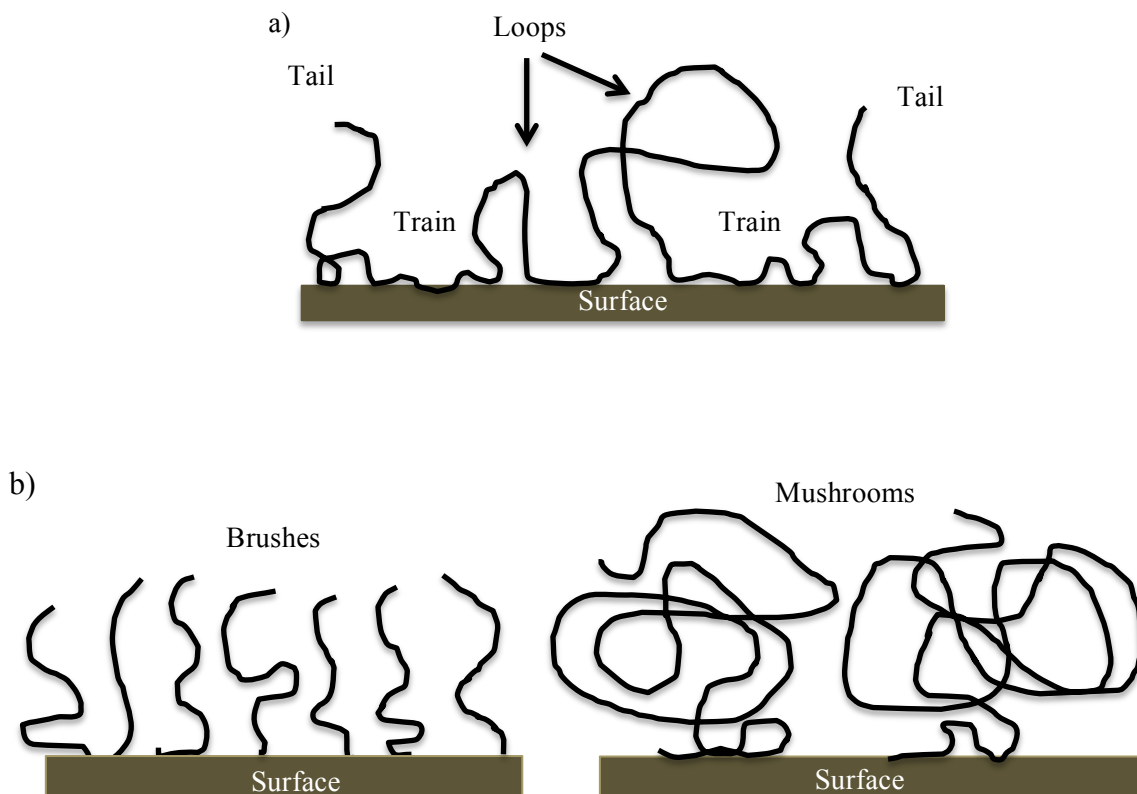
Figure 2. Shematic representation of randomly adsorbed polymer showing a) train, loops, and tails, and b) mushroom and brush structures.

2.3. CHARACTERIZATION TECHNIQUES FOR INTERFACIAL POLYMERS

Polymer based composites are comprised of multicomponent materials such as mixtures of polymers in a polymer blend, fillers and polymers in a reinforcing material, interpenetrating polymer networks, or adsorbed polymers on surfaces. The performance of composite materials depends on the inherent morphology and interactions between the components at interfaces. Therefore, the determination of morphological parameters, such as individual domain sizes, thickness, weight fraction in the mixture, miscibility, composition drifts at interfaces, etc. is essential. However, the exploration of a better characterization technique for these materials has still been challanging. This is because the interfacial interactions generally occur in a nanoscale range, and thus, require extremely sensitive techniques.

Recent developments in the synthesis of various polymer based composites demand rigorous methods for analyzing them. A variety of experimental techniques such as ellipsometry,[28] dielectric relaxation,[29,30] dielectric spectroscopy,[31,32] x-ray reflectivity measurements,[33] electron microscopy (scanning electron microscopy (SEM),[34] confocal microscopy,[35] and transmission electron microscopy (TEM)),[36,37] X-Ray diffraction (XRD), light scattering,[38] electron spin resonance (ESR),[39,40] NMR,[41,42] dynamic mechanical analysis (DMA), and calorimetric measurements[23,43,44] have been developed and used to study the structure and/or dynamics of these materials. Light scattering and microscopy techniques have been extremely useful to study the size, shape, and structure of the domains in a mixture. For example, XRD, light scattering, and neuton scattering have provided valuable information about interfacial thickness, and domain sizes.[36,45] Likewise, SEM and TEM have been used to determine the individual

size, interfacial thickness, and structure of the components in a mixture.[36,45,46] It has been useful to determine the miscibility and distribution of individual components, phase separations in a mixture, surface texture, and morphology of materials. However, sample preparation, especially for TEM, can sometimes be difficult, and the inherent structure of materials might be destroyed during this procedure. In addition, heat generated while exposing the material in the electron beam could damage the structure of the sample resulting artifacts in the measurements.[47,48] Thus, TEM and SEM results can sometimes be misleading. Moreover, these technologies (SEM and TEM) are not always cost effective.

Thermal analysis techniques, such as differential scanning calorimetry (DSC) and dynamic mechanical thermal analysis (DMTA), are very useful to study glass transition temperature (T_g) of polymer-based materials. DSC has been widely used to determine T_g, melting (T_m) and crystallization (T_c) temperatures, heat capacity, enthalpy, and degree of crystallinity (in semi-crystalline polymers) of several polymer based materials. [48,49] This technique has been popular, as it is easy to use, cost effective, fairly rapid, and easy to prepare samples. However, the weak sensitivity and resolution of DSC limit its application usually to the macroscopic properties of the material. In addition, DSC results are not always clear if multiple transitions are present around the same temperatures and are very difficult to separate from one another in complex systems. DMTA has been very popular to study the temperature dependent visco-elastic properties, modulus, coefficient of thermal expansion, and the damping values of the materials.

NMR has become a robust technique for identifying the chemical structures and physical properties of bulk polymers.[50-54] It is a sensitive and non-destructive technique,

can usually be performed with a small amount of analyte. However, the technique

becomes insensitive for interfacial polymers for two reasons: it is difficult to distinguish

the interfacial nuclei from two bulk phases nucleus as both phases might have similar

nuclei of interest, and the amounts (volume or weight fraction) of materials at interfaces

are very small as compared to those of the bulk materials. In some cases, the NMR

technique is superior over other optical techniques such as UV-visible, IR, and

fluorescence as optical clarity of the sample is not required in a NMR experiment. The

insensitivity of NMR for a small fraction of materials at interfaces, however, can be

remedied by two methods. The volume/weight fraction of polymer at interfaces can be

increased by application of high surface area substrates, and polymers at interfaces can

also be highlighted by the selective labeling (isotopic labeling) of the polymers.

Various NMR studies have been done with the aim of understanding the

interactions of polymer segments at interfaces. Early studies of cross polarization transfer

of ^{1}H in poly(vinyl alcohol) (PVA) to ^{29}Si nuclei by Zumbulyadis have shown that there

is a strong interaction between the polymer and silica.[55] The extent of the cross

polarization transfer from the polymer to the silica provided a rough estimation of the

length scale between the polymer segments and the surface. Similarly, solid-state carbon-

13 chemical shifts were used to probe the conformational changes of adsorbed poly-L-

lysine and poly-L-glutamic acid on silica and on hydroxyapatite.[56] The shifts were

consistent with more heterogeneous structures of adsorbed polymers as compared to that

of the bulk. Similarly, van Alsten used relaxation time (T_1) studies on poly(dimethyl

siloxane) (PDMS) adsorbed on modified silica and observed that the T_1 was dependent on

the amount of polymer adsorbed on surface. The relaxation time (T_1) was increased with

surface coverage.[57] Cross-polarization (CP), dipolar decoupling (DD), and magic angle

spinning (MAS) experiments on solid-state carbon-13 has been very common to study the

behavior of polymers adsorbed on surfaces.[53,58-60] Likewise, deuterium (^{2}H) solid-state

NMR has been routinely used to probe the dynamics of the bulk polymer and polymer

segments at different interfaces such as polymer-solvent, polymer-surface, polymer-

polymer, and polymer-air interfaces.[61-64] In these studies, the line shapes of the spectrum

were correlated with the mobility of the polymer segments at different interfaces.

2.3.1. Differential Scanning Calorimetry (DSC):

 Differential scanning calorimetry (DSC) is a thermo-analytical technique, in

which the energy necessary to establish similar temperatures between a sample and a

reference is measured as a function of time and temperature under controlled conditions

(inert atmosphere, temperature, time, and pressure). The amount of heat flow at different

temperatures is measured continuously when the sample is heated or cooled. Several

thermal events such as melting, crystallization, phase change (in liquid crystals,

pharmaceuticals, and organics), and glass transition temperature (T_g) can be measured

both qualitatively and quantitatively using DSC. It can also be used to measure enthalpy

of melting and crystallization, a chemical reaction, glass transition, and chain relaxation

(in polymers), and heat capacity of an analyte.

 The most common design of the differential scanning calorimeter is the heat flux

calorimeter. A simple schematic representation of heat flux calorimeter is shown in

Figure 3. In the figure, T_{fs}, T_{fr}, T_s, and T_r are the temperatures of the furnace on sample

side, furnace on reference side, sample sensor, and reference sensor, respectively. R_s and

R_r are the thermal resistances between sample sensor and furnace, and reference sensor

and furnace, respectively. Q_r and Q_s are the respective heat flow to the sample and the reference. The change in heat flow between sample and reference can also be expressed as:

$$\Delta Q = Q_s - Q_r = \frac{T_s - T_{fs}}{R_s} - \frac{T_r - T_{fr}}{R_r} \tag{2.1}$$

If T_{fs} is equal to T_{fr}, and R_s is equal to R_r, the equation 2.1 can be rearranged as,

$$\Delta Q = \frac{T_s - T_r}{R} = \frac{\Delta T}{R} \tag{2.2}$$

Thus, the differential heat flow is measured with thermocouples while maintaining similar temperatures in the sample and reference compartments.

$$Q_s = \frac{T_s - T_{fs}}{R_s} \qquad\qquad Q_r = \frac{T_r - T_{fr}}{R_r}$$
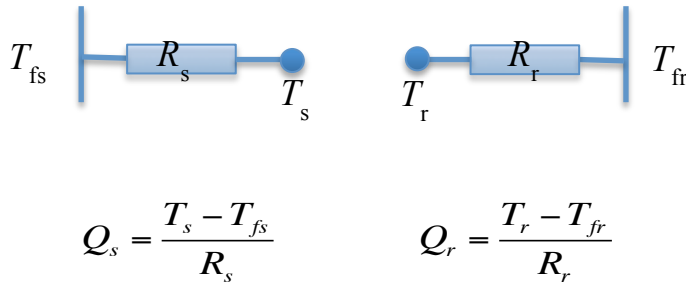
$$\Delta Q = Q_s - Q_r$$

Figure 3. Schematic representation of a heat flux DSC.[65]

Various sensors are involved in the measurement of the heat flow and to maintain similar temperatures inside the DSC cell. For example, Q2000 DSC from TA instruments (New Castle, DE, USA) consists of a body of constantan (a copper-nickel alloy) sensor with a flat surface at the base and a pair of thin-walled closed-end cylinders combined with the base as shown in Figure 4. In the center of the sensor, there is a T-Zero (T_0)

thermocouple (constantan wire and chromel wire). This thermocouple controls the

temperature of the furnace and provides precise temperature control to the sample and the

reference platform. Underneath each sample and reference platform disks, there is a

chromel area detector. This detector acts as an area thermocouple junction to reduce

sensitivity variations in thermal contact between the constantan disk and pans. The

differential temperature (ΔT) between the sample and the reference platforms is measured

by respective chromel wires (chromel wires from sample and reference platforms).
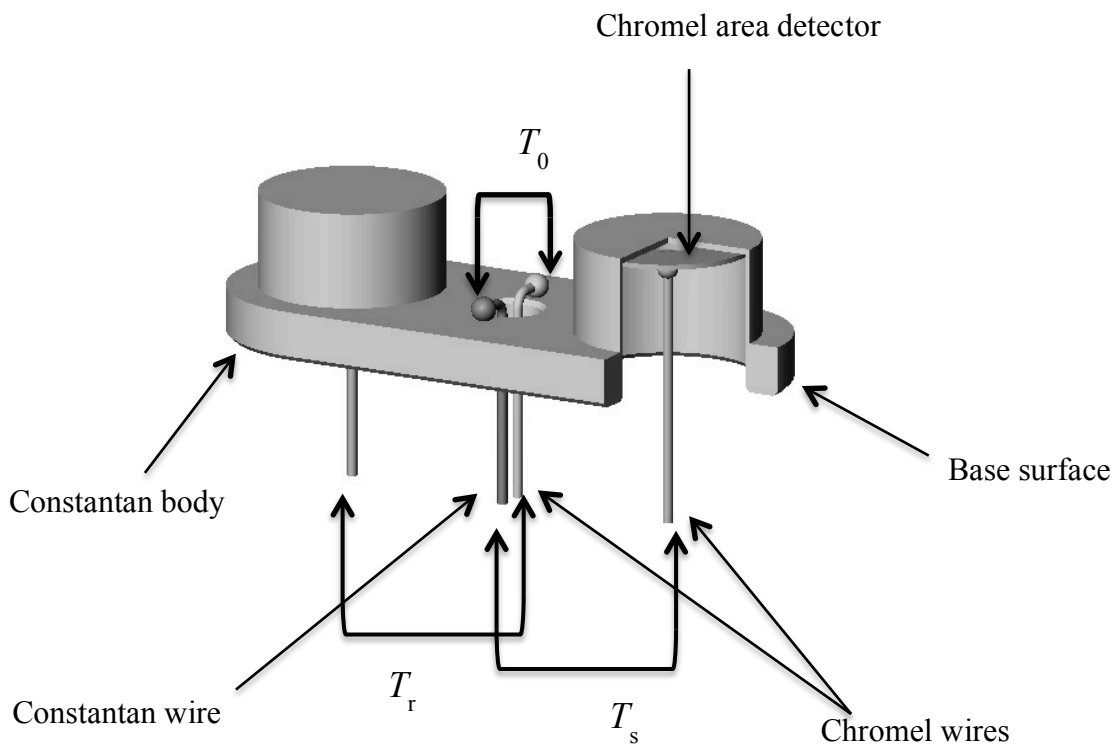
Figure. 4. Sensor assembly for Q2000 DSC (TA Instruments).[65]

In a simple DSC experiment, the sample is either heated or cooled at a specific

heating rate, and the heat flow rate is measured as a function of temperature or time. For

polymeric materials, the sample is heated to a certain temperature (generally above glass

transition or melting temperatures), cooled down to a lower temperature (below T_g), and

heated back to high temperatures. Since the first heating cycle changes the thermal

history of the material, the first cooling cycle or second heating cycle is generally used to

study the thermal events of the material. In some respects, compared to other thermal

analysis techniques, DSC is a simple and robust technique to determine some of the

thermal properties of the material. However, there are some limitations in using DSC.

Sensitivity becomes an issue for polymers with very broad glass transition temperatures.

Likewise, it can be very difficult to separate multiple thermal events occurring around the

same temperatures in a complex system such as polymer blends or composites.

Moreover, the amorphous and crystalline structures of a material are dependent on its

thermal history (temperature and time). Materials can change their structure as a function

of temperature and time. It is always desirable to know how the sample changes during

the experiment in order to determine the original structure of the material. Similarly,

results can be different depending on the method used; for example, heating rate, and

annealing at high temperature, can change the structure of the polymers.

2.3.2. Temperature Modulated Differential Scanning Calorimetry (TMDSC)

In order to properly characterize complex materials, it is necessary to determine if

there are multiple events overlapping around similar temperatures. Since many transitions

such as enthalpy relaxation, evaporation, thermoset cure, and decomposition are kinetic

events (a function of temperature and time), these events depend on the heating rate. In

some cases, these transitions shift to higher temperatures or can even be eliminated when

heated at a higher heating rate. For example, the cold crystallization of a semi-crystalline

polymer can be decreased or can even be eliminated if the sample is heated at a relatively

large heating rate. This is because the polymeric materials may be slower (compared to the heating rate) to arrange (relax) themselves for a transition at any specific temperature. Other transitions may not depend as much on heating rate, rather depend on the heat capacity of the material. In a simple DSC technique, it may be difficult, if not impossible to separate these two, kinetic and thermodynamic events. Temperature modulated differential scanning calorimetry (TMDSC) can be used to separate these events precisely.

TMDSC is an extension of the conventional DSC technique, in which the sample is heated in a way that a sinusoidal modulation (+/- X °C/min) is applied in addition to a continuous heating rate. A general equation that describes the total heat flow rate in a TMDSC experiment is of:

$$\frac{dQ}{dt} = C_P \frac{dT}{dt} + f(T,t) \tag{2.3}$$

where dQ/dt represents total heat flow rate (mW/min) and C_p is the heat capacity (J/g) of the material. dT/dt is the heating rate. The first portion of the equation represents the thermal component, which depends on the heat capacity of the material, and $f(T, t)$ represents the kinetic component of the total heat flow signal. Thus, in TMDSC, the total heat flow can be divided into the reversing heat flow rate ($C_p \, dT/dt$), a thermal component, and nonreversing heat flow rate ($f(T, t)$), a kinetic component of the total heat flow rate. In a TMDSC experiment, the average heating rate provides the total heat flow, while the sinusoidal heating rate provides heat capacity information from the heat flow that responds to a change in the heating rate. When $f(T, t)$ is zero, Equation (2.3) can be rearranged as:

$$C_P = \frac{dQ/dt}{dT/dt} \qquad (2.4)$$

The nonreversing heat flow is the difference between the total heat flow and the reversing heat flow. An example of total, reversing, and nonreversing curves obtained from a TMDSC experiment is shown in Figure 5. Smooth glass transition behavior is often clearly observed in the reversing heat flow, while total heat flow may consist of an overlap of a nonreversing event with a glass transition event.
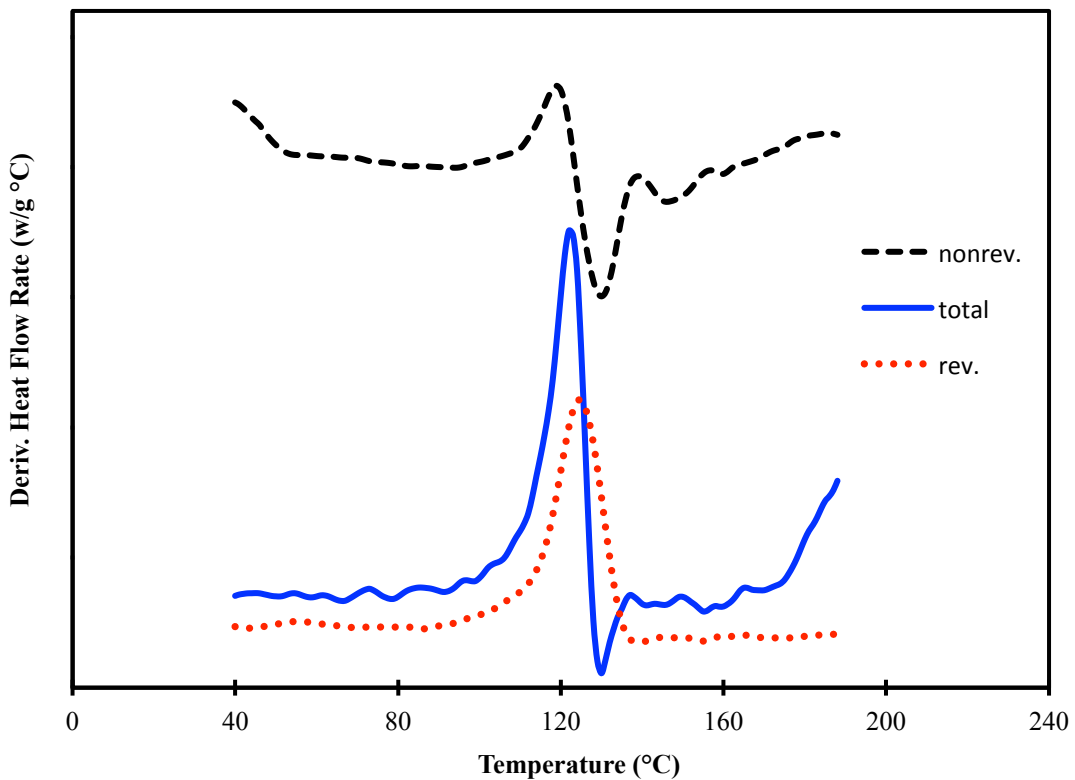
Figure 5. TMDSC thermogram of bulk PMMA showing nonreversing (black dashed line), reversing (red dotted line), and total heat flow (blue solid line) curves.

2.3.3. Heat Capacity Measurement Using TMDSC

TMDSC can be used to measure a number of phenomena beyond the measurements of T_g, T_m, and enthalpy of transitions (melting and crystallization);

20

TMDSC can also be used to measure the absolute heat capacity of different materials

such as metals, metal oxides, polymers, composites, etc. For a polymer composites

system, the heat capacity of the bulk polymer can be compared with its composites and a

correlation between their heat capacities with weight fractions of the polymers in the

composites can be made. Heat capacity measurement techniques are extremely useful for

studying the behavior of polymers and their composites.[66,67] In some studies, this

technique has been used to measure T_g[68] while others have measured degrees of

crystallinity,[69] supercooling,[70] etc. (in crystalline and semi-crystalline polymer). For

example Righitti et al. have estimated the rigid amorphous fraction in semi-crystalline

polymers.[71] Di Lorenzo et al. have studied the devitrification of rigid amorphous

fraction in semi-crystalline polymer like poly(ethylene terephthalate).[72] In some respects

adsorbed polymers are similar to semi-crystalline polymers, where crystals below their

melting temperatures behave like substrates and the polymer segments them are similar to

surface-bound polymers.

In this study, we have used a quasi-isothermal TMDSC technique to measure heat

capacities of the bulk and adsorbed poly(methyl methacrylate) (PMMA). In normal

differential scanning calorimetry, the heating rate of the system may affect the heat

capacity measurement of the sample. This may be especially true for the samples with

very small amounts of adsorbed polymers due to the low thermal conductivity of the

material. The faster the heating rate, the greater the temperature difference between the

sample and the set point temperature of the instrument can be, and consequently the

greater the chance of deviation in the measurement of the heat flow at different

temperatures. In the quasi-isothermal procedure, slow heating rates minimize the

temperature lags and hence, enhance the sensitivity and precision of heat capacity measurements.[73] These measurements allow an understanding of the changes associated with the interaction of the polymer and the substrate.

In a quasi-isothermal technique, a sample is heated to a certain temperature, kept at that temperature for 5-10 minutes, and a sinusoidal modulation of +/- X °C/min, generally 1 °C/120 second, is applied in such a way that the average temperature of the sample does not change by more than a small amount. An example of a quasi-isothermal experiment for the temperature profile as a function of time is shown in Figure 6.
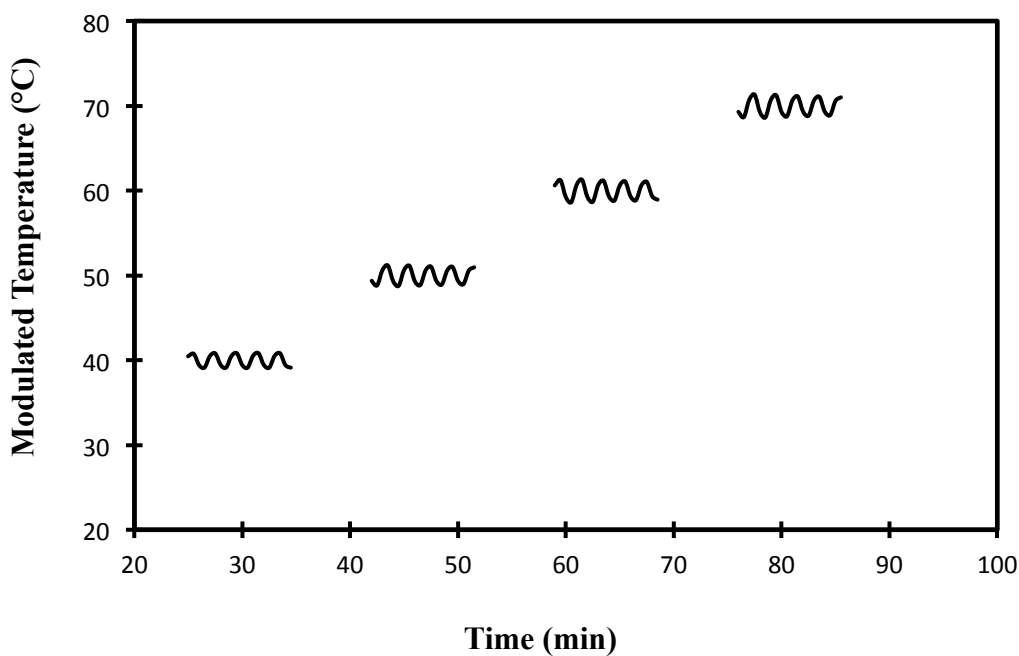
Figure 6. A quasi-isothermal method of heat capacity measurement using TMDSC for the bulk PMMA. A sinusoidal modulation of +/- 1 °C/120 second has been applied to the pseudo-isothermal condition; the average temperature does not change.

After the measurement of the heat capacity at one temperature, the sample is heated to another temperature and the same procedure is repeated. The temperature of the

sample is increased step-wise and the cycle is repeated to obtain heat capacities at different temperatures.

2.3.4. NMR Spectroscopy

NMR spectroscopy is a powerful tool that can be used to obtain physical, chemical, electronic, and structural information about a molecule. For molecules to be NMR active, they must possess nuclei with spin quantum number, $I > 0$. This condition is met when either the mass number (Z) is odd, or Z is even and the atomic number (A) is odd. I is zero for atoms with both A and Z even. When NMR active nuclei are exposed to an external magnetic field, the spins align in different orientations with respect to the applied magnetic field. The possible number of orientations, also called spin states (S), are given by $S = 2I + 1$.

In the presence of an external magnetic field, the nuclear spins precess at a frequency, v_0 (in Hertz), given by the Larmor expression:

$$v_0 = \frac{\gamma B_0}{2\pi}$$
(2.5)

where v_0 is called Larmor frequency, γ is the magnetogyric ratio, and B_0 (in Tesla) is the magnetic field strength and the field direction usually taken along the z-axis in the laboratory frame of reference. The precession frequency of the nuclei depends on the strength of external magnetic field and the magnetogyric ratio. The energy difference between different spin states is given by:

$$\Delta E = -\frac{\gamma h B_0}{2\pi}$$
(2.6)

where h is Planck's constant. The energy associated with this radio-frequency transition (ΔE) is relatively small. This energy is much smaller than the typical thermal energy (kT,

k is the Boltzman constant and T is the temperature) except at very low temperatures. The population distribution of nuclear spins in quantized energy levels is given by Boltzman factor, $e^{-\Delta E/kT}$. At room temperature, all energy levels (ground and excited energy levels) are almost equally populated. Because of the small population difference between the ground and excited states, the intensity of NMR spectra are weaker than the spectra obtained from most other spectroscopic techniques. The sensitivity and the resolution of the NMR spectrum also depends on many other factors, (a) magnetic moment (μ), which depends on the magnetogyric ratio (γ) (rad/T s) of the nucleus, (b) the external magnetic field strength (B_0), (c) natural abundance of the nucleus, and (d) the local field experienced by the nucleus, which in turn depends primarily upon the prevailing electronic factors (largely induction and anisotropy) that cause a change in local electron density around the nucleus.

The types of NMR experiments generally depend on the state of the material. For simplicity, one can divide NMR experiments into those that require techniques suitable for either liquid or solid samples. In liquid NMR spectroscopy, the spectrum results from the averaging of many interactions through isotropic reorientations of the molecules. This usually results in the formation of a narrow spectrum. In contrast, solid spectra are due to anisotropic chemical shifts, dipolar (homonuclear or heteronuclear) interactions, or quadrupolar interactions, and are generally broad. However, these interactions can be reduced by employing various perturbations on original NMR experiments, such as magic angle spinning (MAS). Even though these perturbations require special hardware, NMR instruments can be designed for these experiments.

2.3.5. Solid State Deuterium (^{2}H) NMR Spectroscopy

For solid materials, the Hamiltonian of the nucleus in the presence of an external magnetic field can be described as:

$$H_T = H_Z + H_Q + H_D + H_{CS} + H_J \qquad (2.7)$$

where H_Z, H_Q, H_D, H_{CS}, and H_J represent the Hamiltonians for Zeeman interaction (the interaction of nuclei with external magnetic field), quadrupolar interaction (nuclei with $I > 1/2$), dipolar interactions between nuclei through space, chemical shift anisotropy of the nucleus, and scalar coupling interactions between the nuclei, respectively. For solid state deuterium (^{2}H) NMR spectroscopy, Zeeman, and quadrupolar interactions are dominant over other interactions. Thus, the Hamiltonian for ^{2}H is reduced to:

$$H_T = H_Z + H_Q \qquad (2.8)$$

The interaction of the magnetic moment of deuteron with an external magnetic field causes the nuclear spins to precess around the external magnetic field with a frequency given by a Larmor frequency (ν_0). For a deuterium nucleus, this frequency is 61.39 MHz at 9.4 Tesla (400 MHz ^{1}H frequency). The Zeeman energy levels of the nuclear spin are given by:

$$E = -hm_Z\nu_0 , \text{ or } E = -\hbar m_Z\omega_0 \text{ and } \omega_0 = \gamma B_0 \qquad (2.9)$$

where m_Z is the a quantum number whose values are 1, 0, and -1 for deuteron. ω_0 is the Larmor frequency in rad/sec.

The frequency corresponding to the transitions of the nuclear spins between allowed states (from -1 to 0, and from 0 to +1) depend on two factors (ignoring the asymmetry factor); (a) the deuterium nucleus has electric quadrupole moment, which interacts with the electric field gradient (from the electrons around the nucleus) resulting

25

quadrupolar coupling constant (QCC) given by e^2qQ/h (eQ from deuterium quadrupole moment and eq from electric field gradient), and (b) the orientations of the electric field gradient tensor with respect to the external magnetic field, given by angle θ (angle between the external magnetic field and the electric field gradient tensor). The frequency corresponding to the transitions can be written as:

$$\omega_{0\to-1} = \frac{E(-1)-E(0)}{h} = \omega_0 + \frac{3}{4}\left[\frac{e^2Qq}{h}\right](3\cos^2\theta - 1) \tag{2.10a}$$

$$\omega_{1\to0} = \frac{E(0)-E(1)}{h} = \omega_0 - \frac{3}{4}\left[\frac{e^2Qq}{h}\right](3\cos^2\theta - 1) \tag{2.10b}$$

The expressions (2.10a) and (2.10b) work well when the electric field gradient tensor is axially symmetric with respect to the external magnetic field, as in aliphatic C-D bonds. However, for aromatic C-D bonds, along with some others, the motionally averaged electric field gradient is not axially symmetric.[74] Thus, the modified forms of Eqns. (2.10a) and (2.10b) that accounts for asymmetry caused by an electric field gradient can be written as:

$$\omega_{1\to0} = \frac{E(0)-E(1)}{h} = \omega_0 - \frac{3}{8}\left[\frac{e^2Qq}{h}\right](3\cos^2\theta - 1 - \eta\sin^2\theta\cos^2\phi) \tag{2.11a}$$

$$\omega_{1\to0} = \frac{E(0)-E(1)}{h} = \omega_0 + \frac{3}{8}\left[\frac{e^2Qq}{h}\right](3\cos^2\theta - 1 - \eta\sin^2\theta\cos^2\phi) \tag{2.11b}$$

where η represents asymmetry parameter. The angle ϕ represents the azimuthal orientation of electric field gradient tensor with respect to the external magnetic field.

From expressions (2.10a) and (2.10b), it can be observed that the doublet spacing depends on the angle between the C-D bond to the direction of the applied magnetic field (θ). In the presence of molecular motions, however, the doublet spacing depends on the

26

orientation and the motion of the deuteron with respect to the molecular symmetry axis and the external magnetic field. The pictorial representation of the transition between different states in a deuterium nucleus is shown in Figure 7.

Zeeman Interaction + Quadrupole Interaction

$$\omega_{0\to-1} = \frac{E(-1)-E(0)}{h} = \omega_0 + \frac{3}{4}\left[\frac{e^2Qq}{h}\right](3\cos^2\theta - 1)$$

$$\omega_{1\to0} = \frac{E(0)-E(1)}{h} = \omega_0 - \frac{3}{4}\left[\frac{e^2Qq}{h}\right](3\cos^2\theta - 1)$$

$$\omega_0 + \frac{3}{4}\left[\frac{e^2Qq}{h}\right](3\cos^2\theta - 1) \quad \omega_0 \qquad \omega_0 - \frac{3}{4}\left[\frac{e^2Qq}{h}\right](3\cos^2\theta - 1)$$

Frequency (rad/sec)
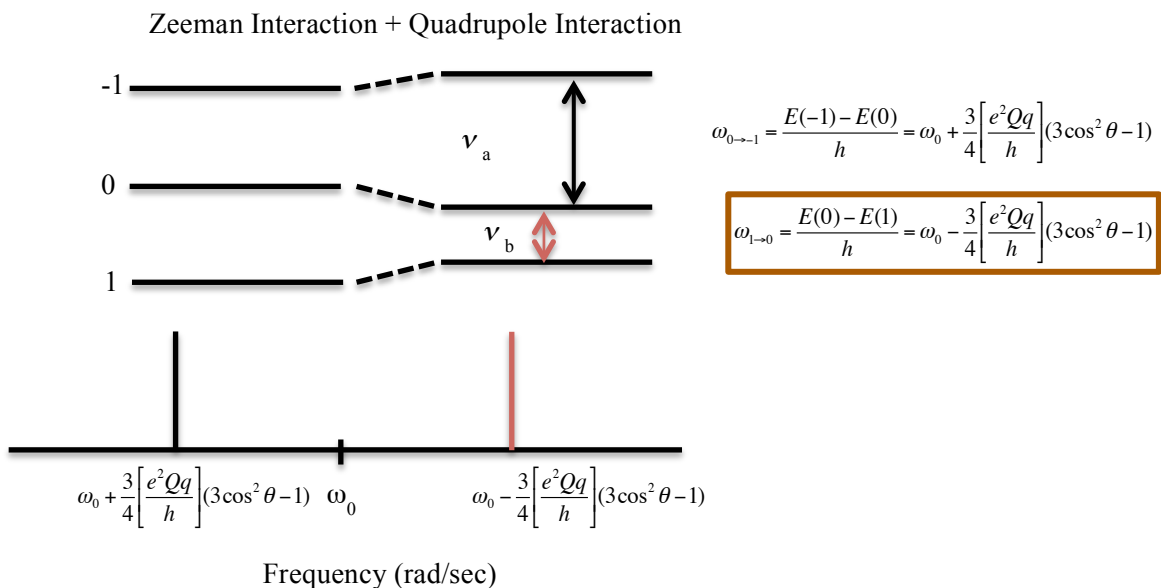
Figure 7. The quadrupolar splitting of nuclei with spin quantum number, I = 1.

The resonance frequency of a deuterium nucleus depends on the angle θ that a C-D bond makes with an external magnetic field. For a single crystal, in a static condition, if there is only one type of C-D bond orientation, a doublet spectrum is obtained. In the case of amorphous polymers, where C-D bond takes all possible orientations (θ = 90° to 0°) with respect to external magnetic field, a Pake powder pattern is obtained as shown in Figure 8. The maximum intensity is obtained when θ is 90°, the situation where C-D bond orientation is perpendicular to the external magnetic field. When θ is 0°, the intensity would be at a minimum. In this situation, the C-D bond is oriented parallel to

the external magnetic field. The intensity of each orientation can be described as the

latitude of a sphere with equal intensity as shown in Figure 8.
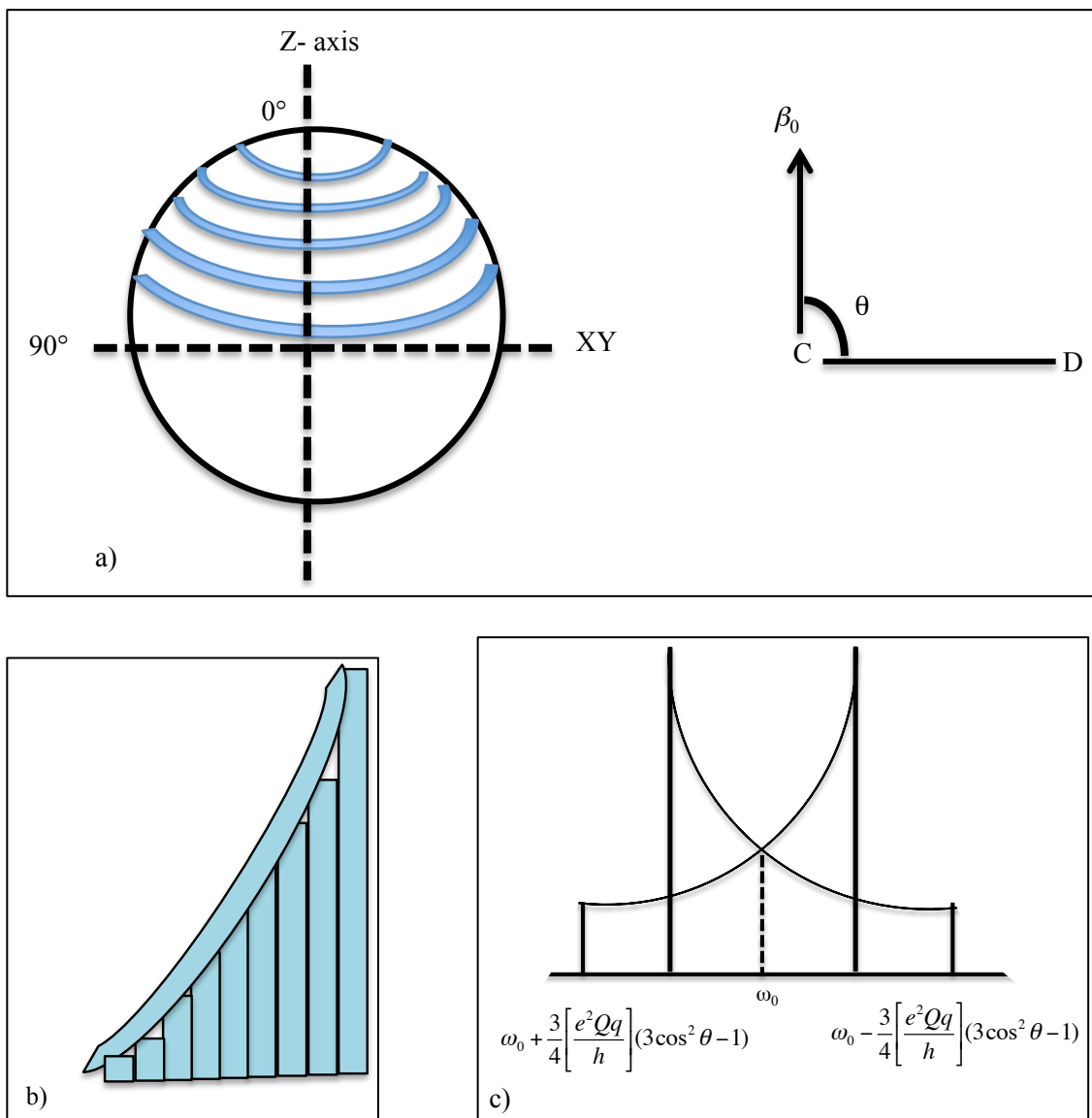
Figure 8. Pictorial representation of how deuterium NMR line shape originates. a) A

sphere is divided into latitudes of equal frequency; the orientation of the C-D bond vector

perpendicular to the external magnetic field generates a maximum intensity and is a

minimum when the bond vector is parallel. b) A half portion of Pake power pattern of

deuterium spectrum for all possible orientations of C-D bonds with respect to the external

magnetic field. c) A complete Pake powder pattern for deuterium resulted from both transitions (m = - 1 to 0) and (m = +1 to 0).
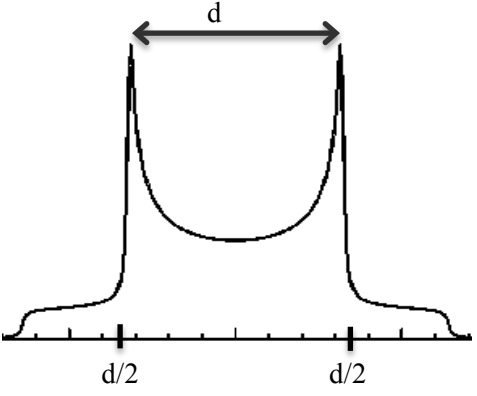
The line shape of the deuterium Pake power pattern can provide detailed information about the structure and the motion of the segments in polymers. For glassy polymers, the static C-D bond results in the splitting of doublets with three-fourths of quadrupole coupling constant (QCC). The presence of other local motions such as the rotation of a methyl or phenyl group, ring flip in a phenyl ring, or two-site hop, changes the line shape of deuterium power pattern. In this situation, the angular dependence of deuterium powder pattern takes the form of:
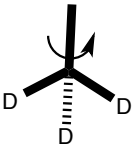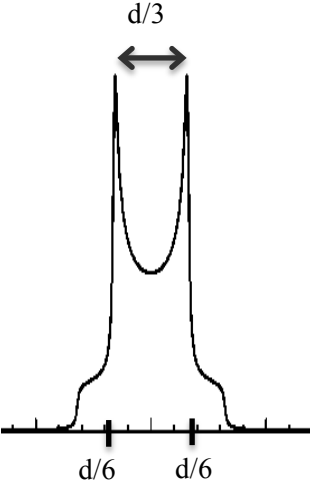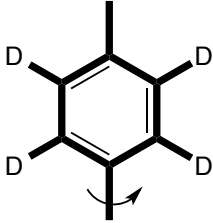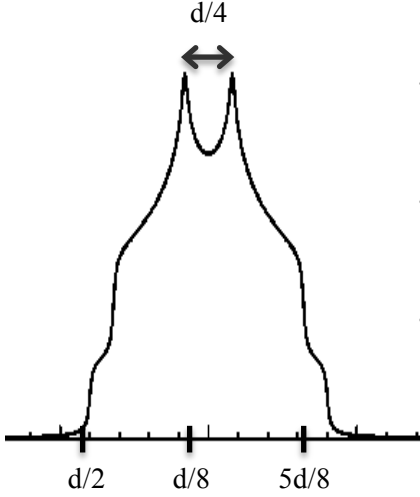
$$3\cos^2\theta(t) - 1 = \frac{1}{2}(3\cos^2\alpha(t) - 1)(3\cos^2\phi - 1) \tag{2.12}$$
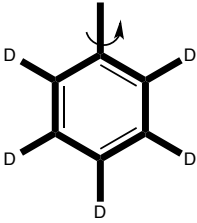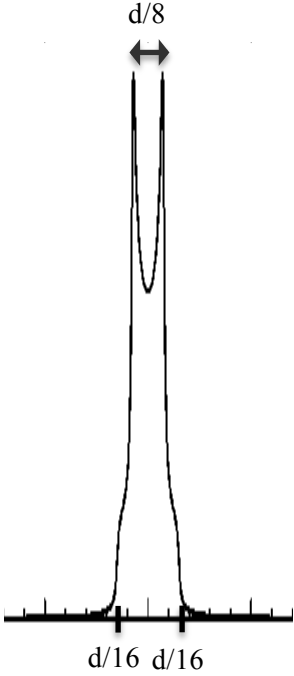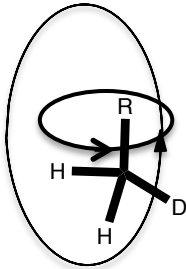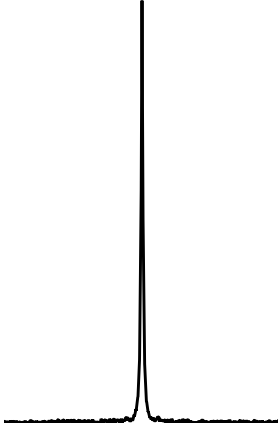
where, the first term (with $\alpha(t)$) on the right hand side represents orientations of the deuterium nucleus with respect to the external magnetic field. The second term (ϕ) represents the orientation of C-D bond with respect to the symmetry axis. For the methyl group rotating around the symmetry axis, the angle (ϕ) becomes 70.5°. Thus, the term $3\cos^2\theta(t)-1$ is reduced to one third of its static analog. Since the QCC of a static methyl group is in the order of 150 to 170 kHz, the methyl group rotation decreases this value to 50 to 57 kHz. Similarly, for deuterated phenyl rings with 180° ring flips, or rotation of phenyl ring around 1,4 symmetry axis, cause the deuterium line width to decrease from their static analog. For example, for 180° phenyl ring flips, one can observe a series of bumps (shoulders) following the major horns separated by (1/4)QCC. For the electric field gradient (EFG) tensor component that is perpendicular to the flip axis, there will be

29

no effect of ring flip motion, a bump corresponding to a half of the static QCC is

obtained. However, the position of deuteron is changed by 120° in the flip process,

another side band can be observed at (5/8)QCC (static) with major peaks at (1/8)QCC

(static) as shown in Table 1. In the case of a molecule with phenyl ring in a constant

rotation motion around 1,4 axis, the averaging of all orientations reduce the width of the

deuterium powder pattern to one-eighth of its static analog.

Table 1. NMR line shapes corresponding to various types of motion of groups in a

molecule.[75] The symbol "d" is used to replace the quadrupole coupling constant (QCC)

of the deuterium Pake powder pattern. The spectra were obtained using Dr. H. W.

Spiess's WebLab (NMR WebLab 4.5) simulations.

Motion type	Bond	Spectrum
A) Static C-D bond	C — D	

B) Methyl group rotation		
C) 180° ring flip		

D) Phenyl ring rotation		
E) Isotropic motion		

Solid-state deuterium NMR has been commonly used to study molecular motions.

Unlike that for a liquid sample, a quadrupole echo sequence is generally used for solid-

state deuterium spectra. This is because in a typical solid-state NMR experiment, the

magnetization in the time domain decays very rapidly in the transverse direction. This

results in a loss of some of the signals during the dead time, the time required for receiver

to recover from strong pulse. The application of the quadrupole echo eliminates much of this problem as the spectra are generated from the maximum point of an echo signal as shown in Figure 9(a). The pulse sequence for a quadrupole echo experiment can be written as, $90°_X - \tau_1 - 90°_Y - \tau_2 -$ acquisition. Two 90° pulses each with 90° out of phase are applied in succession with a delay time (τ_1) in between them. The first 90° pulse orients the nuclear magnetization to Y-axis (according to "$90°_X - \tau_1 - 90°_Y - \tau_2 -$ acquisition" pulse sequence). After some time τ_1, the nuclear spins diphase. The application of a second 90° pulse and waiting for τ_2 refocuses the nuclear spins generating an echo signal. A schematic picture diagram showing formation of an echo signal is shown in Figure 9(b). This is an example of a Hahn echo experiment. However, it is impossible to draw a vector picture diagram for quadrupole echo experiment. The echo signal is left shifted and Fourier transformed to generate the deuterium powder pattern.

a)
Pulse   Pulse   Echo

τ_1 τ_1

$90°_X$ $90°_Y$ Acquisition
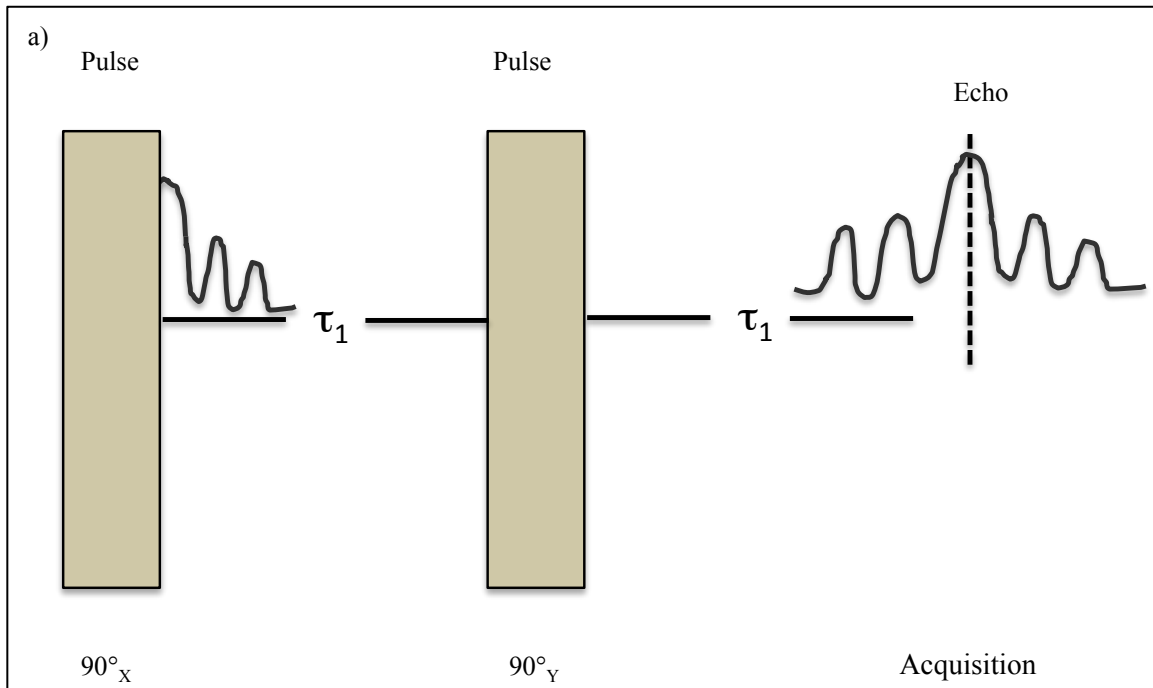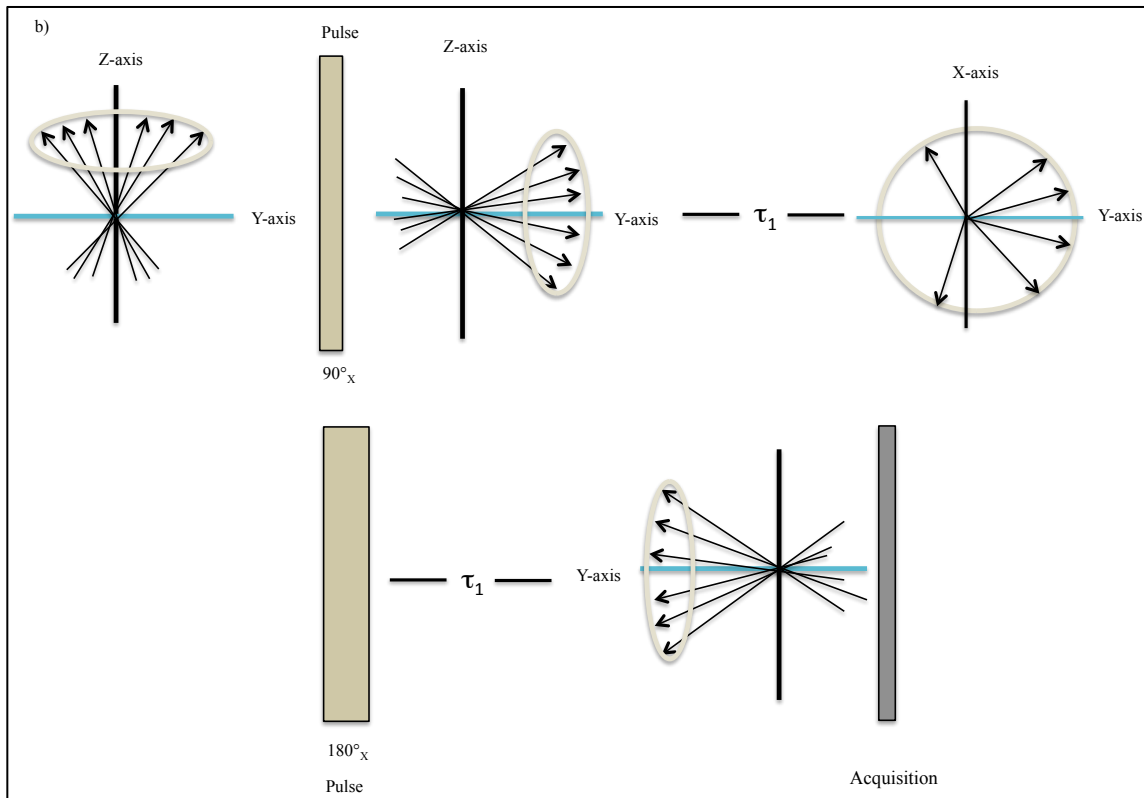
Figure 9. (a) A pulse sequence for quadrupolar echo experiment, and (b) vector diagram that shows the formation of an echo after applying two pulses (90° and 180° along X-axis) with a time τ_1 (tau1) in between the pulses. This is an example that shows the formation of an echo, however, vector picture diagram does not work for a quadrupole echo experiment.

2.4 REFERENCES

(1) Fleer, G. J.; Cohen-Stuart, M. A.; Scheutjens, J. M. H. M.; Cosgrove, T.; Vincent, B. *Polymers at Interfaces;* Chapman & Hall: London, **1993**.

(2) Van der Beek, G. P.; Cohen Stuart, M. A.; Fleer, G. J.; Hofman, J. E. *Langmuir* **1989**, *5*, 1180-1186.

(3) Van der Beek, G. P.; Stuart, M. A. C.; Fleer, G. J.; Hofman, J. E. *Macromolecules* **1991**, *24*, 6600-6611.

(4) Silberberg, A. *J. Chem. Phys.* **1968**, *48*, 2835-2851.

(5) Felter, R. E.; Ray Jr, L. N. *J. Colloid Interface Sci.* **1970**, *32*, 349-360.

(6) Linden, C. V.; Leemput, R. V. *J. Colloid Interface Sci.* **1978**, *67*, 63-69.

(7) Cohen Stuart, M. A., Scheutjens, J. M. H. M., Fleer, G. J. *J. Polym. Sci. Polym. Phys. Ed.* **1980**, *18*, 559-573.

(8) Roe, R. J. *Adhesion and Adsorption of Polymers;* Plenum, New York, **1980**. 629.

(9) Lee, L. T.; Somasundaran, P. *Langmuir* **1989**, *5*, 854-860.

(10) Chakraborty, A. K.; Golumbfskie, A. J. *Annu. Rev. Phys. Chem.* **2001**, *52*, 537-573.

(11) Bouchaud, E.; Daoud, M. *J. Phys. France* **1987**, *48*, 1991-2000.

(12) O'Shea, J.-P.; Qiao, G. G.; Franks, G. V. *J. Colloid Interface Sci.* **2010**, *348*, 9-23.

(13) Wiśniewska, M. *Appl. Surf. Sci.* **2012**, *258*, 3094-3101.

(14) Steinby, K.; Silveston, R.; Kronberg, B. *J. Colloid Interface Sci.* **1993**, *155*, 70-78.

(15) Kozlov, M.; McCarthy, T. J. *Langmuir* **2004**, *20*, 9170-9176.

(16) Silberberg, A. *J. Chem. Phys.* **1968**, *48*, 2835-2851.

(17) Roe, R. J. *J. Chem. Phys.* **1974**, *60*, 4192-4207.

(18) Ober, R., Paz, L., Taupin, C., Pincus, P., Boileau, S. *Macromolecules* **1983**, *16*, 50-55.

(19) Griot, O., Kitchener, J. A. *Trans. Faraday Soc.* **1965**, *61*, 1026-1031.

(20) Linse, P. *Soft Matter* **2012**, *8*, 5140-5150.

(21) Kolthoff, I. M., Gutmacher, R. E., Kahn, A. *J. Phys. Chem* **1951**, *55*, 1240-1246.

(22) Kulkeratiyut, S.; Kulkeratiyut, S.; Blum, F. D. *J. Polym. Sci. Pt. B-Polym. Phys.* **2006**, *44*, 2071-2078.

(23) Blum, F. D.; Young, E. N.; Smith, G.; Sitton, O. C. *Langmuir* **2006**, *22*, 4741-4744.

(24) Kabomo, M. T.; Blum, F. D.; Kulkeratiyut, S.; Kulkeratiyut, S.; Krisanangkura, P. *J. Polym. Sci., Part B: Polym. Phys.* **2008**, *46*, 649-658.

(25) Langmuir, I. *J. Am. Chem. Soc.* **1918**, *40*, 1361-1403.

(26) Jenkel, E., Rumbach, B. *Z. Electrochem.* **1951**, *55*, 612.

(27) de Gennes, P. G. *Adv. Colloid Interface Sci.* **1987**, *27*, 189-209.

(28) Keddie, J. L.; Jones, R. A. L.; Cory, R. A. *Faraday Discuss.* **1994**, *98*, 219-230.

(29) Fukao, K.; Miyamoto, Y. *Europhys. Lett.* **1999**, *46*, 649-654.

(30) Fukao, K.; Miyamoto, Y. *Phys. Rev. E* **2000**, *61*, 1743-1754.

(31) Hartmann, L.; Kratzmuller, T.; Braun, H. G.; Kremer, F. *Macromol. Rapid Commun.* **2000**, *21*, 814-819.

(32) Bauer, C.; Bohmer, R.; Moreno-Flores, S.; Richert, R.; Sillescu, H.; Neher, D. *Phys. Rev. E* **2000**, *61*, 1755-1764.

(33) Wallace, W. E.; Vanzanten, J. H.; Wu, W. L. *Phys. Rev. E* **1995**, *52*, R3329-R3332.

(34) Hudec, I.; Sain, M. M.; Kozankova, J. *Polym. Test.* **1991**, *10*, 387-397.

(35) Zammarano, M.; Maupin, P. H.; Sung, L.-P.; Gilman, J. W.; McCarthy, E. D.; Kim, Y. S.; Fox, D. M. *ACS Nano* **2011**, *5*, 3391-3399.

(36) Annighofer, F., Gronski, W. *Makromol. Chem.* **1984**, *185*, 2231.

(37) Washiyama, J.; Creton, C.; Kramer, E. J. *Macromolecules* **1992**, *25*, 4751-4758.

(38) Zhang, K.; Gui, Z.; Chen, D.; Jiang, M. *Chem. Commun.* **2009**, 6234-6236.

(39) Robb, I. D., Smith, R. *Polymer* **1977**, *18*, 500-504.

(40) Kobayashi, K., Yajima, H. Imamura, Y., Endo, R. *Bull. Chem. Soc. Japan* **1990**, *63*, 1813-1815.

(41) Okuom, M. O.; Metin, B.; Blum, F. D. *Langmuir* **2008**, *24*, 2539-2544.

(42) Fernandez, V. L.; Reimer, J. A.; Denn, M. M. *J. Am. Chem. Soc.* **1992**, *114*, 9634-9642.

(43) Porter, C. E.; Blum, F. D. *Macromolecules* **2000**, *33*, 7016-7020.

(44) Sargsyan, A.; Tonoyan, A.; Davtyan, S.; Schick, C. *Eur. Polym. J.* **2007**, *43*, 3113-3127.

(45) Roe, R. J. *Appl. Crystallogr.* **1982**, *15*, 182-189.

(46) Reading, M., Hourston, D. J. *Modulated Temperature Differential Scanning Calorimetry: Theoretical and Practical Applications in Polymer Characterisation.;* Springer: Dordrecht, The Netherlands, **2006**.

(47) Thomas, D. A. *In Advances in Preparation and Characterization of Multi-polymer Systems;* Ambrose, R. J., Aggarwal, S. L. Eds.; John Wiley and Sons: New York, **1978**.

(48) Vesely, D. *In Polymer Blends and Alloys;* Folks, M. J., Hope, P. S., Eds.; Blackie Academic & Professional: London, **1993**.

(49) *Handbook of Thermal Analysis and Calorimetry: Applications to Polymers and Plastics.;* Cheng, S. Eds.; Elsevier: Amsterdam, The Netherlands, **2002**. Vol. *3*,

(50) Schmidt-Rohr, K., Spiess, H. W. *Multidimensional Solid-state NMR and Polymers;* Academic Press: London, **1994**.

(51) Heatley, F. *Solid State NMR of Polymers* Mathias, L. J. Eds.; John Wiley & Sons, Ltd: Plenum, New York, **1991**. Vol. *30*,

(52) McBrierty, V.; Packer, K. *Nuclear Magnetic Resonance in Solid Polymers;* Cambridge University Press: Cambridge, **1993**. 202.

(53) Harris, R. K. *Nuclear Magnetic Resonance Spectroscopy;* Wiley: New York, **1985**.

(54) Sanders, J. K. M., Hunter, B. K. *Modern NMR spectroscopy;* Oxford University Press: Oxford **1987**.

(55) Zumbulyadis, N.; O'Reilly, J. M. *Macromolecules* **1991**, *24*, 5294-8.

(56) Fernandez, V. L.; Reimer, J. A.; Denn, M. M. *J. Am. Chem. Soc.* **1992**, *114*, 9634-9642.

(57) Van Alsten, J. *Macromolecules* **1991**, *24*, 5320-5323.

(58) Blum, F. D. *Coll. Surf.* **1990**, *45*, 361-376.

(59) Sinha, B. R.; Blum, F. D.; O'Connor, D. *J. Appl. Polym. Sci.* **1989**, *38*, 163-171.

(60) Blum, F. D.; Sinha, B.; Schwab, F. C. *Polym. Mater. Sci. Eng.* **1988**, *59*, 302-305.

(61) Lin, W.-Y.; Blum, F. D. *J. Am. Chem. Soc.* **2001**, *123*, 2032-2037.

(62) Hetayothin, B.; Blum, F. D. Effect of Structure and Plasticizer on the Glass Transition of Adsorbed Polymer. Ph.D. Thesis, Missouri University of Science and Technology, **2010**.

(63) Hetayothin, B.; Cabaniss, R. A.; Blum, F. D. *Macromolecules* **2012**, *45*, 9128-9138.

(64) Metin, B.; Blum, F. D. *Langmuir* **2009**, *26*, 5226-5231.

(65) Waguespack, L., Blaine, R. *A Technical Report*; TA Instruments.

(66) Marti, E.; Kaisersberger, E.; Moukhina, E. *J. Therm. Anal. Calorim.* **2006**, *85*, 505-525.

(67) Carini, G.; D'Angelo, G.; Tripodo, G.; Bartolotta, A.; Di Marco, G.; Lanza, M.; Privalko, V. P.; Gorodilov, B. Y.; Rekhteta, N. A.; Privalko, E. G. *J. Chem. Phys.* **2002**, *116*, 7316-7322.

(68) Hempel, E.; Kahle, S.; Unger, R.; Donth, E. *Thermochim. Acta* **1999**, *329*, 97-108.

(69) Chen, H. P.; Cebe, P. *Macromolecules* **2009**, *42*, 288-292.

(70) Nishimoto, Y.; Ichimura, Y.; Kinoshita, R.; Teramoto, Y.; Yoshida, H. *Thermochim. Acta* **1991**, *179*, 117-124.

(71) Righetti, M. C.; Di Lorenzo, M. L.; Tombari, E.; Angiuli, M. *J. Phys. Chem. B* **2008**, *112*, 4233-4241.

(72) Di Lorenzo, M. L.; Righetti, M. C.; Cocca, M.; Wunderlich, B. *Macromolecules* **2010**, *43*, 7689-7694.

(73) Ding, E. Y.; Cheng, R. S. *Thermochim. Acta* **2001**, *376*, 133-139.

(74) Jelinski, L. W. *Deuterium NMR of Solid Polymers: High-resolution NMR Spectroscopy of Synthetic Polymers in Bulk;* Komoroski, R. A. Eds.; VCH Publishers, Inc: New York, **1986**. Vol. *7*.

(75) Jelinski, L. W. *Annu. Rev. Mater. Sci.* **1985**, *15*, 359-377.

CHAPTER 3

THERMAL PROPERTIES OF PMMA ON SILICA USING TEMPERATURE-
MODULATED DIFFERENTIAL SCANNING CALORIMETRY[*]

3.1. ABSTRACT

The behavior of an amorphous polymer, poly(methyl methacrylate) (PMMA),

adsorbed on silica was studied using temperature-modulated differential scanning

calorimetry (TMDSC). A two-component model, based on loosely-bound polymer with a

glass transition temperature (T_g) (similar to that of the bulk polymer) and a tightly-bound

polymer (with a T_g higher than that of the loosely-bound polymer) was used to interpret

the thermograms. Increased sensitivity allowed the two transitions in the thermograms to

be quantified much more accurately than in previous work. Linear regression analysis of

the ratio of the area under two transitions with composition yielded the amount of tightly

bound polymer, $m_B'' = 1.21$ +/- 0.21 mg PMMA/m^2 silica. Two methods of analyzing the

thermograms, fitting with a Gaussian-Lorentzian (GL) cross distribution function and

perpendicular drop (PD) method, yielded similar results for the amount of tightly-bound

[*]*Bal K. Khatiwada,*[a] *Boonta Hetayothin,*[b] *Frank D. Blum*[a]
[a]Department of Chemistry, Oklahoma State University, Stillwater, Oklahoma, 74078,
USA
[b]Department of Chemistry and Materials Research Center, Missouri University of
Science and Technology, Rolla, Missouri 65409, USA

polymer on the surfaces with the GL method having a statistically better fit to the model. The ratio of heat capacity increments of loosely bound and tightly bound polymer, $\Delta C_{pA}/\Delta C_{pB}$, around the glass transition, indicated the relative mobility of the two components. It was found that the ΔC_{pA} was about three times as large as that of ΔC_{pB} suggesting that the tightly bound polymer had a much smaller change in mobility through glass transition region.

3.2. INTRODUCTION

The understanding of the physical properties of polymer chains near surfaces and interfaces has attracted attention in recent years owing to their impact in many technological advances, such as electronic packaging, drugs, paints, coatings, adhesion, detergents, composites, and many more.[1,2] Bulk properties are not always assignable to interfacial polymers because their behavior can be very different from those of the bulk polymers.[1,3] For example, in thin polymer films on solid substrates, the changes in glass transition temperatures (T_g) are dependent on the nature of the substrate, as well as on the thickness of the polymer films.[3-5] Previously, ellipsometric studies on polystyrene adsorbed on silica had reported that the T_g decreased with decreased film thickness[6,7] while similar studies on poly(methyl methacrylate) (PMMA) on silica reported an increased T_g.[8,9] Apparently conflicting results likely result from the details of the interactions and modification of the polymer at the interface. Typically, the physical properties of adsorbed polymers are more complex than those in bulk since they involve multiple components, including polymers and substrates. These adsorbed polymers may also be spatially heterogeneous.[5,10]

The study of complex materials such as adsorbed polymers is not generally easy to perform macroscopically, as the dimensions of such material on surfaces are on the order of 100 Å or less. Some experimental techniques, such as, spectroscopic ellipsometry,[8,11] neutron[3,12,13] and x-ray[14,15] reflectometry, and positron lifetime spectroscopy[16,17] have been used to study the local structure or thickness changes in the polymer layer. Other studies based on NMR,[18,19] ESR[20,21] and FTIR[22-24] have been successful in studying such interfaces. These techniques are very sensitive to the small amounts of material on the surfaces and have been used to examine the dynamics and segmental heterogeneity of the bound polymer.[24] These techniques are either very specific to the nature of the material, for example, transmission FTIR can be used only for particles that do not scatter much infrared radiation, and are surface localized, i.e., the effect of surface can be seen on those segments that are directly bound to the surface. The use of NMR and ESR is not prevented by the presence of solid fillers or by the optical clarity of the sample. However, surface studies may be limited to very small amounts of material on the surface and substrates with high surface areas and spectroscopic labels may be required.

Differential scanning calorimetry (DSC) is perhaps the most widely accepted technique for studying the thermal properties of polymers, including polymers adsorbed on surfaces.[25] This technique, in particular, is widely used to measure the glass transition temperature (T_g) of materials. The addition of temperature modulation[26] brought many advantages to the field, although its interpretation is often far from simple.[27] In particular, temperature modulated DSC (TMDSC) brought about considerable understanding of the behavior of adsorbed polymers.[28-30]

Previous studies on small amounts of poly(methyl methacrylate) (PMMA) adsorbed on silica reported that the PMMA glass transition temperature (T_g) broadened and shifted to a higher temperature than the bulk polymer.[29,30] This exact behavior depended on the adsorbed amounts[29,30] and also surface treatments.[31] The small amounts of adsorbed polymers require the use of very large surface-area substrates, but the consequent sensitivity problems hamper these studies. While good progress has been made, it has been difficult to quantify the calorimetric results with good accuracy. In the present study, we extend the use of temperature-modulated differential scanning calorimetry (TMDSC) with improved sensitivity and more sophisticated data analysis methods to achieve more accurate characterization of thermal behavior of PMMA on the surface of silica. These measurements are also extended to both larger and smaller adsorbed amounts, and it is shown that the bound segment model holds to over twice the original range studied. The results provide a greatly improved estimate of the amount of tightly-bound polymer and the DC_p's in the glass transition region.

3.3. BOUND-SEGMENT MODEL

A two-state model, based on loosely-bound polymer (component A, T_g similar to, but not necessarily equal to that of the bulk polymer) and tightly-bound polymer (component B, T_g significantly higher than that of the loosely-bound polymer) was used to interpret the thermograms on the adsorbed polymer on surfaces.[30] In this model, tightly-bound polymer is that most closely associated with the silica surface so that the dynamics of its segments are altered compared to the bulk-like segments. With increasing adsorbed amounts, the tightly-bound material was added first, followed by the

completion of this "tightly-bound" or "bound-segment layer" of an amount m_B" (in mg

polymer/m^2 silica surface). After that, additional polymer adsorbed is "loosely-bound".

The normalized polymer mass, m'_p, is defined as the total mass of adsorbed

polymer (e.g., as measured from thermal gravimetric analysis, TGA) divided by the mass

of silica used, which is the sum of the normalized masses for the two adsorbed polymer

components, A and B, or:

$$m'_p = m'_{pA} + m'_{pB} \tag{3.1}$$

The ratio of the heat flow changes of components A and B in the transition

regions, given by r, is related to the ratios of the specific heat capacities of the

components, or:

$$r = \Delta Q_A/\Delta Q_B = m'_{pA}\,\Delta C_{pA}/(m'_{pB}\,\Delta C_{pB}) \tag{3.2}$$

where the ΔQ's represent the heat flows and the ΔC_p's represent the changes in specific

heat capacity in the glass transition region. From equations (2) and (3), a linear equation

can be made, or:

$$r = (m'_p - m'_{pB})\,\Delta C_{pA}/(m'_{pB}\,\Delta C_{pB})$$

$$= [\Delta C_{pA}/(m'_{pB}\,\Delta C_{pB})]m'_p - \Delta C_{pA}/\Delta C_{pB} \tag{3.3}$$

This equation predicts that r should be a linear function of m'_p, a value that can easily be

converted to the adsorbed amount (mg polymer/m^2 silica) when surface area of silica is

known (in this case, 200 m^2/g). At adsorbed amounts where the bound layer of tightly-

bound polymer is fully developed, m'_{pB} should be a constant. Above this amount,

additional polymer adds to the loosely-bound polymer component. The slope and

intercept of the line can be used to calculate the amount of tightly bound polymer and the

ratio of the changes in specific heat capacity for loosely-bound and tightly-bound polymer.

The polymer behavior at the interface may also be characterized in terms of a bound fraction, f_B, which was taken as the ratio of the mass of bound polymer at the interface to the total amount of polymer.[1] This ratio can be expressed as a function of the experimental observable, r, as:

$$f_B = m'_{pB}/m'_p = m_{pB}/m_p = m''_{pB}/m''_p = 1/(1 + r\Delta C_{pB}/\Delta C_{pA}) \qquad (3.4)$$

where the ratio is the same, regardless of how the amount of polymer is normalized (i.e., per mass of silica, mass in sample, or per surface area). The fraction of tightly-bound polymer may then be compared to other measurements.[1,23,24,29,30]

3.4. EXPERIMENTAL

High molecular mass PMMA with M_w of 4.5×10^5 g/mol and polydispersity (PD) of 2.6 (Aldrich Chemical Co., Milwaukee, WI), was characterized with light scattering, gel permeation chromatography, and NMR,[23] and Cab-O-Sil M-5P silica with specific surface area of 200 m^2/g (Cabot Corporation, Tuscola, IL) were used as received.

To prepare the samples, different amounts of PMMA were dissolved in toluene in test tubes. Silica (Cab-O-Sil, 300 mg) was first wetted with toluene and then added to the polymer solutions. Adsorption of the polymer was carried out by shaking the sample tubes in a mechanical shaker for 2 days. The composites were then dried by bubbling air through the tip of a pasture pipette at the bottom of the tubes. The air-dried samples were put under vacuum at 60 °C for 2 days to remove any residual solvent. The compositions (amount of adsorbed polymer) were determined using Mettler Toledo TGA (TGA/DSC1

Thermogravimetric Analyser). The samples were heated from 40 °C to 600 °C at a heating rate of 10 °C/min. Air was used as a purge gas with flow rate of 50 mL/min. The major degradation for bulk PMMA started at around 220 °C, while the PMMA in the composites started degradation at around 280 °C. The accuracy and the validity of the method were verified with degradation of bulk PMMA, bulk silica, and PMMA/silica mixtures. After heating, the residual material contained only silica and the adsorbed amounts of polymer on silica were calculated based on the masses of PMMA and silica, and the specific surface area of the silica. The adsorbed amounts were verified after TMDSC measurements by opening the pans and analyzing those samples with TGA.

The thermal behavior in the glass transition region was measured with a TA Instruments model Q2000 MDSC (TA Instruments, New Castle, DE). The sample pans were referenced against empty pans of very similar mass and the cell purged with nitrogen gas at a flow rate of 50 mL/min. For PMMA, the samples were held at 25 °C for 2 min, heated to 200 °C at a rate of 3.0 °C/min with a modulation amplitude of +/- 1.0 °C, and a period of 60 s, then held for 2 min, cooled to 25 °C at the same rate, and finally held at 25 °C for 2 min in order to standardize the effects of previous thermal history. After the first heating and cooling scan, the second heating scan was applied with the same conditions as the first. The samples were not subjected to temperatures in excess of 200 °C in order to avoid the possibility of thermal degradation. The thermograms reported were determined using the second heating scans. The calorimetric results are shown as differential reversing heat flow rates (dQ_{rev}/dT) vs. temperature. A 15 °C smoothing was applied to the thermograms to reduce the higher-frequency noise and

46

highlight the transition, without significantly distorting the thermograms for the adsorbed polymers.

Two methods were chosen to estimate the area under the transitions in the (dQ_{rev}/dT) plots; the perpendicular drop method (TA Universal Analysis V4.2E software) and fitting of plots with Gaussian-Lorentzian mixed distribution (GL) function as shown in Figure 1. The GL function is a product function of Gaussian/Lorentzian functions[32] as represented by:

$$f(x) = \frac{a}{[1 + \frac{4M(x - x_0)^2}{w^2}] \exp[\frac{4\ln 2(1 - M)(x - x_0)^2}{w^2}]} \qquad (3.5)$$

where M is the G/L mixing ratio, w is the width, x_0 is the peak center and a is the amplitude. The value of M is 1 for a pure Lorentzian and 0 for a pure Gaussian function. w is the FWHM (full width at half maximum) for pure Gaussian and Lorentzian functions, but may be slightly higher (less than 10%) for the mixed functions.

In each case, a straight baseline was chosen, the transitions were split into two components, and the areas under each component were integrated. In the perpendicular drop (PD) method, the two overlapping transitions were separated by a line segment that was drawn perpendicular to the baseline at the temperature where it was believed that the two transitions could be separated like that in 1.1. For the GL cross distribution function a baseline subtraction was made for the ease of fitting. The resulting curves were fitted with the GL function (Origin software). Sometimes the peaks themselves were sufficient for the tops to be reported at the center of the transitions (T_g). In other cases, the GL fittings allowed the tops of the fitted components to be used as the T_g's.
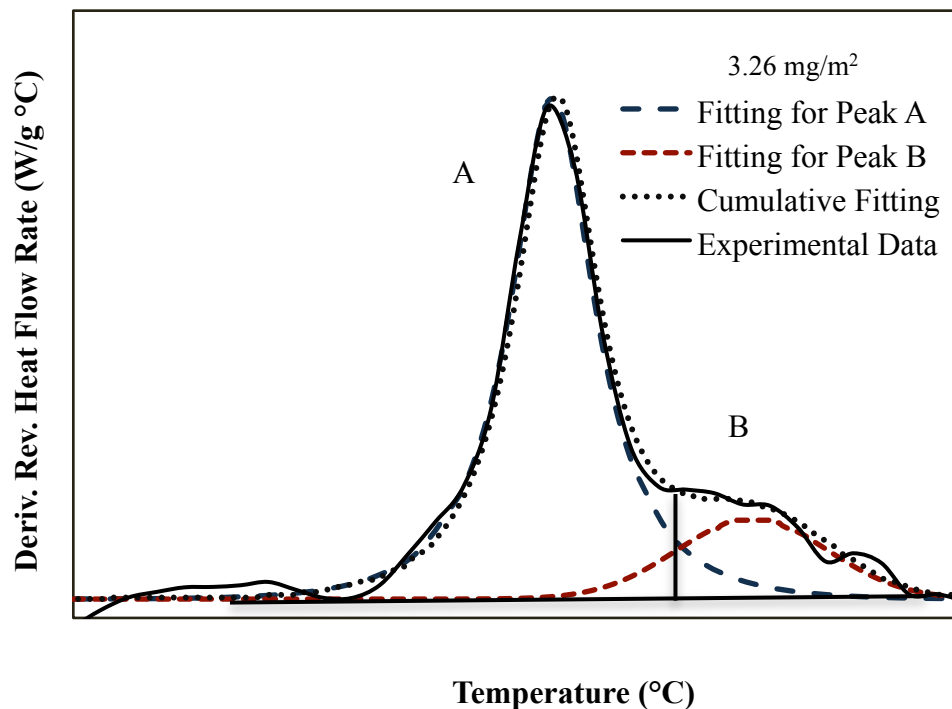
Figure 1. Examples of fittings from the perpendicular drop method and Gaussian-Lorentzian cross distribution (GL) function. In perpendicular drop method, a perpendicular line segment is drawn to separate the two peaks. For the GL method, the two components (dashed), and cumulative fitting (dotted) is compared to the experimental thermogram.

3.5. RESULTS

The thermograms for samples with different amounts of PMMA adsorbed on silica are shown in Figure 2. The thermograms for the adsorbed polymer samples were shifted vertically for clarity of the peaks. The intensity of the bulk PMMA sample was reduced to fit on the same figure as the adsorbed samples. Bulk PMMA has a T_g of about 125 °C (at 3.0 °C/min) consistent with earlier studies.[30]
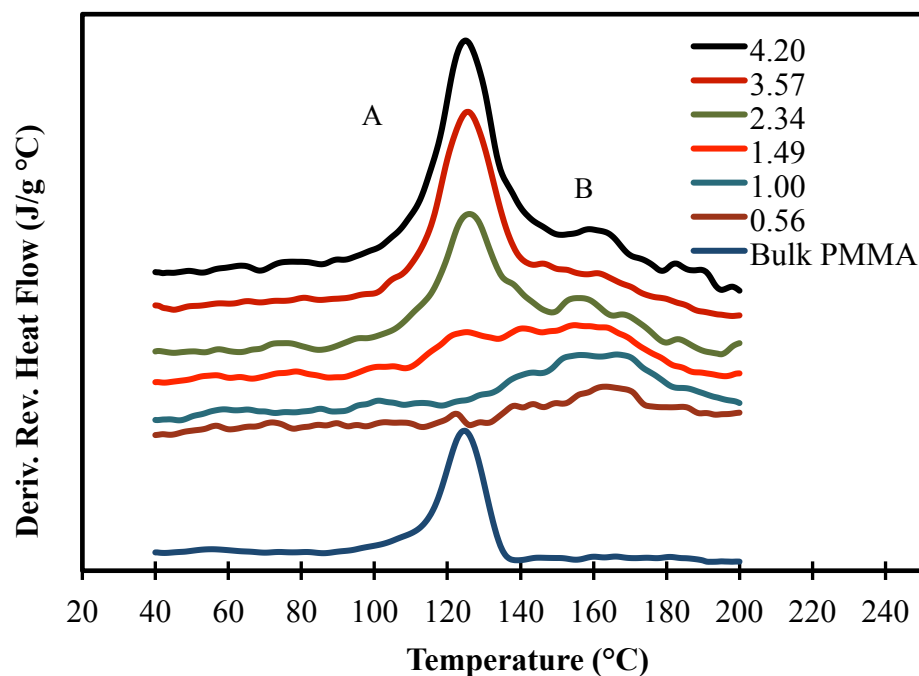
Figure 2. TMDSC thermograms of various adsorbed amounts of PMMA adsorbed on silica. The thermograms are shown in the order presented in the figure legend. The numerical values are the adsorbed amounts, m''_p, expressed in mg of PMMA/m^2 silica. The symbols A and B are used to distinguish two transitions in the thermogram.

The sample with the lowest adsorbed amount, $m''_p = 0.56$ mg/m^2, showed a thermal transition centered around 170 °C. This temperature was 45 °C above the transition for the bulk polymer. For the 1.00 mg/m^2 sample, a greater intensity was found as expected, because there was more adsorbed polymer in that sample. The transition had components at lower temperature, in the 140 to 170 °C range, but these temperatures were still significantly higher than the transition for the bulk polymer. At 1.49 mg/m^2, the intensity of the transition in the higher temperature range increased a little more. The intensity in this high-temperature region was roughly constant for samples with larger adsorbed amounts. The 1.49 mg/m^2 sample was the lowest adsorbed amount sample that

showed intensity in the region of the bulk polymer, i.e., loosely-bound polymer. At larger

adsorbed amounts, the thermograms for the adsorbed polymers showed two distinct peaks

for the loosely-bound component (A) and the tightly-bound component (B). For these

samples, the A transition was not very different from the bulk polymer and B component

was centered at a higher temperature, 161.3 +/- 3.0 °C (SD). The standard deviation was

estimated from the measurements of T_g of all of the PMMA samples with different

adsorbed amounts. The relative area under A transitions increased as the adsorbed

amounts increased, while those of B transitions remained roughly constant.

A plot of the ratios (r) for the areas under the A and B transitions was a linear

function of the total relative mass of polymer (m'_p), obtained by dividing the mass of

polymer with mass of silica)[30] and is shown in Figure 3. Adsorbed amounts over a wide

range of compositions (0.56 - 4.20 mg polymer/m^2 silica) were used. The uncertainties in

the points are roughly the size of the data point symbols. A linear relationship of r versus

adsorbed amount of polymer with positive slope was obtained. As described in eq. 3, the

intercept of the line yields a ratio of the heat capacity increments, $\Delta C_{pA}/\Delta C_{pB}$, and the

slope yields $\Delta C_{pA}/(m'_{pB} \Delta C_{pB})$. Therefore, the amount of tightly-bound polymer can be

readily obtained from a linear regression. The measurements for samples below m'_{pB}

show only one distinct peak at higher temperature (tightly bound), and hence, the r values

are zero. These points are included in 1.3 to show that there is no loosely-bound polymer

in those samples.
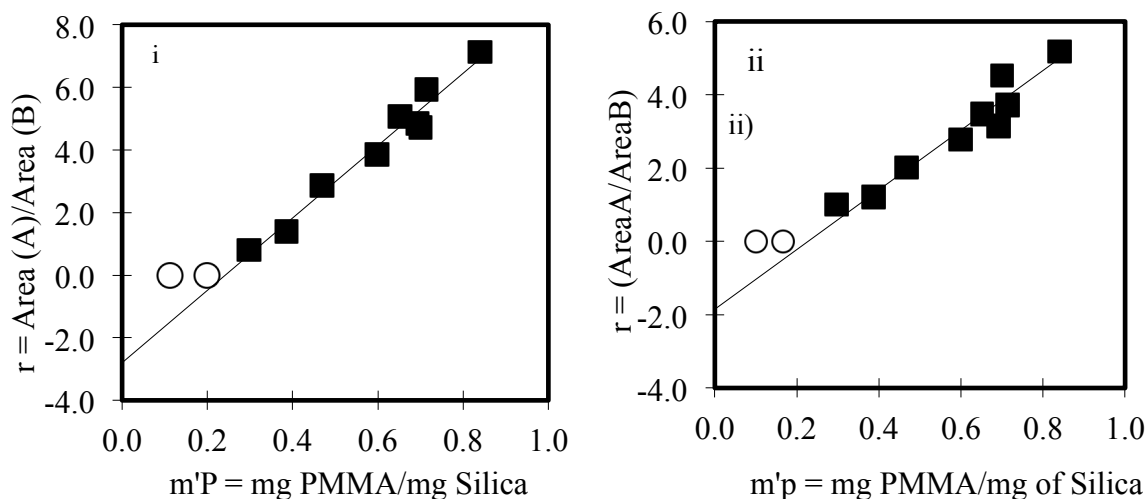
Figure 3. Plots of ratio (*r*) of the areas under transitions A and B, as a function of the adsorbed amounts (mg PMMA/ m^2 silica) for PMMA adsorbed on silica. The areas under the peaks were obtained from fitting the thermograms with i) the GL shape function and ii) with the perpendicular drop method.

Two methods have been used to calculate the area under each peak, fitting curves with Gaussian-Lorentzian (GL) distribution and using the perpendicular drop (PD) method (Thermal Advantage software, TA Instruments, New Castle, DE). The summary of the results obtained from the GL fitting is presented in Table 1.

Table 1. Properties of the peaks A and B obtained from fitting of thermograms with Gaussian-Lorentzian cross (GL) function for different adsorbed amounts.

m''_p (mg/m^2)	Peak Area (J/g °C)			FWHM (°C)		T_g, center (°C)		M	
	a_A x 10^4	a_B x 10^4	a_B/m_{pB} x 10^4	Peak A	Peak B	Peak A	Peak B	Peak A	Peak B

0.56	0	0.59	2.69	N/A	33.3	N/A	160.6	N/A	0.000
1.00	0	1.17	5.78	N/A	41.4	N/A	158.9	N/A	0.000
1.49	0.82	1.01	5.42	24.8	34.7	125.0	156.7	0.998	0.002
1.93	1.45	1.04	5.93	25.5	37.9	124.6	158.0	0.999	0.001
2.34	2.19	0.76	4.61	18.9	30.7	126.0	159.4	0.996	0.001
2.99	2.64	0.69	4.52	19.8	34.4	125.2	157.8	1.000	0.002
3.26	2.81	0.56	3.79	18.2	27.5	125.9	163.9	0.903	0.090
3.46	2.67	0.55	3.85	18.2	33.4	125.9	160.4	0.837	0.082
3.50	3.42	0.73	5.09	16.5	32.4	125.9	162.9	0.950	0.997
3.57	3.00	0.51	3.58	17.4	29.0	125.5	160.5	0.997	0.004
4.20	3.60	0.51	3.84	17.9	20.7	124.9	160.4	0.999	0.744
Bulk PMMA	N/A	N/A	N/A	12.5 $(8.5)^{a}$	N/A	124.0	N/A	0.523	N/A

a. The T_g for the bulk polymer measured without broadening.

The ratio (r) for GL method was calculated from the area under each peak obtained from the fitting as shown in Table 1. Similar results were obtained for the slope and intercepts from both fittings. Least-squares fits of the data with the GL fitting yields a slope of 11.58 +/- 0.74 (S.D) and intercept of -2.81 +/- 0.46 (S.D.). Similarly, for the plot based on the PD method, a slope of 7.78 +/- 0.77 (S.D.) and intercept of -1.62 +/- 0.47 (S.D.) was obtained. The ratios of the intercept to the slope from least-square fits yield the amount of tightly-bound polymer per mass of silica (m'_{pB}). Converting this amount from per mass silica to per m^2 silica surface yields m''_B = 1.21 +/- 0.21 (S.D.) mg/m^2 and 1.19 +/- 0.33 (S.D.) mg/m^2 from fitting the thermograms with the GL and PD,

respectively. The intercept of the plot yields the ratio $\Delta C_{pA}/\Delta C_{pB}$, found to be 2.81 +/- 0.46 (S.D.) and 1.62 +/- 0.47 (S.D.) for GL and PD, respectively.

It is useful to consider the intensities of the transitions for the bound polymers (a_B) divided by the mass of bound polymer, m_{pB}, or a_B/m_{pB}. Since the TMDSC measurements were obtained per total mass of sample (m), the measured quantity was proportional to the transition intensity per mass of sample or a_B/m_{pB}. To convert this ratio from the measured quantity (a_B/m) based on the mass of the sample to the mass of bound polymer, a multiplicative factor, proportional to the ratio of the mass of bound polymer to the total mass may be used. In our case, this can be done in terms of the adsorbed amount of polymer (m''_p in mass polymer/m^2 silica) and the value of m''_B derived from the model. Since both of these values were per m^2 silica, the ratio can be made on this basis with the conversion of surface area to mass of silica using the specific surface area (SSA, 200 m^2/g in this case). The resulting formula is:

$$\frac{a_B}{m_{PB}} = (\frac{a_B}{m})(\frac{1 + m''_P \times SSA}{m''_B \times SSA}) \tag{3.6}$$

In Table 1, the values of a_B/m_{pB} are relatively constant with the exception of the 0.56 mg/m^2 sample which does not have any loosely-bound polymer and its intensity was about half of that of the 1.00 mg/m^2 sample.

Fitting of the peaks with GL shape function allowed us to measure other parameters that are characteristics of the peaks. The full width at half maximum (FWHM), an important parameter that is used to signify the broadness of the peak, was found to be 8.5 °C without broadening and 12.5 °C with broadening for the bulk polymer. For adsorbed polymer, FWHM was found to be 19.7 +/- 3.2 °C (S.D.) and 32.3 +/- 5.5 °C (S.D.) for peaks A (loosely bound) and peak B (tightly bound), respectively. The standard

deviation was estimated from the values of the FWHM of all of the polymer samples with different adsorbed amounts. The FWHM for the bulk polymer was narrower than either the loosely-bound or tightly-bound polymer. The broadening of T_g was particularly evident when polymer was adsorbed on surface. The center of the peaks, which can also be assigned as the T_g, for loosely bound and tightly bound polymer were 125.4 +/- 0.5 (S.D.) and 160.0 +/- 2.1 (S.D.), respectively. The mixing ratio, which takes the value of 0 for a pure Gaussian function and 1 for pure Lorentzian function, is also shown in Table 1 for each sample. Generally, the nature of peak A was more like Lorentzian than Gaussian. The opposite was true for peak B.

For samples at adsorbed amounts below m''_B (taken as 1.21 mg/m^2), the entire polymer was tightly-bound. For samples above m_B the fraction of tightly-bound polymer was calculated using equation 4 (r.h.s.) for each sample. The smooth curve was drawn from the model with $m''_B = 1.21$ (equation 4, l.h.s.). The results of the data and curve are shown in Figure 4. The bound fraction decreased smoothly with increased adsorbed amount. For comparison, the data for the bound fractions of the same polymer on silica from FTIR are also shown.[33]
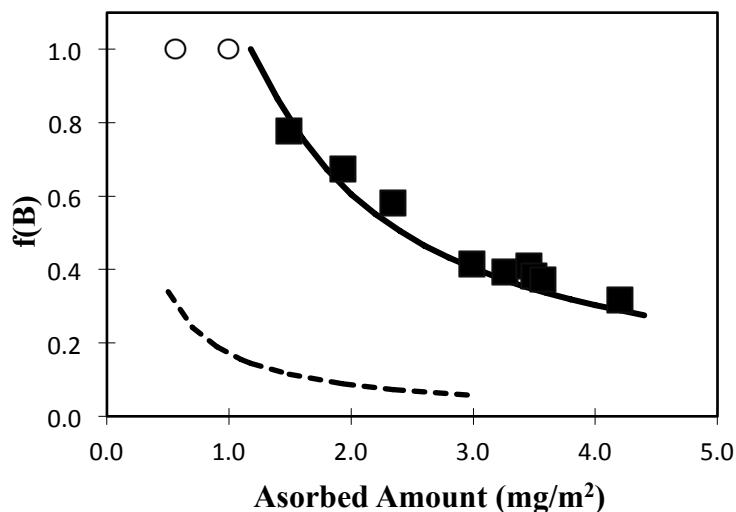
Figure 4. The tightly-bound fraction of PMMA on silica as a function of the adsorbed amount for samples with adsorbed amounts greater than (filled squares) and less than (open circles) m''_B. The smooth curve is based on the model with fixed amount of tightly bound polymer of $m''_B = 1.21$ mg/m^2. Shown for comparison are the composite of results for PMMA of different molecular masses and solvents from FTIR.[33]

3.6. DISCUSSION

Two distinct peaks were found in the MDSC curves and were labeled A and B. The much higher sensitivity of the instrument used in this study allowed them to be clearly observed. In previous measurements,[30] two peaks were also observed in the thermograms, but they were difficult to distinguish and consequently, it was very difficult to integrate each peak with accuracy or determine where some of the peaks started and stopped. Since transition A was at a temperature similar to, but slightly higher than that for the transition of the bulk polymer, it can be identified with "loosely-bound" polymer. For very small amounts of adsorbed polymer, there was no loosely-bound polymer, as can be seen in the thermograms for samples of less than m''_B (1.21 mg/m^2) PMMA on

55

silica as in Figure 2. This loosely-bound material becomes evident at larger adsorbed amounts and its nature was more like that of the bulk polymer, for example, as in the 4.2 mg/m^2 sample of PMMA on silica in 1.2.

The transition B was found at a temperature that was significantly higher than that for the loosely-bound polymer, indicative of lower mobility polymer. It was referred to as "tightly-bound polymer". This elevated transition for tightly-bound polymer was reported in studies for polymers adsorbed on surfaces, but only when there was a strong interaction between the polymer and substrate.[28,30,34,35] Such an attraction can come from a specific interaction, such as hydrogen bonding between the polymer and a solid surface and this interaction exists in the PMMA/silica system. Tightly-bound polymer does not, for example, occur with weak interactions such as those as in polystyrene/silica.[29] The width of the transition for tightly-bound polymer was significantly broader than both loosely-bound and bulk polymer. The broadening of the T_g is an important characteristic of a multi-component material, such as adsorbed polymer, and is due to a loss in the cooperative large-amplitude motions.[25] The presence of a strong interaction between the polymer and the substrate, such as H-bonding on the surface has been demonstrated with FTIR on the carbonyl peak of PMMA on silica.[23,36,37] The stretching frequency of the bound carbonyls was shifted to lower frequency when PMMA was adsorbed on silica. This shift to lower frequency was due to the interaction of polymer carbonyl with surface hydroxyl group and, hence, weakening the bond.[1]

The amount of tightly-bound polymer (m_{pB}) and the corresponding thicknesses (based on the bulk densities) of the polymer adsorbed on silica were calculated based on the slope and intercept obtained from linear fit. The amounts of tightly-bound polymer

from both analysis methods (GL and PD methods) yielded similar results. The error estimates from the GL fitting were distinctly less than those from the PD method. In addition, they also allow a less arbitrary start/stop of the two transitions, which means a more reasonable estimate of the widths of the different transitions. For this reason, we have chosen to base the reported values on the GL analysis. The amount of 1.21 +/- 0.21 mg/m^2 was obtained for the tightly-bound polymer. Using the density of the bulk polymer, this adsorbed amount corresponds about 1 nm of PMMA that is tightly-bound. These results were consistent with earlier results.[30] The data to test the model, in this work, was extended to half as much at the lower end and twice as much at the higher end as in the previous work.

The ratio $\Delta C_{pA}/\Delta C_{pB}$ was also estimated from the intercept from linear fit model. The ratio of 2.81+/- 0.46 (S.D.) from GL analysis suggest that previous measurements overestimated this value by a factor of almost 2 times larger than this measurement.[30] The reason for this discrepancy is may be the sigmoidal base line that was used to calculate the area under each peak of TMDSC thermograms in the previous work. Differences in the estimation of the amount of tightly-bound polymer and ratio $\Delta C_{pA}/\Delta C_{pB}$ was observed in similar measurements done by using different methods of integrating the peaks.[38] Nevertheless, the quantity ΔC_{pB} is definitely less than that of ΔC_{pA}. This is consistent with the notion that the restriction in the mobility of polymer segments on surface limits the freedom of the polymer above glass transition temperature. In other words, mobility of the tightly-bound polymer on the surface above glass transition temperature was reduced compared to the bulk polymer.

The bound fractions, based on fixed amounts of tightly-bound polymer as shown in Figure 4, ranged from 1 to 0.30 as a function of adsorbed amount over the concentration range (1.0 to 4.2 mg/m^2) studied. Fontana and Thomas first reported the bound fraction estimation for poly(alkyl methacrylate) on silica using IR spectroscopy. They obtained values of bound fractions from 0.3 to 0.4 for adsorbed poly(lauryl methacrylate) on silica in organic solvents.[22] Similar results were obtained when poly(ethylene ortho-phthalate) was adsorbed on silica in CCl$_4$ based on ellipsometric measurements.[39] Results from ESR (which are similar to NMR[1,18]) measurements were, however, higher than (in the range of 1 to 0.5) from IR over a similar range of concentrations, consistent with the notion that the estimation of bound fraction depends on different experimental technique used.[24,30] NMR and ESR techniques are not only sensitive to the segments that are directly bound, but also the segments that are a few Ångstroms from surface.[33] In contrast, shifts in carbonyl frequencies in IR spectrum are only sensitive to segments that are directly attached to the surface,[1,24,33] resulting lower estimates of bound fractions. It is obvious that our present results resemble NMR and ESR results in terms of the bound fractions. In a sense, the DSC measurements are more like those from NMR and ESR.

Previously, ^{2}H NMR studies on adsorbed poly(methyl acrylate) and poly(vinyl acetate) on silica reported that the segmental mobility of the polymer on surface was spatially heterogeneous with respect to the segment position.[19,40] The segments near the polymer-air interface were more mobile (lower T_g) than those in the bulk polymer while the segments that were close to the silica surface were less mobile (higher T_g). This notion was verified by studies done on a system where unlabeled polymer was placed on

the top of labeled polymer, causing the regions of high mobility to disappear.[41] One might expect that such behavior should be observed in the TMDSC measurements as well. Clearly, an increased T_g of as much as 35-45 °C was easily observed here and the amount of the tightly-bound polymer seemed to level off after $m''_B = 1.21$ mg/m^2, consistent with NMR studies on similar systems. On the other hand, the regions of high mobility (for example, those at the polymer/air interface) are difficult to distinguish with TMDSC. The small amount of this material and its proximity to the bulk-like polymer glass transition makes this small amount of thermal activity difficult to determine, even at our level of sensitivity. In this case, the NMR experiment is a more sensitive technique in the glass transition region and the two experiments are complementary and consistent. The results from both TMDSC and NMR suggest that the broadening of glass transition temperature is evident when there is a strong interaction between polymer and surface.

3.7. CONCLUSIONS

This work has extended previous studies to provide more accurate measurements for materials with small amount of PMMA adsorbed on silica. These measurements, with greater sensitivity, more advanced data analyses, and taken over a wider range of compositions, provide a real opportunity to better understand the behavior of adsorbed PMMA. A simple two-component model was used to estimate the amount of tightly bound polymer, which was found to be constant after m''_B of 1.21 mg/m^2 and have a T_g of as much as 35-45 °C higher than bulk PMMA. The use of the Gaussian-Lorentzian model fit the data better than that of the perpendicular drop method. The model also predicted a change in heat capacity ratio in the glass transition region for the loosely-bound and

tightly bound polymer or $\Delta C_{pA}/\Delta C_{pB} \sim 3.0$. This value is significantly lower than previously estimated. It is indicative of the tightly-bound polymer being less mobile than bulk polymer in the glass transition region.

3.8. REFERENCES

(1) Fleer, G. J.; Cohen-Stuart, M. A.; Scheutjens, J. M. H. M.; Cosgrove, T.; Vincent, B. *Polymers at Interfaces;* Chapman & Hall: London, **1993**.

(2) Feast, W. J.; Munro, H. S. *Polymer Surfaces and Interfaces;* Wiley: Chichester; New York, **1987**.

(3) Lin, E. K.; Kolb, R.; Satija, S. K.; Wu, W.-l. *Macromolecules* **1999**, *32*, 3753-3757.

(4) Fukao, K.; Miyamoto, Y. *Europhys. Lett.* **1999**, *46*, 649-654.

(5) Fryer, D. S.; Nealey, P. F.; de Pablo, J. J. *Macromolecules* **2000**, *33*, 6439-6447.

(6) Keddie, J. L.; Jones, R. A. L.; Cory, R. A. *Europhys. Lett.* **1994**, *27*, 59-64.

(7) Singh, L.; Ludovice, P. J.; Henderson, C. L. *Thin Solid Films* **2004**, *449*, 231-241.

(8) Keddie, J. L.; Jones, R. A. L.; Cory, R. A. *Faraday Discuss.* **1994**, *98*, 219-230.

(9) Grohens, Y.; Hamon, L.; Reiter, G.; Soldera, A.; Holl, Y. *Eur. Phys. J. E* **2002**, *8*, 217-224.

(10) Gregory, J. *Polym. Int.* **1995**, *36*, 102-102.

(11) Grohens, Y.; Brogly, M.; Labbe, C.; David, M.-O.; Schultz, J. *Langmuir* **1998**, *14*, 2929-2932.

(12) Wu, W. L.; Orts, W. J.; Vanzanten, J. H.; Fanconi, B. M. *J. Polym. Sci. Pt. B-Polym. Phys.* **1994**, *32*, 2475-2480.

(13) Wu, W. L.; Vanzanten, J. H.; Orts, W. J. *Macromolecules* **1995**, *28*, 771-774.

(14) Orts, W. J.; Vanzanten, J. H.; Wu, W. L.; Satija, S. K. *Phys. Rev. Lett.* **1993**, *71*, 867-870.

(15) Reiter, G. *Macromolecules* **1994**, *27*, 3046-3052.

(16) Jean, Y. C.; Zhang, R.; Cao, H.; Yuan, J.-P.; Huang, C.-M.; Nielsen, B.; Asoka-Kumar, P. *Phys. Rev. B* **1997**, *56*, R8459-R8462.

(17) DeMaggio, G. B.; Frieze, W. E.; Gidley, D. W.; Zhu, M.; Hristov, H. A.; Yee, A. F. *Phys. Rev. Lett.* **1997**, *78*, 1524-1527.

(18) Barnett, K. G.; Cosgrove, T.; Vincent, B.; Cohen-Stuart, M.; Sissons, D. S. *Macromolecules* **1981**, *14*, 1018-1020.

(19) Blum, F. D.; Xu, G.; Liang, M.; Wade, C. G. *Macromolecules* **1996**, *29*, 8740-8745.

(20) Hommel, H. *Adv. Colloid Interface Sci.* **2008**, *141*, 1-23.

(21) Afif, A.; Hommel, H.; Legrand, A. P. *Colloids Surf., A* **1996**, *111*, 177-184.

(22) Fontana, B. J.; Thomas, J. R. *J. Phys. Chem.* **1961**, *65*, 480-487.

(23) Kulkeratiyut, S.; Kulkeratiyut, S.; Blum, F. D. *J. Polym. Sci. Pt. B-Polym. Phys.* **2006**, *44*, 2071-2078.

(24) Blum, F. D.; Krisanangkura, P. *Thermochim. Acta* **2009**, *492*, 55-60.

(25) Wunderlich, B. *Thermal analysis of polymeric materials;* Springer: Berlin; New York, **2005**.

(26) Gill, P. S.; Sauerbrunn, S. R.; Reading, M. *J. Therm. Anal.* **1993**, *40*, 931-939.

(27) Simon, S. L. *Thermochim. Acta* **2001**, *374*, 55-71.

(28) Porter, C. E.; Blum, F. D. *Macromolecules* **2000**, *33*, 7016-7020.

(29) Porter, C. E.; Blum, F. D. *Macromolecules* **2002**, *35*, 7448-7452.

(30) Blum, F. D.; Young, E. N.; Smith, G.; Sitton, O. C. *Langmuir* **2006**, *22*, 4741-4744.

(31) Kabomo, M. T.; Blum, F. D.; Kulkeratiyut, S.; Kulkeratiyut, S.; Krisanangkura, P. *J. Polym. Sci. B: Polym. Phys.* **2008**, *46*, 649-658.

(32) Kojima, I.; Kurahashi, M. *J. Electron Spectrosc. Relat. Phenom.* **1987**, *42*, 177-181.

(33) Krisanangkura, P.; Packard, A. M.; Burgher, J.; Blum, F. D. *J. Polym. Sci. B: Polym. Phys.* **2010**, *48*, 1911-1918.

(34) Priestley, R. D.; Ellison, C. J.; Broadbelt, L. J.; Torkelson, J. M. *Science* **2005**, *309*, 456-459.

(35) Madathingal, R. R.; Wunder, S. L. *Langmuir* **2010**, *26*, 5077-5087.

(36) Sakai, H.; Imamura, Y. *Bull. Chem. Soc. Jpn.* **1980**, *53*, 1749-50.

(37) Frantz, P.; Granick, S. *Macromolecules* **1995**, *28*, 6915-6925.

(38) Hetayothin, B.; Blum, F. D. Effect of structure and plasticizer on the glass transition of adsorbed polymer. Ph.D. thesis, Missouri University of Science and Technology, **2010**.

(39) Peyser, P.; Tutas, D. J.; Stromberg, R. R. *J. Polym. Sci. A: Polym. Chem.* **1967**, *5*, 651-663.

(40) Metin, B.; Blum, F. D. *Langmuir* **2009**, *26*, 5226-5231.

(41) Lin, W.-Y.; Blum, F. D. *J. Am. Chem. Soc.* **2001**, *123*, 2032-2037.

CHAPTER 4

HEAT CAPACITIES OF ADSORBED POLY(METHYL METHACRYLATE) ON

SILICA[*]

4.1. ABSTRACT

The heat capacities of samples made from very small amounts of poly(methyl

methacrylate) adsorbed onto high surface-area silica (Cab-O-Sil) were measured using

temperature-modulated differential scanning calorimetry (TMDSC) using a quasi-

isothermal method. The composition-dependent heat capacities of the adsorbed samples

were markedly less than those predicted from a simple mixture model below (glassy),

above (rubbery) and near the glass transition (T_g) of the bulk polymer. A two-state model,

comprised of tightly- and loosely-bound polymer (bound segment model), was

successfully used to interpret the data and the heat capacities of the tightly-bound

polymer were found to be 70-80% (glassy region) and 70-94% (rubbery region) of that of

the bulk polymer. The amount of tightly-bound polymer was estimated to be about 1.2

mg/m^2 for both the glassy and rubbery regions, consistent with heat flow measurements.

More detailed models with exponential dependencies of the heat capacity, and either zero

and non-zero intercepts were also used to fit the experimental data.

[*]Bal K. Khatiwada and Frank D. Blum
Department of Chemistry, Oklahoma State University, Stillwater, OK, 74078, United
States

A *transitional model*, with a non-zero heat capacity for the first amount of polymer adsorbed was the most useful for fitting the data for the polymer alone on the surface. This model allowed, for the first time, an estimate of the heat capacity of the initial polymer adsorbed. The fractional heat capacity of the initially adsorbed polymer, relative to bulk, increased with temperature from 0.3 (well below) to 0.8 (well above the bulk T_g). It was also possible to estimate the exponential dependence of the development from the initial heat capacities to the bulk heat capacity as 0.42 to 0.56 mg/m^2, suggesting a distance scale consistent with the notion of a tightly-bound amount.

4.2. INTRODUCTION

When two or more than two different types of materials are brought together, the properties of the resulting mixtures can be additive or be very different from the weighted sum of their properties. The properties of the mixture are additive when neither component affects the properties of the other. However, mixing of materials together often changes the properties of one or both of them, especially when interfacial interactions exist, like van der Waals, H-bonding or ionic interactions. Such interactions are crucial in a variety of applications, especially when those applications are based on interfacial properties.[1] Many studies have been conducted with the aim of understanding the properties of interfacial materials, especially on the nanoscale range, with a variety of solid substrates and polymers.[1-8] The increased interest in such nanoscale materials is because of the dramatic improvements in properties possible due to differences in the components. For example, interfacial polymers will likely have properties that are different than those of bulk polymers. In the present work, we explore one aspect of the

changes in interfacial properties associated with adsorption of poly(methyl methacrylate)

(PMMA) on a silica surface, namely, the heat capacity of very small amounts of adsorbed

polymer.

A variety of experimental techniques such as ellipsometry,[9] dielectric

relaxation,[10,11] dielectric spectroscopy,[12,13] x-ray reflectivity measurements,[14]

adhesion,[15] and calorimetric measurements[6,16,17] have been used to study the structure

and dynamics of the interfacial polymers. A key property that was extensively studied

was the glass transition temperature, T_g, and its dependence on film thickness. It has been

found that the glass transition temperature of the absorbed polymers could decrease,

increase or not change compared to the bulk polymer. Sometimes these experimental

results were not definitive regarding the mechanism and dynamics of polymer chains near

the interface. However, there are many experimental results suggesting that the restriction

of mobility caused by attractive interactions of the interface, which does not affect the

entire material, but remains within a few nanometers from surfaces.[3] The existence of

such an interfacial layer was shown by many techniques.[3,18-20] In some cases, the

interfacial layer appeared to be totally immobilized,[17,19,21,22] while in others, a second

glass transition temperature or at least a shoulder at higher temperature in calorimetric

measurement were seen.[16,23] Fourier transform infrared spectroscopy (FTIR) studies on

the adsorbed poly(methyl methacrylate) (PMMA) on a silica surface have demonstrated

the presence of bound carbonyls on the surface of silica.[24-28] Studies of the glass

transition temperature (T_g) of PMMA on silica (DSC measurements) have reported the

presence of second glass transition at higher temperature for small-adsorbed amounts of

polymer.[6,16] The existence of such an interfacial layer for PMMA/silica system was confirmed by a variety of other techniques.[6,28-30]

Heat capacity measurement techniques are extremely useful for studying the behavior of polymers[31] and their blends[32]. In some studies, this technique was used to measure the T_g[33] (in amorphous polymers) while others measured degrees of crystallinity,[34] super cooling,[35] etc. (in crystalline and semi crystalline polymers). Heat capacity measurements can also be used to study the segmental heterogeneity in miscible polymer blends.[32,36] For example, Righitti et al. estimated the rigid amorphous fraction in semi-crystalline polymers.[37] Di Lorenzo et al. studied the devitrification of rigid amorphous fraction in semi-crystalline polymer like poly(ethylene terephthalate).[38] In some respects adsorbed polymers are similar to semi-crystalline polymers, where crystals below their melting temperatures behave like substrates and the polymer segments near them are similar to surface-bound polymers. In some areas of research, such as in filled polymers, the terms tightly and loosely-bound polymer has been used[39] in contrast to rigid amorphous fraction.

In this work, measurements of the heat capacities of very small amounts of adsorbed PMMA on silica have been made. These measurements have allowed an understanding of the changes associated with the interaction of the polymer and the substrate. A slow heating technique (quasi-isothermal method) has been used to measure the heat capacities of the silica, the polymer and the surface adsorbed samples. In normal differential scanning calorimetry, the heating rate of the system may affect the heat capacity measurement of the sample. This may be especially true for our samples with small amounts of adsorbed polymers. The faster the heating rate, the greater the

temperature difference between sample and the set point temperature of the instrument can be, and consequently, the greater the chance of deviation in the measurement of the heat flow at different temperatures. In the quasi-isothermal procedure, slow heating rates minimize the temperature lags and hence, enhances the sensitivity and precision of heat capacity measurements.[40]

4.3. EXPERIMENTAL

High molecular mass PMMA with M_w of 4.5×10^5 g/mol (Aldrich Chemical Co., Milwaukee, WI) and Cab-O-Sil M-5P (Cabot Corporation, Tuscola, IL) silica with specific surface area of 200 m^2/g were used as received. Different amounts of PMMA (from 30 to 300 mg) were dissolved in 7 ml of toluene in test tubes. Silica (Cab-O-Sil, 300 mg) was wetted with 3 ml of toluene and then added to the polymer solutions.

The adsorption of the polymer was achieved by shaking the mixtures in sample tubes in a mechanical shaker for 2 days. The samples were then dried by bubbling air through the tip of a Pasteur pipette at the bottom of the tube. The air-dried samples were put under vacuum at 60 °C for 2 days to remove any residual solvent. Portions of samples from different positions in the dried materials were then collected. Samples dried in this way were found to vary in composition by less than 4% between the top, middle and lower portions for higher adsorbed amounts (for more than 3 mg polymer/m^2 silica) and less than 2% for lower adsorbed amounts (for less than 3 mg polymer/m^2 silica). The compositions (amount of adsorbed polymer on surface) were determined using a TA Instruments (New Castle De, USA) Model 2950 Thermogravimetric Analysis (TGA) instrument. The samples were heated from 40 – 600 °C at a heating rate of 10 °C/min.

Air was used as a purge gas with flow rate of 50 mL/min. The accuracy and the validity of the method were verified with degradation of bulk PMMA, bulk silica, and PMMA/silica mixtures. The residual material contained only silica and the adsorbed amounts of polymer on silica were calculated based on the masses of PMMA and silica, and the specific surface area of the silica.

The heat capacities of the polymer, silica, and the surface samples were measured using the quasi-isothermal temperature modulated differential scanning calorimetry (TMDSC) technique with a Q2000 DSC (TA Instruments). The samples were first annealed at 140 °C for 20 min, cooled to 40 °C with a ramp rate of 20 °C/min, to ensure that the samples had similar thermal histories. After TMDSC runs, the samples were re-weighted to determine the mass of any solvent remaining in the sample. Typically, around 0.5 to 1% mass loss was found after annealing. Samples used for heat capacity measurements were later subjected to TGA analysis for accurate determination of the composition of each sample. The heat capacity was measured every 10 degrees with the system kept isothermal for 10 min before each heat capacity measurement. A sinusoidal modulation of amplitude 1 °C with a period of 120 s was used to measure the heat capacities of all of the samples. The sample pans were referenced against an empty pan. A baseline calibration was performed through the heating of empty cells. Temperature and heat capacity calibrations were performed with indium and sapphire, respectively. Since the silica particles, including many of those with adsorbed polymers, were very light, fluffy and did not have good thermal conductivity, their heat capacities were measured after pressing the sample into pellets in an FTIR pellet press. FTIR measurements were made on the pellets to test if compressing of the samples caused any

apparent deformation of the polymer on surface. The resulting FTIR spectra in the

carbonyl and surface hydroxyl regions looked very similar to the measurements done on

salt plates (sample was put in between two NaCl salt plates) even though there was a

small amount of light scattered from the pellets. The pressure applied to make the DSC

pellets (less than 70000 kPa or 10000 PSI) was much less than that used for making FTIR

pellets (more than 350,000 kPa or 50,000 PSI).

4.4. MODELING OF HEAT CAPACITIES OF INTERFACIAL MATERIALS

For adsorbed polymers, the heat capacities measured were a function of the

amount and nature of each component. A simple model is a mixture model, where the

heat capacity of the adsorbed sample is a simple mass-weighted superposition of the heat

capacities of polymer and silica. The hypothesis in this model is effectively an

assumption that polymer and silica behave independently when the polymer is adsorbed.

The predicted heat capacity for the sample is:

$$C_{P(composite)}(T) = C_{PP}(T)M_P + C_{PS}(T)M_S$$

$$(4.1)$$

where C_{PP} and C_{PS} are the specific heat capacities (in J/g °C) of the pure polymer (p) and

silica (s) and M's are their mass fractions. It is reasonable to assume that the heat capacity

of the silica did not vary with added polymer; however, it is likely that the properties of

the polymer were affected by the silica.

An example of the dependence of the heat capacities on composition (mass

fraction of polymer) for some adsorbed samples is shown in Figure 1 for the

PMMA/silica system at 120 °C. The purpose of this plot is to illustrate how varying

compositions (silica vs PMMA) contribute to the prediction of the mixture model and to

demonstrate that the mixture model has the right shape, but does not adequately describe the data. It is obvious from Figure 1 that the general shape of the model (top line) is dictated by the differing heat capacities of the two components, with the PMMA having a larger heat capacity than the silica. It is also obvious that the experimental data falls below the prediction from the mixture model. We propose that this difference is caused by the alteration of the heat capacity of the polymer due to the presence of the silica and its interaction with the polymer.
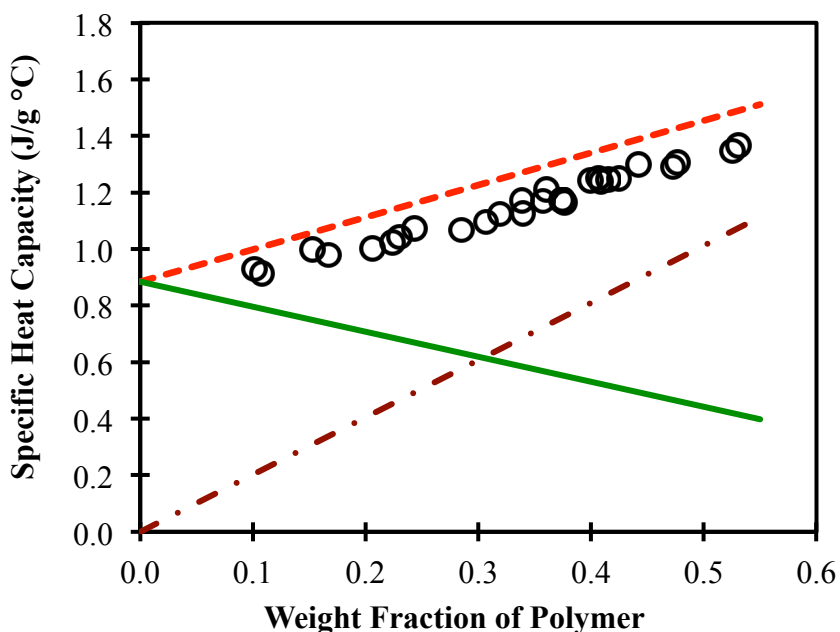

Figure 1. Heat capacities for PMMA adsorbed on silica at 120 °C as a function of weight fraction of polymer. The prediction from the simple mixture model (top, dashed line) is shown along with the contributions from the silica (solid line, decreasing with weight fraction of polymer) and polymer (dot-dashed line, increasing with weight fraction of polymer).

The adsorption of a polymer on a silica surface should result in a restriction of the mobility of some of the segments at the polymer silica interface, if an attractive interaction occurs. In this respect, adsorbed polymers can be considered to be similar to semi-crystalline polymers, where the crystalline domains reduce the mobility of neighboring amorphous segments. Chen and Cebe[34] applied a three-state model in which the heat capacity of a semi-crystalline polymer, just above the glass transition temperature, was given by the heat capacity of solid crystal, rigid amorphous polymer and rubbery polymer.

Since a simple mixture model clearly does not fit the data for our adsorbed polymer systems, a more appropriate model, taking the interface into consideration has been explored. It is a two-state polymer model; in which the polymer is divided into two components, a tightly-bound polymer, with reduced heat capacity (denoted by C'_{PP}), and a loosely-bound polymer, with a heat capacity similar to bulk (denoted by C_{PP}). Since the tightly-bound polymer would be associated with the silica surface, some modification to ultimately account for the surface area of the substrate must be made. An appropriate way to do this is to consider the behavior of the polymers to be scaled based on the adsorbed amount, AA (in mg polymer/m^2 surface). In effect, there is a certain amount of adsorbed polymer, m_B'' (in mg polymer/m^2 surface) which has its properties altered by the substrate interface. This polymer has a reduced heat capacity of $C_{PP}f$, where f represents the fractional of the heat capacity of the tightly-bound polymer. When the adsorbed amount, AA is greater than m_B'' ($AA > m_B''$), the heat capacity of the composite is given by the contributions of the loosely-bound (bulk-like, first term) polymer, tightly-bound polymer (second term) and silica (third term) of the sum, or:

$$C_{P(composite)}(T) = C_{PP}M_P \frac{(AA - m_B^{''})}{AA} + C_{PP}fM_P \frac{m_B^{''}}{AA} + M_S C_{PS} \qquad (4.2)$$

When the amount of polymer is less than the full amount of tightly-bound polymer, $AA \leq m_B^{''}$, equation 2 becomes:

$$C_{P(composite)}(T) = C_{PP}fM_P + C_{PS}M_S \qquad (4.3)$$

In this model, $m_B^{''}$ and f are parameters which can be fit to the data.

If one assumes that the heat capacity of the silica is unaffected in the adsorbed samples, its contribution may be subtracted from the heat capacity of the adsorbed samples. This deconvolution can expose the behavior of polymer alone. In addition, for the polymer alone, a monomorphic model for the tightly-bound polymer is unrealistic, as shown in Figure 1. If the data is sufficiently precise, a layered model might better mimic the adsorbed polymer. A simple form is an exponential dependence of the heat capacity on the adsorbed amount or:

$$C_P = \frac{\int_0^{AA} [C_{PP}(1 - \exp^{-\frac{AA'}{a}})dAA']}{AA} = \frac{[AA + a(\exp^{-\frac{AA}{a}} - 1)]C_{PP}}{AA} \qquad (4.4)$$

where C_P represents the heat capacity of just the polymer in the sample (the silica contribution is subtracted out) and a describes the length scale of the transition of the polymer as its heat capacity becomes bulk-like. The implication of this model is that the polymer nearest to the surface has zero heat capacity and exponentially increases to its bulk value. If the initial polymer adsorbed lies very flat on the surface, this may reasonably approximate the situation, however, it is unlikely that the polymer configurations on the surface would be very flat.[41] In contrast, the initial polymer

adsorbed may have more of a random coil configuration.[41,42] Then, the heat capacity of isolated, adsorbed polymers should be non-zero.

One way to account for a non-zero heat capacity for isolated polymers is through a modified exponential model with a non-zero heat capacity (intercept) for very small amounts of adsorbed polymer. We refer to this model is referred to as *transitional model* where the heat capacity transitions from an initial value for the close-in polymer segments to bulk with an exponential dependence. The resulting heat capacity is given by:

$$C_P = \frac{[\int_0^{AA} \{C'_P(1 - \exp^{-\frac{AA'}{a}}) dAA'\} + AA \times C_{PP}f]}{AA}$$

$$= \frac{[\{AA + a(\exp^{-\frac{AA}{a}} - 1)\}C'_P + AA \times C_{PP}f]}{AA} \tag{4.5}$$

where we have chosen to formulate the C_p in terms of $C_{PP}f$, the heat capacity of the initial polymer on the surface given by some fraction of the bulk heat capacity and C'_P which is the incremental heat capacity. In this formulation, $C_{PP}(\text{bulk}) = C_{PP}f + C'_P$. The parameters in this model are a and f.

The best fits of the heat capacity data to these models were done by iteration in which the sum of the squares of residuals were minimized by changing the parameters using statistical analysis system (SAS) software (SAS Institute Inc., Cary, NC, USA). The uncertainties in the parameters were estimated by varying each parameter independently from the set of best fit values until the best fit data points are increased or decreased by 1.96×S.D, which represents a 95% confidence interval. The S.D.

corresponds to the standard deviation of the residuals. The uncertainties in the parameters were determined by using SAS software.

4.5. RESULTS

The amounts of polymer adsorbed on the different samples were determined from the mass losses from TGA measurements and are shown in Figure 2. Bulk silica and bulk polymer were used to verify the validity of the measurements in the extremes of the composition range. Over the temperature range studied (40 – 700 °C), all of the PMMA degraded, while silica had very little mass loss (less than 0.5%), mainly from adsorbed water molecules. From the derivative curves (Fig. 4b), a two-step degradation was observed for the bulk PMMA, while adsorbed samples had a single-step degradation. The major degradation for adsorbed samples started at higher temperatures (around 360 °C) and increased as the amount of adsorbed polymer decreased (around 390 °C) for the two polymers with the smallest adsorbed amounts reported in Figure 2b.
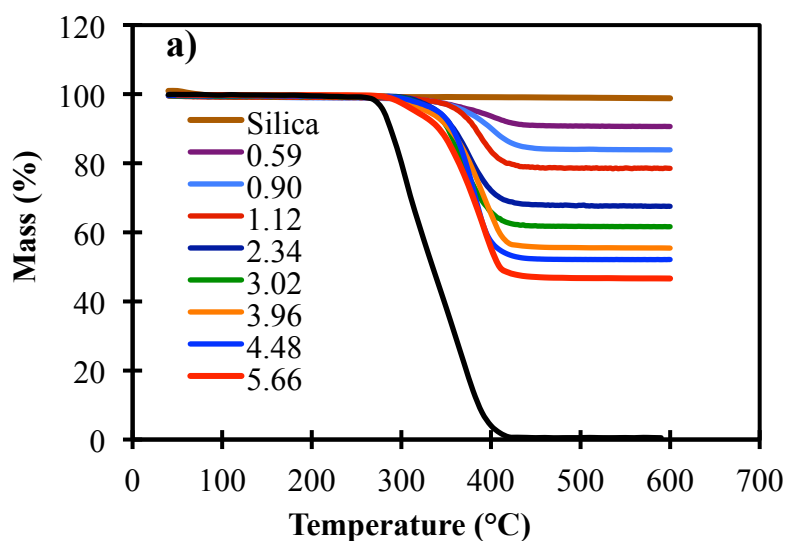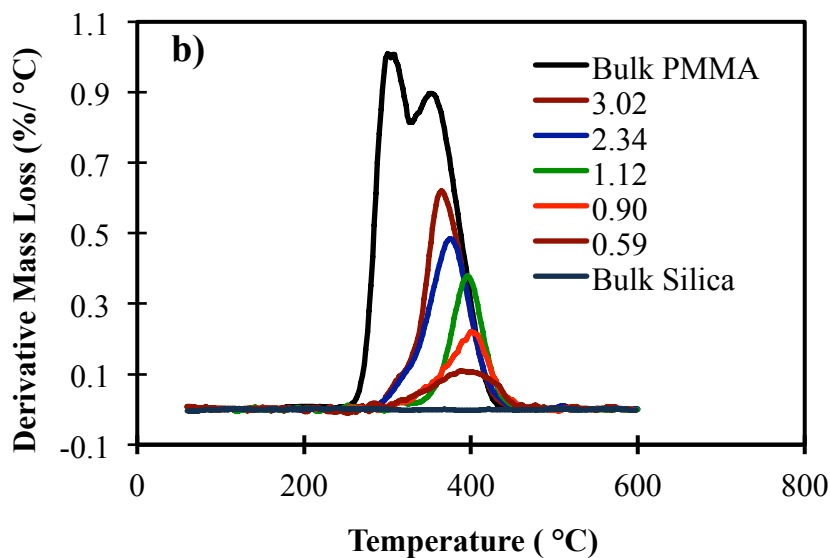
Figure 2. Mass loss of silica, PMMA on silica and PMMA as a function of the adsorbed amount of polymer plotted in a) weight-loss mode and b) derivative mode to see the structure more clearly. The curves are in the order as shown in the legends.

The TMDSC thermograms for bulk PMMA and some of the samples with different adsorbed amounts on silica are shown in Figure 3. The thermograms for different adsorbed amounts were shifted vertically so that each transition can be seen clearly. The intensity of the bulk polymer was reduced to fit with the other thermograms. To reduce the noise, a 15 °C smoothing was done for all samples. The glass transition temperature (T_g) for bulk PMMA was centered around 125 °C (at a TMDSC ramp rate of 3.0 °C/min), consistent with previous studies.[16] For the sample with lowest adsorbed amount, $AA = 0.41$ mg/m^2, the glass transition peak was very weak and difficult to discern, although it was consistent with a very broad transition, ranging from 100 °C to 190 °C. This sample represents the limit of our ability to measure the thermal behavior for this type of sample. When the amount of adsorbed polymer was increased to 0.59

mg/m^2, a single transition was observed at higher temperature centered at 170 °C. This temperature was 45 °C higher than that of the bulk polymer. As the amount of adsorbed polymer increased, the higher temperature portion of the transition increased in intensity until the amount of polymer adsorbed reached around 1.12 mg/m^2. At 1.49 mg/m^2, two peaks, labeled as component A (loosely-bound, transition temperature close to bulk) and component B (tightly-bound, higher transition temperature) were observed. For all adsorbed samples, there appeared to be no thermal activity after 190 °C. As the amount of adsorbed polymer increased, the intensity under peak A increased for adsorbed amounts above 1.12 mg/m^2 sample. For these larger adsorbed amount samples, a relatively constant intensity per gram of polymer under peak B was found.
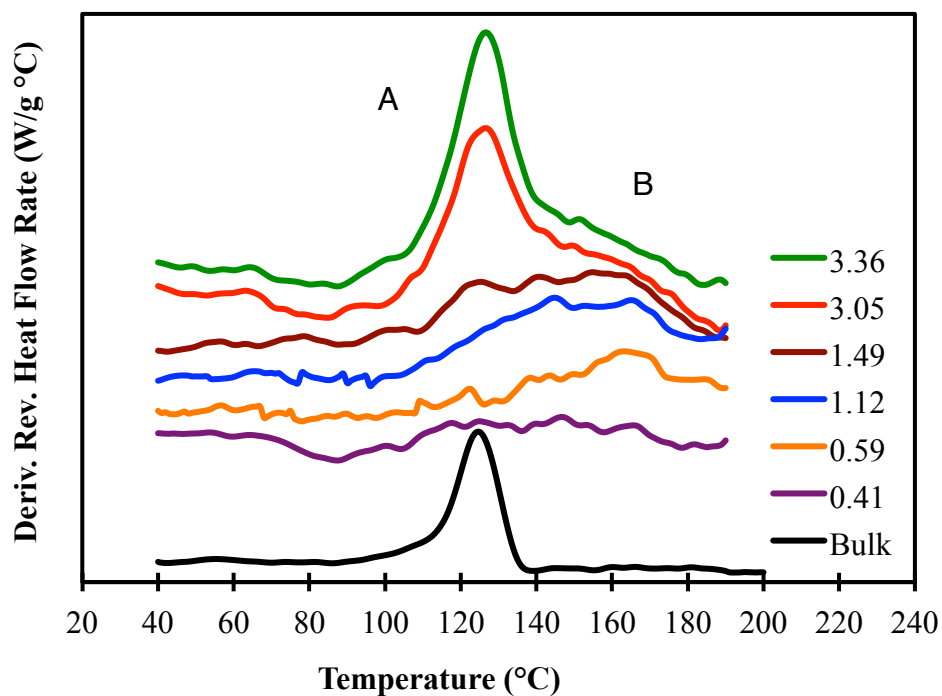
Figure 3. TMDSC thermograms for bulk and adsorbed PMMA on silica at different adsorbed amounts in mg polymer/m^2 silica. The order in the legend is the order of the curves on the left hand part of the curve.

The measured specific heat capacities for the bulk polymer, silica, and adsorbed samples (represented by symbols) are shown in Figure 4. In the figure, only a few of the measurements made are shown for the sake of clarity. Due to relatively low heat capacity of silica with respect to the polymer, the curves (for the adsorbed samples) were higher in heat capacity with increased adsorbed amounts. For the sample with the smallest amount of adsorbed polymer, 0.60 mg/m^2, the heat capacity increased linearly with an increase in temperature with almost no jump in heat capacity, i.e., no glass transition was suggested. This is in contrast with the behavior of samples with more adsorbed polymer in them. However, the slope of the curve changed with temperature near the range of the bulk T_g suggesting very broad and weak glass transition. With increased amount of adsorbed polymer (greater than 1.49 mg/m^2), more bulk-like glass transition behavior was observed with an intensity increasing with additional adsorbed polymer.
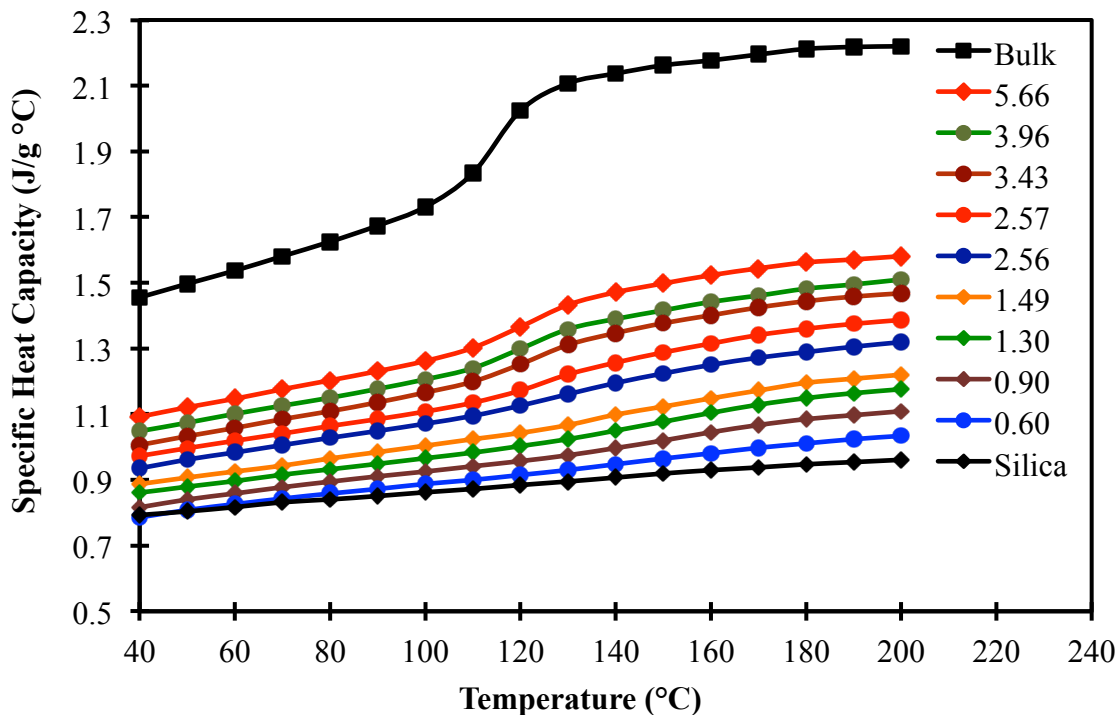
Figure 4. Specific heat capacities of bulk PMMA, silica, and composites as a function of temperature. The symbols represent the measured heat capacities and curves are to aid the eye and are in the order given in the legend.

Given that the changes in heat capacities of the adsorbed samples are dominated by the changes in composition and the heat capacity of the silica is unlikely to change with composition, it is instructive to examine the heat capacity of adsorbed polymer alone. This can be accomplished by subtracting the contribution of the silica. The heat capacities of the polymer alone, thus calculated, were fitted with four different models to try to understand the behavior of adsorbed polymer on surface as shown in Figure 5. The mixture model overestimates the heat capacity of adsorbed polymer and, on the polymer alone basis, was flat with a fixed per gram contribution from the polymer. Obviously, the adsorption of polymer on surface lowered the heat capacity of the polymer. The bound

segment model, in which the polymer layers on surface are divided into two types, tightly-bound and loosely bound polymer, fits experimental data pretty well except for very small amounts of adsorbed polymer. The simple exponential model also fits data reasonably well. However, it is unlikely that the heat capacity of very small amount of adsorbed polymer approaches to zero. The exponential model with a non-zero intercept, called *transitional model* as represented by Eq. 5., fits the data very well. To the first approximation, both the bound segment and transitional models fit experimental similarly, however, the transitional model fits better statistically than bound segment model.
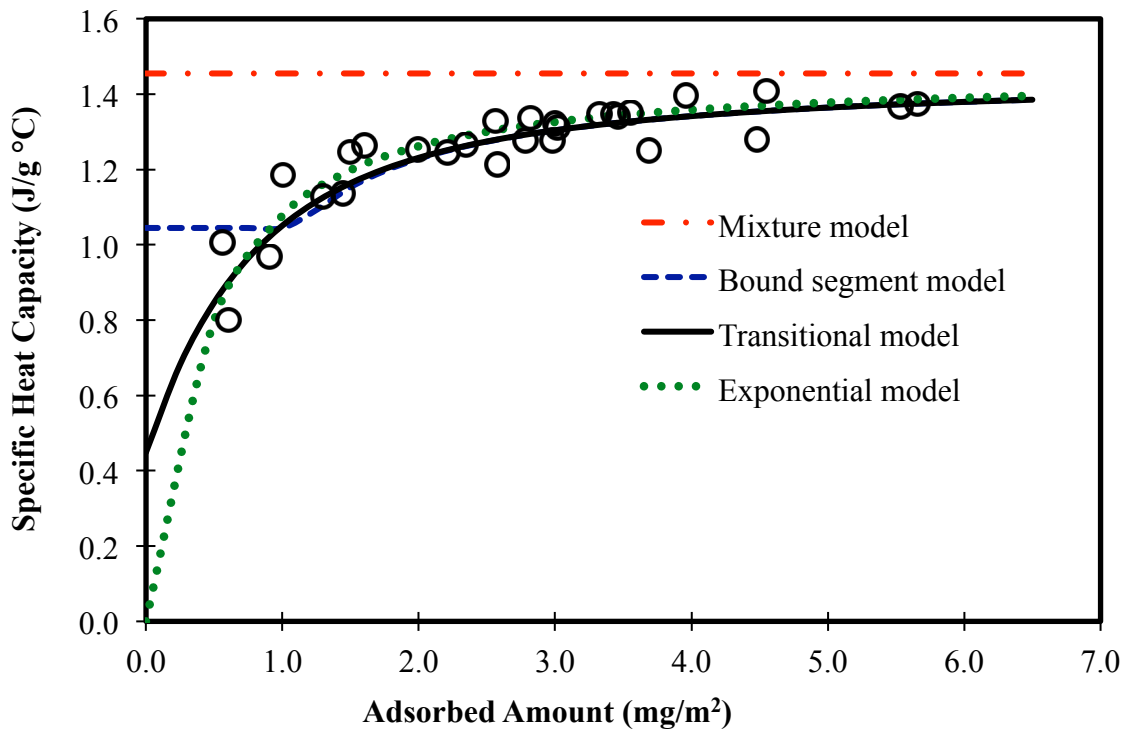
Figure 5. Heat capacities of the adsorbed polymer alone (calculated by subtracting the heat capacity of the silica from total heat capacity) adsorbed on surface at different adsorbed amounts showing prediction from mixture, bound segment, exponential, and transitional model at 40° C.

The fitting of the heat capacities for the polymer alone adsorbed on surface with bound segment model and transitional model in three different regions; below, around, and above the bulk T_g are shown in Figure 6. Similar fittings at other temperatures are provided in APPENDIX E. From the fittings of the heat capacity data with bound segment model, it was observed that the amount of tightly-bound polymer varied with temperature as shown in Figure 7a. Well above and well below the bulk T_g, the amount of tightly-bound polymer was found to be around 1.20 mg/m^2. This value increased significantly around the bulk T_g, where a maximum value was observed. The heat capacity of tightly-bound polymer was found to be temperature dependent. Below the bulk T_g, the heat capacity of the tightly-bound polymer was around 70 – 80% of the bulk heat capacity. This fraction increased with increased temperature and approached the bulk heat capacity well above the bulk T_g.
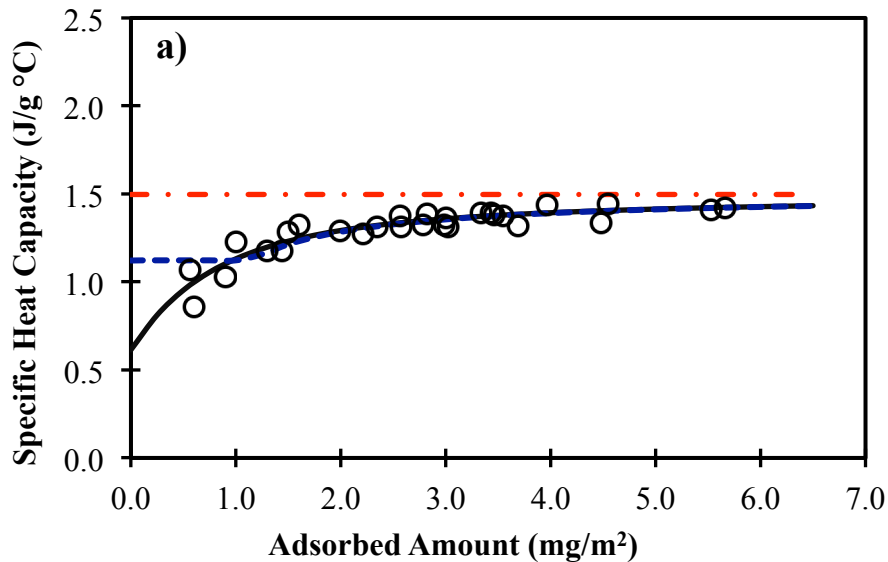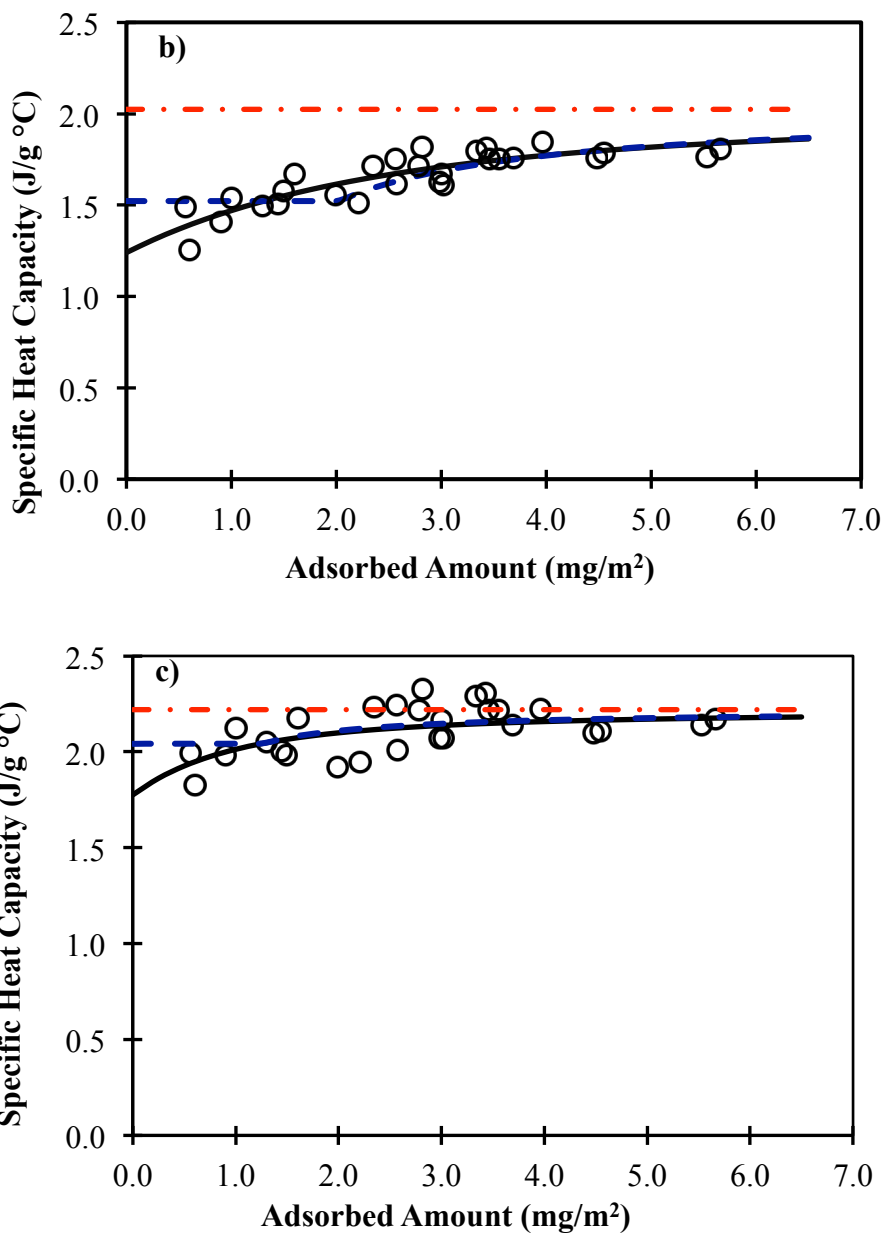
Figure 6. Heat capacities of adsorbed polymer alone at different adsorbed amounts showing the prediction from bound segment model (- - -) and transitional model (—) for a) 50 °C, below; b) 120 °C, near; and c) 200 °C, above the bulk T_g. The dot-dashed line on the top represents the heat capacity of bulk polymer at the temperatures noted.

The variation of the fractional heat capacities of first polymer that goes on surface (*f*), obtained from intercepts, and exponential parameter (*a*) as a function of temperature as determined from the transitional model is shown in Figure 7b. The fractional heat capacity increased with increasing temperature. The parameter, "*a*", indicated the steepness of the transition of heat capacity of adsorbed polymer towards its bulk value. The value of "a" varied with temperature; it was lowest at the two extremes in temperatures and increased near the bulk T_g with highest value at the bulk T_g, as shown in Figure 7b.
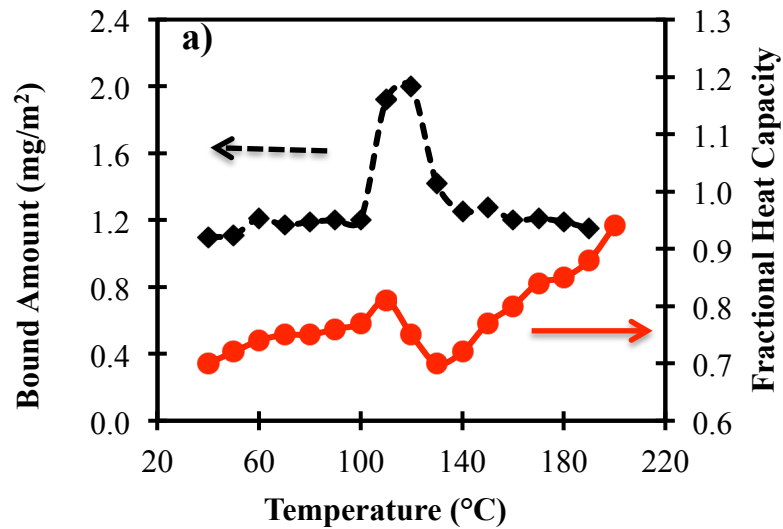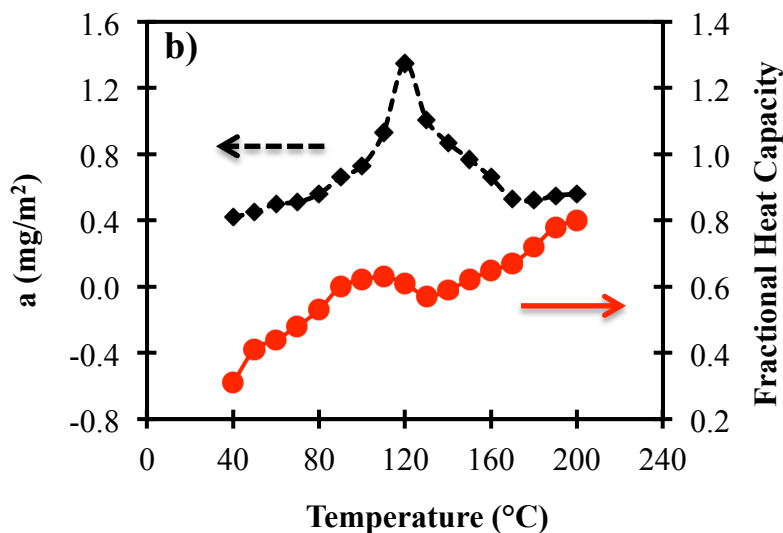
Figure 7. Plots for a) tightly-bound amount and its heat capacity for bound segment model, and b) the exponential parameter (*a*) and intercept (*f*) for transitional model at different temperatures.

4.6. DISCUSSION

Two major degradation regions, characterized by (T_{max}), temperature at which the rate of mass loss is maximum, were observed for the bulk polymer starting at around 280 °C and 320 °C. This behavior is different than that reported in previous measurements by Zhang et al.[43] The difference is likely due to the different tacticities and the methods of polymerization. Thermal degradation studies by McNeill[44] on PMMA synthesized with different techniques has reported that polymer synthesized by free radical methods showed two step degradation, while only one step transition at high temperature was observed for polymer synthesized using ionic methods. Sazanov et al. obtained similar results for PMMA synthesized by ionic techniques.[45] The lower temperature degradation in former is believed to be because of the presence of weak linkages. For example, a head to head linkage between the free radicals or a double bond at the end of the chain from

disproportionation is the cause for the first major degradation in this polymer.[44,46] However, two-stage degradation was not observed for the adsorbed polymers.

For small amounts of adsorbed polymer (<1.12 mg/m^2), the major decomposition temperatures (T_{max}) were centered around 380 - 390 °C; about 100 °C higher than the low temperature degradation step for the bulk polymer. The increases in degradation temperatures were due to the H-bonding of polymers with surface silanols. A previous thermogravimetric study on adsorbed PMMA suggested that bound PMMA degrades at higher temperatures than bulk PMMA.[47] In contrast, the behavior of isotactic and syndiotactic PMMA on silica exhibited degradation temperatures dependent on amount of adsorbed polymer; higher adsorbed amounts had lower T_{max} than bulk for both polymers.[43] While lower adsorbed amounts had T_{max}s similar to bulk for syndiotactic PMMA, however, the isotactic polymer had very complex thermal degradation. This difference is likely due to different stereo-regularity of the PMMAs used, and hence, different pathways for degradation.

Two distinct transitions were observed in the MDSC thermograms and were labeled with A and B. The transition A was at a temperature similar to, but slightly higher than that for bulk polymer, and hence, was called "loosely-bound polymer". Similar glass transition behavior for loosely-bound polymer and the bulk polymer was confirmed using many other techniques.[5,6,16,17,28] For very small amounts of adsorbed polymer, there was no loosely-bound polymer, as observed in the thermograms for adsorbed amounts less than 1.12 mg/m^2 in Figure 3. The transition B was centered at a temperature significantly higher than (around 45° higher for lowest adsorbed amount) that for the loosely-bound polymer, indicative of lower mobility polymer. This fraction was referred to as "tightly-

bound polymer". Previous studies on adsorbed polymers on surfaces have reported that the T_g is increased when there was a strong interaction between polymer and surface.[5,6,16,48] Since there was so little material associated with these transitions, they were difficult to observe using most standard samples and measurement techniques. Previously,[16,49] a linear fit model based on the area under the peaks for loosely-bound and tightly-bound polymer has been used for the estimation of amount of tightly-bound polymer. These measurements provided an estimate of the amount of tightly-bound polymer, its T_g, and a rough estimate of the heat capacity change at the T_g.

In this study, the measured heat capacities were interpreted using the mixture model, bound segment model, and exponential models with either zero or finite intercepts (transition model). Each represented a sequential improvement of the analysis of the data. The mixture model clearly shows that the interaction of the polymer with the silica is not "ideal". The assumption that the polymer heat capacity is affected by the interaction of the polymer and silica, yields an estimate of the heat capacity of the adsorbed polymer. The resulting data can be interpreted in terms of a bound segment model, where polymer segments close to the surface are tightly-bound and those far from the surface is loosely-bound as shown in Figure 8. This kind of heterogeneous behavior of polymer is expected when there is some kind of strong interaction between the polymer and the surface, for example, H-bonding or ionic interactions. The presence of segmental heterogeneity in adsorbed polymer was demonstrated using deuterium NMR studies of adsorbed poly(vinyl acetate)[50] and poly(methyl)acrylate on silica surface.[51-55] Molecular dynamics simulation studies also revealed the presence of segmental heterogeneity when polymer is adsorbed on surface.[56]
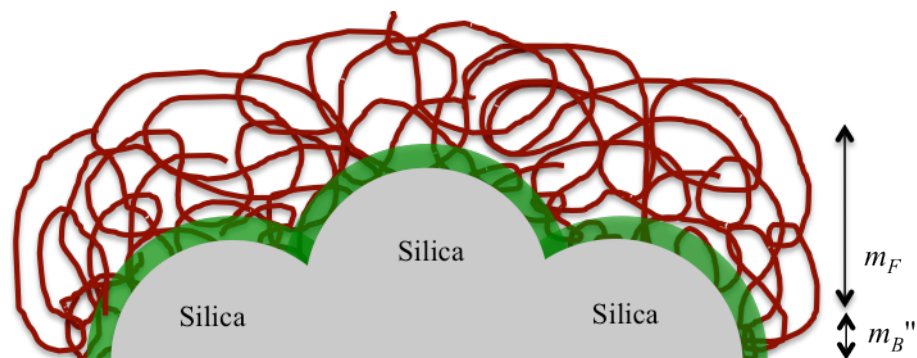
Figure 8. Schematic representation of adsorbed PMMA on Cab-O-Sil silica showing a) two state model comprised of loosely-bound (green shaded, m_F) and tightly-bound polymer (m_B''). The polymer coil size and silica particles (10 nm of diameter) are drawn roughly to scale. The thickness corresponding to tightly bound polymer is about 1 nm.

The use of the bound segment model allowed the quantification of the amount of tightly-bound polymer and its heat capacity. The amount of tightly-bound polymer was found to depend on temperature. However, the amount of tightly-bound polymer was found to be fairly constant well below and above the bulk T_g. In these two ranges, the average amounts of tightly-bound polymer (m_B'') were found to be 1.17 ± 0.04 (1 S.D.) mg/m^2 and 1.21 ± 0.05 (1 S.D.) mg/m^2 respectively. These values, shown in Table 1, were slightly lower (around 9 %, but within experimental error) than previous measurements from heat-flow curves, using a less sensitive instrument,[16] and similar to the measurements done by Khatiwada et al.[49] The amount of tightly-bound polymer, based on bulk density of 1.2 g/cm^3, corresponds to a polymer thickness of 1 nm, if the polymer layer was flat and uniform. Around the bulk glass transition, the amount of tightly-bound polymer approached a value of 2.0 mg/m^2. In this range, the polymer segments that were attached on the surface, as well as some segments close to the bound segments, remained

in the glassy state. In other words, the higher fraction of the tightly-bound segments was due to the elevated T_g of some of the segments. As the temperature increased well above the bulk T_g, more segments became rubbery leaving only small amount of motionally restricted polymer on surface.

The heat capacity of tightly-bound polymer was estimated to be around $70 - 80\%$ of that of the bulk polymer at below and through the bulk T_g. The reduction in heat capacity of tightly-bound polymer was due to the reduction in mobility of polymer adsorbed on surface. Previously, NMR studies on similar systems also reported the presence of heterogeneous mobility of polymer segments at the interface.[28,53,55] Similar studies on glass transition behavior of adsorbed polymers on surfaces have reported that polymers that were tightly-bound on surface, showed weak glass transition behavior at higher temperatures.[5,6,16,57] The estimation of step change in heat capacity (ΔC_P) for tightly-bound polymer also reported the reduction of heat capacity when polymer was bound on the surface.[16] The heat capacity of tightly-bound polymer increased with increased temperature, approaching the bulk value well above the bulk T_g. This result suggests that tightly-bound polymer relaxes slowly over a wide temperature range and only approaches bulk like behavior well above bulk T_g, which is before it undergoes degradation. Studies on devitrification (relaxation) of rigid amorphous fraction (RAF) in semi-crystalline materials also suggested that RAF relaxes step by step before the melting temperature of the crystal is reached.[34,58] In this context, crystals are considered similar to surfaces in semi-crystalline material. Moreover, the TMDSC measurements on adsorbed polymer also suggested that the tightly-bound polymer relaxes at higher temperature.[6,16] However, some studies on adsorbed polymers on surface systems have

reported that the tightly-bound (rigid amorphous fraction) polymer does not relax before the degradation temperature is reached.[17]

Table 1. Tightly bound amounts (m_B'') and exponential parameter (a) from the bound-segment model and transitional model below, around and above the bulk T_g respectively.

Parameter	Below[a] (40 -90 °C)	Near[a] (110 -120 °C)	Above[a] (150 -200 °C)
m_B'' (mg/m^2)	1.17 +/- 0.08	1.96 +/- 0.12	1.21 +/- 0.10
			1.30 +/- 0.34[b]
			1.21 + /- 0.42[c]
a (mg/m^2)	0.55 +/- 0.22	1.14 +/- 0.60	0.56 +/- 0.11

[a] relative to the bulk T_g

[b,c] from heat flow curves obtained from TMDSC measurements by Blum et al.[16] and Khatiwada et al.[49] The uncertainties are from the standard deviation and represent the 95% confidence interval.

Polymers adsorbed on surfaces may not just form two layers with different heat capacities as immobilizing one part of the polymer chain at the interface affects the mobility of neighboring segments. The effect of immobilization decreases as the polymer segments are moved further away from the surface and eventually attains bulk-like mobility where there is fairly negligible effect of the surface on the polymer segments. Hence, the heat capacity of polymer alone (adsorbed on surface) can be better described with the application of model in which the heat capacity increases with distance from the surface, e.g., an exponential model. The exponential model can be developed with a non-

zero (transitional model) or zero (exponential model) intercept. At first glance, it looks like both models fit the data reasonably well up to the range of adsorbed amounts studied. However, It is unlikely that the heat capacities of very small amounts of adsorbed polymer approach zero as predicted by the simple exponential model (represented by dotted line in the figures). Adsorbed polymers tend to have coiled configurations on surfaces.[41,42] Computer simulation studies of adsorbed polymers on surfaces have suggested that the polymers retain more random coil configurations when adsorbed from theta or poor solvents.[59] However, this phenomenon is highly dependent on polymer surface interaction parameter, the density of the polymer adsorbed and molecular mass.

At some level, it seems like all four models fit experimental heat capacity reasonably well. However, the transitional model fits the data better than the simple exponential model. The transitional model describes the behavior of surface adsorbed polymer better than any other model described above, especially for adsorbed polymer with lowest adsorbed amounts. However, the bound-segment model is useful, especially for an estimate the amount of tightly-bound polymer on the surface and comparison with data from other experiments where a similar model is used.

From the heat capacity data interpreted with the transitional model at different temperatures, it was observed that the fractional heat capacity of first polymer that goes on surface was smaller than that of the bulk polymer at all temperatures, as shown in Figure 7b. The reduction in heat capacity was due to the reduction in mobility of polymer chains that are bound to the surface, as mentioned above. This result was consistent with weak nature (lower C_p) of transition B in TMDSC measurements as shown in Figure 3. The parameter (a), which indicated the rate of increase in the heat capacity of adsorbed

polymer towards its bulk value, was smaller on either side of the bulk T_g, as shown in Figure 7b. Values of $a = 0.4$ to 0.5 mg/m^2 correspond to 1.2 to 1.5 for obtaining 95% of the bulk heat capacity. This estimate is quite consistent with that from heat flow curves (1.2 mg/m^2) for the amount of tightly bound polymer. The heat capacity of adsorbed polymer transitions to bulk heat capacity more sharply with polymer thickness at temperatures well below and above bulk T_g, but considerably slower near the bulk T_g. Well below the bulk T_g, the polymer on surface was all glassy and the extra constraints on mobility had only minimal effects on the rest of the polymer on the surface. Most surface segments were very similar to bulk. Well above the bulk T_g, all polymer segments became rubbery leaving very few segments, which were directly bound on the surface, with altered heat capacity. Consistent with the NMR data from similar systems, the presence of a motional gradient was largest in the bulk T_g region.[54,55]

4.7. CONCLUSIONS

In the present study, the usefulness of heat capacity measurements to probe the behavior of PMMA adsorbed on silica has been demonstrated. TGA and MDSC techniques were consistent with the presence of tightly-bound polymer at polymer-silica interface. The heat capacity of bound polymer was found to be lower than that of the bulk polymer. A two state model, the bound segment model, was used to estimate the amount of tightly-bound polymer and its heat capacity on surface. However, the model, which divided the polymer layers into two segments, was an oversimplification; the bound polymer segments reduced the mobility of polymer segments next to them, and so on.

Nevertheless, this model provided an estimate of the amount of tightly bound polymer, in this case about 1.2 mg/m^2, which was similar to that, estimated from heat flow curves.

Perhaps a more realistic model, referred to as the transitional model, has been used to probe the heat capacity of polymer alone on the surface. Interpretation of the data with this model provides two significant parameters with new insight. The fractional heat capacity, f, of the polymer initially bound to the surface was estimated to have a heat capacity from 0.3 to 0.8 of that of the bulk polymer, increasing monotonically with temperature. We believe that this is the first time that this value has been determined. The heat capacity of the polymer that is bound on the surface was shown to transition to the bulk heat capacity with additional adsorbed polymer. For temperatures above and below the bulk T_g, the heat capacity increases exponentially with a distance parameter, a, of 0.43 to 0.56 mg/m^2 providing a first estimate of distance scale for the effect of the surface.

4.8. REFERENCES

(1) Alcoutlabi, M.; McKenna, G. B. *J. Phys.: Condens. Matter* **2005**, *17*, R461-R524.

(2) Paul, D. R.; Robeson, L. M. *Polymer* **2008**, *49*, 3187-3204.

(3) Arrighi, V.; McEwen, I. J.; Qian, H.; Prieto, M. B. S. *Polymer* **2003**, *44*, 6259-6266.

(4) Winey, K. I.; Vaia, R. A. *MRS Bull.* **2007**, *32*, 314-319.

(5) Madathingal, R. R.; Wunder, S. L. *Langmuir* **2010**, *26*, 5077-5087.

(6) Porter, C. E.; Blum, F. D. *Macromolecules* **2000**, *33*, 7016-7020.

(7) Moniruzzaman, M.; Winey, K. I. *Macromolecules* **2006**, *39*, 5194-5205.

(8) Ramanathan, T.; Abdala, A. A.; Stankovich, S.; Dikin, D. A.; Herrera-Alonso, M.; Piner, R. D.; Adamson, D. H.; Schniepp, H. C.; Chen, X.; Ruoff, R. S.; Nguyen, S. T.; Aksay, I. A.; Prud'homme, R. K.; Brinson, L. C. *Nat. Nanotechnol.* **2008**, *3*, 327-331.

(9) Keddie, J. L.; Jones, R. A. L.; Cory, R. A. *Faraday Discuss.* **1994**, *98*, 219-230.

(10) Fukao, K.; Miyamoto, Y. *Europhys. Lett.* **1999**, *46*, 649-654.

(11) Fukao, K.; Miyamoto, Y. *Phys. Rev. E* **2000**, *61*, 1743-1754.

(12) Hartmann, L.; Kratzmuller, T.; Braun, H. G.; Kremer, F. *Macromol. Rapid Commun.* **2000**, *21*, 814-819.

(13) Bauer, C.; Bohmer, R.; Moreno-Flores, S.; Richert, R.; Sillescu, H.; Neher, D. *Phys. Rev. E* **2000**, *61*, 1755-1764.

(14) Wallace, W. E.; Vanzanten, J. H.; Wu, W. L. *Phys. Rev. E* **1995**, *52*, R3329-R3332.

(15) Blum, F. D.; Gandhi, B. C.; Forciniti, D.; Dharani, L. R. *Macromolecules* **2005**, *38*, 481-487.

(16) Blum, F. D.; Young, E. N.; Smith, G.; Sitton, O. C. *Langmuir* **2006**, *22*, 4741-4744.

(17) Sargsyan, A.; Tonoyan, A.; Davtyan, S.; Schick, C. *Eur. Polym. J.* **2007**, *43*, 3113-3127.

(18) Kirst, K. U.; Kremer, F.; Litvinov, V. M. *Macromolecules* **1993**, *26*, 975-980.

(19) Miwa, Y.; Drews, A. R.; Schlick, S. *Macromolecules* **2006**, *39*, 3304-3311.

(20) Mammeri, F.; Rozes, L.; Le Bourhis, E.; Sanchez, C. *J. Eur. Ceram. Soc.* **2006**, *26*, 267-272.

(21) Lee, D. C.; Jang, L. W. *J. Appl. Polym. Sci.* **1996**, *61*, 1117-1122.

(22) Vieweg, S.; Unger, R.; Hempel, E.; Donth, E. *J. Non-Cryst. Solids* **1998**, *235*, 470-475.

(23) Tsagaropoulos, G.; Eisenberg, A. *Macromolecules* **1995**, *28*, 6067-6077.

(24) Johnson, H. E.; Granick, S. *Macromolecules* **1990**, *23*, 3367-3374.

(25) Enriquez, E. P.; Schneider, H. M.; Granick, S. *J. Polym. Sci. Part B:, Polym. Phys.* **1995**, *33*, 2429-2437.

(26) Berquier, J.-M.; Arribart, H. *Langmuir* **1998**, *14*, 3716-3719.

(27) Kulkeratiyut, S.; Kulkeratiyut, S.; Blum, F. D. *J. Polym. Sci. Pt. B-Polym. Phys.* **2006**, *44*, 2071-2078.

(28) Blum, F. D.; Krisanangkura, P. *Thermochim. Acta* **2009**, *492*, 55-60.

(29) Hartmann, L.; Gorbatschow, W.; Hauwede, J.; Kremer, F. *Eur. Phys. J. E* **2002**, *8*, 145-154.

(30) Fryer, D. S.; Peters, R. D.; Kim, E. J.; Tomaszewski, J. E.; de Pablo, J. J.; Nealey, P. F.; White, C. C.; Wu, W. L. *Macromolecules* **2001**, *34*, 5627-5634.

(31) Marti, E.; Kaisersberger, E.; Moukhina, E. *J. Therm. Anal. Calorim.* **2006**, *85*, 505-525.

(32) Carini, G.; D'Angelo, G.; Tripodo, G.; Bartolotta, A.; Di Marco, G.; Lanza, M.; Privalko, V. P.; Gorodilov, B. Y.; Rekhteta, N. A.; Privalko, E. G. *J. Chem. Phys.* **2002**, *116*, 7316-7322.

(33) Hempel, E.; Kahle, S.; Unger, R.; Donth, E. *Thermochim. Acta* **1999**, *329*, 97-108.

(34) Chen, H. P.; Cebe, P. *Macromolecules* **2009**, *42*, 288-292.

(35) Nishimoto, Y.; Ichimura, Y.; Kinoshita, R.; Teramoto, Y.; Yoshida, H. *Thermochim. Acta* **1991**, *179*, 117-124.

(36) Song, M.; Hammiche, A.; Pollock, H. M.; Hourston, D. J.; Reading, M. *Polymer* **1995**, *36*, 3313-3316.

(37) Righetti, M. C.; Di Lorenzo, M. L.; Tombari, E.; Angiuli, M. *J. Phys. Chem. B* **2008**, *112*, 4233-4241.

(38) Di Lorenzo, M. L.; Righetti, M. C.; Cocca, M.; Wunderlich, B. *Macromolecules* **2010**, *43*, 7689-7694.

(39) McBrierty, V.; Packer, K. *Nuclear Magnetic Resonance in Solid Polymers;* Cambridge University Press: Cambridge, **1993**. 202-206.

(40) Ding, E. Y.; Cheng, R. S. *Thermochim. Acta* **2001**, *376*, 133-139.

(41) Fleer, G. J.; Cohen-Stuart, M. A.; Scheutjens, J. M. H. M.; Cosgrove, T.; Vincent, B. *Polymers at Interfaces;* Chapman & Hall: London, **1993**.

(42) Hiemenz, P. C. *Polymer Chemistry, The Basic Concepts;* Marcel Dekker, Inc.: Madison Avenue, New York, **1984**.

(43) Zhang, B.; Blum, F. D. *Thermochim. Acta* **2003**, *396*, 211-217.

(44) McNeill, I. C. *Eur. Polym. J.* **1968**, *4*, 21-30.

(45) Sazanov, Y. N.; Skvortsewich, E. P.; Milovskaya, E. B. *J. Therm. Anal. Calorim.* **1974**, *6*, 53-58.

(46) Grassie, N.; Farish, E. *Eur. Polym. J.* **1967**, *3*, 305-315.

(47) Aruchamy, A.; Blackmore, K. A.; Zelinski, B. J. J.; Uhlmann, D. R.; Booth, C. *Mater. Res. Soc. Symp. Proc.* **1992**, *249*, 353-361.

(48) Priestley, R. D.; Ellison, C. J.; Broadbelt, L. J.; Torkelson, J. M. *Science* **2005**, *309*, 456-459.

(49) Khatiwada, B. K.; Hetayothin, B.; Blum, F. D. *Macromol. Symp.* **2013**, *327*, 20-28.

(50) Blum, F. D.; Xu, G.; Liang, M.; Wade, C. G. *Macromolecules* **1996**, *29*, 8740-8745.

(51) Lin, W.-Y.; Blum, F. D. *Macromolecules* **1998**, *31*, 4135-4142.

(52) Lin, W.-Y.; Blum, F. D. *Macromolecules* **1997**, *30*, 5331-5338.

(53) Metin, B.; Blum, F. D. *J. Chem. Phys.* **2006**, *125*, 054707 (1-9).

(54) Lin, W.-Y.; Blum, F. D. *J. Am. Chem. Soc.* **2001**, *123*, 2032-2037.

(55) Metin, B.; Blum, F. D. *Langmuir* **2010**, *26*, 5226-5231.

(56) Smith, G. D.; Bedrov, D.; Borodin, O. *Phys. Rev. Lett.* **2003**, *90*, 226103 (1-4).

(57) Kabomo, M. T.; Blum, F. D.; Kulkeratiyut, S.; Kulkeratiyut, S.; Krisanangkura, P. *J. Polym. Sci., Part B: Polym. Phys.* **2008**, *46*, 649-658.

(58) Huo, P. T.; Cebe, P. *Macromolecules* **1992**, *25*, 902-909.

(59) Chremos, A.; Glynos, E.; Koutsos, V.; Camp, P. J. *Soft Matter* **2009**, *5*, 637-645.

CHAPTER 5

INTERACTION OF GRAPHENE AND GRAPHENE OXIDE WITH POLY(VINYL

ACETATE)[*]

5.1 ABSTRACT

Deuterium (^{2}H) solid-state NMR and differential scanning calorimetry (DSC)

were used to probe the interfacial interactions of poly(vinyl acetate) (PVAc-d_3)

incorporated with graphene oxide. Graphene oxides (GO) were prepared by the oxidation

of graphene by the modified Hummer's method. The glass transition behavior of the bulk

and PVAc-d_3/GO composites was determined by temperature modulated DSC.

Incorporation of the PVAc-d_3 with the GO significantly reduced the thermal intensity of

the glass transition. In fact, the glass transitions of the PVAC-d_3/GO samples from DSC

almost disappeared (very weak and broad) when the composition of the polymer was

50% or less (w/w). In contrast, for PVAc/silica composites, it was possible to observe the

glass transition behavior of the composites, even with 10% (w/w) of the polymer

composition. ^{2}H NMR measurements were carried out to understand the dynamics of the

polymer segments incorporated with the GO. In contrast to the behavior for the bulk

[*]Bal K. Khatiwada,[a] Krishna Bastola,[b] Ranji Vaidyanathan,[b] and Frank D. Blum[a]
[a]Department of Chemistry, Oklahoma State University, Stillwater, OK 74078 USA
[b]Helmerich Research Center, Oklahoma State University, 700 North Greenwood Avenue,
HRC-200, Tulsa, OK 74106 USA

polymer, the polymer segments incorporated with GO showed heterogeneous mobility. The Pake powder patterns of PVAc-d_3/GO samples had resonances from polymer segments that were more mobile and less mobile than the bulk polymer.

5.2. INTRODUCTION

Some polymer-based composites are synthesized by incorporating reinforcing materials such as carbon fibers, glass fibers, polyhedral oligomeric silsesquioxane (POSS), nanoclays, carbon nanotubes (CNTs), graphene, and graphene oxide, etc. in the polymer matrix. The performance of these composites depends, among other things, on the compatibility of the polymer matrix with the reinforcing material. Usually, incorporation of nanoparticles as reinforcing materials enhances the performance of a composite even at low loadings of the reinforcing materials due to the high surface area of the nanomaterial. However, in the case of graphene-polymer based composites, the dispersion of graphene sheets in a polymer matrix is difficult to achieve due to the strong interactions between the graphene sheets via π-π stacking and van der Waals interactions. The problem of aggregation can occasionally be remedied by dispersion of the particles prior to mixing with polymer matrix. Various techniques such as ultra sonication, solvent exfoliation,[1,2] addition of surfactant,[3-5] polymerization in situ,[6] and functional modification of the particles, etc. can be used to disperse the particles. For example, it has been shown that the graphene sheets can be exfoliated by ultra-sonication of graphene in the presence of N-methyl pyrrolidone (NMP) solvent.[1,2,6] However, the extent of dispersion by this technique is relatively poor and often the sheets collapse back to multi layer graphene sheets. Moreover, this process of solvent exfoliation is not economically

feasible due to the high cost; and the high boiling point of the NMP solvent makes the dispersed graphene difficult to collect.

The dispersion and the stability of the graphene sheets can sometimes be improved by intercalation of a polymer or a surfactant in between the sheets. The intercalation of the polymers can be achieved by either simple mixing of polymer with graphene sheets followed by sonication of the mixture,[7-9] in situ polymerization of intercalated monomers,[10] etc. However, these techniques for graphene dispersion can be problematic, especially when the dispersion of the sheets at the molecular level is desired. One way of improving the dispersion of graphene sheets is by surface modification. Modification can often be achieved by introduction of functional groups on the surface of the sheets, such as oxidation of graphene into graphene oxide (GO),[11,12] reductive alkylation of fluorinated graphene,[13] diazonium salt of surfactant wrapped graphene sheets,[14] and ionic liquid functionalized graphene sheets.[15] Among those, the exfoliation of graphene using strong oxidizing agents to produce GO is a frequently used approach. The GO can be converted back to pristine graphene[16-18] for its various applications.

Exfoliated GO can be well dispersed in different polar solvents such as water, tetrahydrofuran (THF), dimethyl formamide (DMF), NMP, and ethylene glycol,[19] which makes GO a good candidate as a reinforcing filler to produce various polymer based composites/nanocomposites. Due to high mechanical strength of GO, incorporation of small amount of the GO in a polymer matrix can significantly enhance the mechanical properties of the composite.[20,21] Unlike graphene, GO has a significant number of oxygen groups (on the basal plane and edges) that can interact with polymers with polar

functional groups (carbonyl, ester, ether, amide, ester, etc.), such as, poly(vinyl alcohol) (PVA), poly(vinyl acetate) (PVAc), poly(ethylene oxide) (PEO), poly(methyl methacrylate) (PMMA), polyvinylpyrrolidone (PVP). The interactions can be H-bonding or dipole-dipole interactions. When there are strong interactions between the groups, one can imagine that the performance of composites made with GO and these polymers can be superior over graphene/polymer composites.

Research on incorporation of GO into polymer matrix have become increasingly widespread due to its enhanced mechanical properties,[22-24] impermeability to gases,[25-27] good electrical conductivity (after in situ reduction of the GO in the GO/polymer composites to generate graphene/polymer composites),[18,28,29] ease of dispersibility in many solvents,[19] and high surface area of the material. Few studies on the synthesis of PMMA/GO have been conducted by solvent-blending or in situ polymerization.[30-32] Liu et al. have synthesized PVAc intercalated GO composites by an in situ polymerization of the vinyl acetate monomer in between the GO layers.[33] Similarly, Zhang et al. synthesized PVAc grafted GO composites by γ-ray induced graft polymerization.[34] Pinto et al. have used a solvent-blending technique to prepare PVAc/GO composites. The composites can be chemically reduced to obtain well-dispersed PVAc/graphene composites.[24] Similar studies have been conducted to understand the alteration of the physical properties of the polymers associated with incorporation of GO into the polymer matrix.[20,22,23,25,26,35-37] Composites made using a single layer of GO show significant property enhancement even at GO loadings of less than 1%. The focus of these studies was to analyze the effect of GO on the mechanical properties of the composites with the addition of a relatively small amount of GO. To the best of our knowledge, no rigorous

studies on why the properties of the polymer were significantly altered by incorporation of GO were made.

The focus of this study is to understand the interactions of the polymer with GO via the thermal and dynamical properties of the polymer segments in polymer/GO composites. PVAc/GO composites have been synthesized by mixing the polymer with the GO in ethanol. Temperature modulated differential scanning calorimetry (TMDSC) has been used to study the glass transition behavior of the bulk polymer and the polymer/GO composites. The dynamics of the polymer in polymer/GO composites has been studied with ^{2}H NMR spectroscopy.

5.3. MATERIALS AND METHODS

5.3.1. Materials

Graphene nano platelets (xGNP® grade M) were purchased from XG Sciences, Michigan. Deuterated (^{2}H) PVAc-d_3 was previously synthesized as described[38] and was used without any additional treatment. The weight average (M_W) and the number average (M_n) molecular mass of the polymer were reported as 68,000 and 20,000 g/mol, respectively.

5.3.2. Synthesis of Graphene Oxide

Graphene oxide was synthesized from graphene nano platelets using modified Hummer's method.[39] In this method, graphene nano platelets (1 wt% equivalent of 6 g) were mixed with 9:1 equivalent mixture of concentrated H_2SO_4 (18 M) and H_3PO_4 (14.8 M) (720:80 mL). The mixture was put in an ice bath and 6 wt% equivalent of $KMnO_4$ (36 g) was slowly added to the mixture with constant stirring. The resultant mixture was

stirred at 90 °C for 12 h. The reaction mixture was cooled to room temperature and poured into a beaker with 800 g of ice containing 12 mL of 30% H_2O_2. The mixture was filtered through a 300 μm polyester fiber filter. The filtrate was centrifuged at 4000 rpm for 4 h and the solid graphene oxide was collected. The solid material was washed in succession with 400 mL of water, 400 mL of 30% HCl, and 400 mL of ethanol twice. The solid material was further washed with 400 mL of water and 400 mL of ethanol in succession until the pH of the mixture was close to neutral. The final wash of the GO was obtained by filtering the mixture through a PTFE membrane of 0.45 μm pore size. The filtered GO was dispersed in ethanol for making PVAc/GO composites.

5.3.3. Preparation of PVAc/GO Composites

The GO in ethanol mixture was sonicated for a half an hour using Microson ultra sonicator (Misonix Inc. Farmingdale, NY) prior to its application for composite preparation. The concentration of GO in mg/mL was determined by taking 3 mL of the mixture and drying it in an aluminum pan. Different amounts of PVAc were dissolved in ethanol and mixed with GO dispersion to achieve compositions of 90.7%, 70.8%, 50.4%, and 34.2% of PVAc in the PVAc/GO composites. The mixture was sonicated for another half an hour for homogeneous mixing of GO with PVAc. The composite mixtures were dried in glass petri dishes and further dried in a vacuum oven for 3 days. Composites dried for 3 days had some residual solvent. For further drying, they were left in the vacuum oven for a month.

5.3.4. TMDSC Measurements

For the TMDSC studies, 5 mg of bulk PVAc and PVAc/GO composites were placed in an aluminum pan, covered with an aluminum lid obtained from TA Instruments

(TA Instruments, New Castle, DE) and pressed with a DSC pan press (TA Instruments). The samples were referenced against an empty pan with a lid and purged with N_2 gas with a flow rate of 50 mL/min. The samples were ramped from -40 °C to 130 °C with a ramp rate of 3 °C/min and modulation of +/- 1 °C/min and held isothermal at 130 °C for 2 min to eliminate the thermal history of the samples. The samples were cooled down to -40 °C, kept isothermal for 2 min, and heated back to 130 °C with 2 min isothermal at this temperature as well. The same ramp rate as that of the first heating cycle was used for the rest of the cycles. Q2000 DSC (TA Instruments) was used for the thermal measurements. Glass transition behavior of the bulk polymer and its adsorbed samples were determined from second heating cycle. The results are presented as a differential reversing heat flow rate (dQ_{rev}/dT) versus temperature. A 10 °C smoothing was applied for all samples to reduce the high-frequency noise from modulation and highlight the weak glass transition behavior of the adsorbed samples.

5.3.5. Solid-state Deuterium (^{2}H) NMR Study

The ^{2}H NMR spectra were obtained using a Tecmag Discovery 400 MHz NMR spectrometer equipped with a high-power amplifier, a fast digitizer and a Bruker Ascend^{TM} 400 WB wide bore magnet. A fixed-frequency wide-line probe (Doty Scientific, Columbia, SC) with a 8 mm (diameter) sample coil was used. The samples were put in a 7.5 mm wide and 20 – 25 mm long thin wall NMR tube and inserted into the NMR coil bore. The quadrupole-echo pulse sequence (delay – 90y – τ – 90x – τ – acquisition) was used with a ^{2}H frequency of 61.48 MHz. The 90° pulse width of 3.2 µs and an echo time (τ) of 32 µs were used. The probe was tuned at each temperature prior to collecting the data. The raw data was left shifted so that the Fourier transform was

started from the top of the echo. Approximately 256-1024 scans were collected depending on the amounts of the polymer in the adsorbed samples. The spectra were taken at intervals of 10 °C from 20 to 130 °C, depending on the composition of the sample. The spectra were processed using the MestRenova software package (Mnova) (Santiago de Compostela, Spain).

5.4. RESULTS

5.4.1. TMDSC Study

Thermal properties of the bulk PVAc-d_3 and PVAc-d_3/GO composites were studied using TMDSC. The reversing heat flow was plotted in derivative mode as a function of temperature. A 10 °C smoothing was used for all the bulk and adsorbed samples. The thermograms for the bulk and adsorbed samples are shown in Figure 1. For the bulk PVAc-d_3, the glass transition temperature was found to be 42.8 °C. When the amount of polymer was 90.7% in the PVAc-d_3/GO (referred to as the 90.7% PVAc-d_3/GO) sample, the T_g was reduced to 39 °C. The slight reduction in T_g for 90.7% PVAc-d_3/GO sample might be due to the broadening of the glass transition signal. The width (full width at half maximum (FWHM)) of the glass transition was broadened from 8 °C for the bulk PVAc to 12 °C for 90.7% PVAc/GO sample. As the amount of PVAc was reduced, the intensity of the glass transition behavior was significantly reduced, as can be observed for 70.8% of PVAc-d_3/GO sample. The FWHM of the glass transition was significantly broadened to 21 °C for 70.8% of PVAc-d_3/GO sample. As the amount of the PVAc-d_3 was further reduced to 50.4 and 34.2% in the PVAc-d_3/GO samples, the glass transition behavior was hard to observe. The curves appeared almost flat with baseline of

103

the curves slightly higher than that of the bulk PVAc above the bulk T_g.
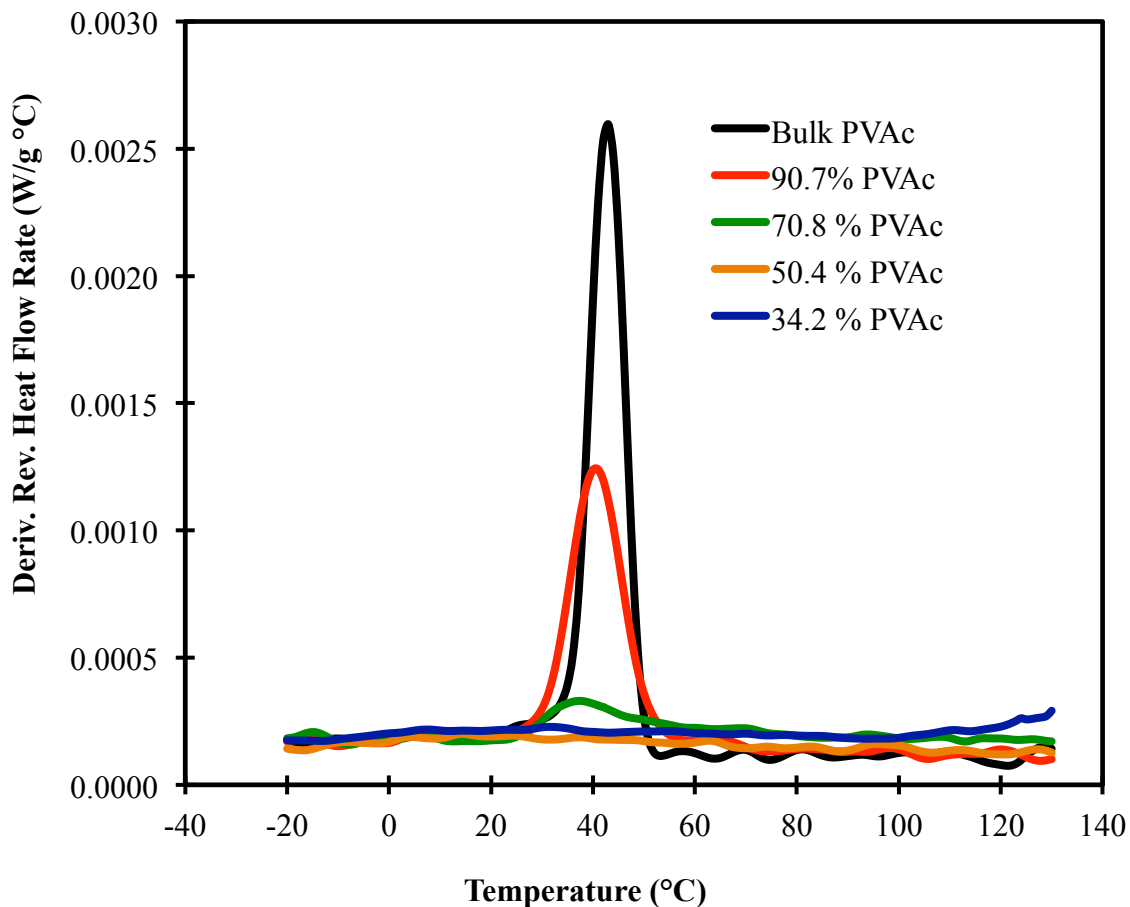

Figure 1. MDSC thermograms of the bulk PVAc and PVAc-d_3/GO composites. The heat flow plot is in the derivative mode and the peak temperature is reported as the glass transition temperature (T_g).

5.4.2. ^{2}H NMR study

^{2}H NMR spectrum of the bulk PVAc-d_3 at 20 °C is shown in Figure 2. At 20 °C, a Pake powder pattern was obtained indicating that the polymer was in the glassy state on the NMR time scale. To a first approximation, the Pake powder pattern appeared similar to what is expected for deuterated methyl group undergoing rapid rotation about its

symmetry axis. The PVAc-d_3 showed an intense powder pattern with a splitting of 44.3 kHz taken at the base of the horns. Upon close examination at the top of the horns, it can be observed that the horns were curved inwards with a smaller separation of 37.6 kHz. The tail of the spectrum extended to a width of 83.7 kHz as shown in Figure 2.
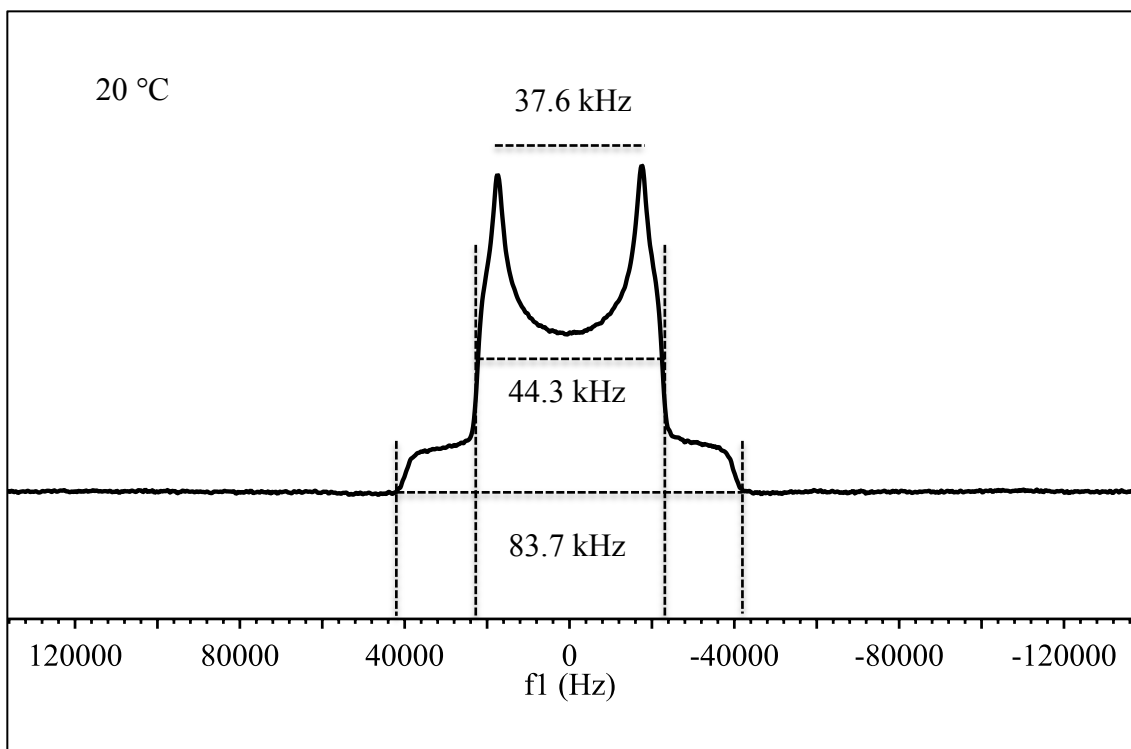
Figure 2. ^{2}H Pake powder pattern of the bulk PVAc-d_3 at 20 °C showing width of the powder pattern for the glassy PVAc-d_3. Lines drawn at the top, middle, and at the bottom of the spectrum shows the width of the Pake pattern at the top, middle and tails of the horns.

The ^{2}H NMR spectra for the bulk PVAc-d_3 were collected at different temperatures starting at 20 °C as shown in Figure 3. At low temperatures (20-60 °C), the Pake powder pattern persisted with well-defined horns. The Pake pattern collapsed at 70 °C, where the spectrum became a broad single peak. A very small peak was observed at

105

the middle of the broad peak. As the temperature of the sample was increased, the middle

sharp peak started to become more intense, and narrower at higher temperatures. At 90

°C, a relatively sharp single peak was observed indicating that the polymer became more
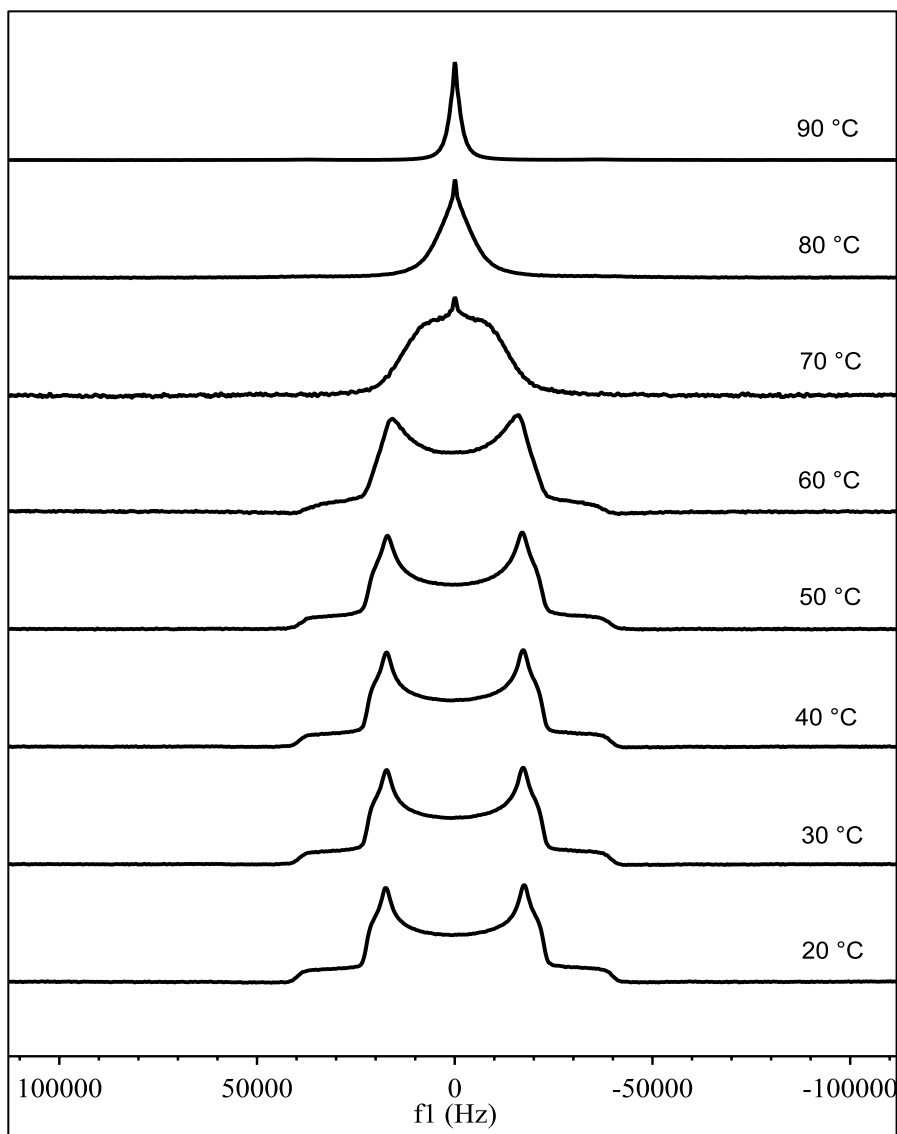
mobile as the polymer become rubbery.

Figure 3. ^{2}H solid-state NMR spectra of bulk PVAc-d_3 as a function of temperature.

The ^{2}H NMR spectra of 34.2%, 50.4%, 70.8%, and 90.7% of PVAc-d_3/graphene

oxide (GO) composites are shown in Figure 4, 5, 7, and 8, respectively. For PVAc-d_3/GO

composites, the ^{2}H NMR spectra looked very different from that of the bulk polymer. For

a composite with a relatively small amount of the polymer (34.2% of PVAc-d_3), the

spectrum had unique features. Unlike the bulk polymer, the Pake pattern had a small peak

at the middle of the broad powder pattern even at 20 °C. As the temperature was

increased from 20 °C to higher temperatures, the intensity of the middle peak increased

with side horns from the powder pattern loosing intensity, but remaining intact. Unlike

the bulk polymer, some intensity of the Pake powder pattern remained intact even at the

highest temperature studied, 130 °C.

As the amount of the polymer increased from 34.2% to 50.4 % of PVAc-d_3, the

majority of the spectra looked similar to that of 34.2%. However, after a careful

examination of the spectra, it was observed that the appearance of the middle peak started

at 30 °C, instead of 20 °C as in 34.2% composite. It is also important to note that the

middle component of the spectrum was more intense for the 34.2% sample than 50.4%

sample. As the temperature increased, the intensity of the middle peak increased while

the intensity of the powder pattern decreased. Unlike that for the bulk polymer, the horns

of the Pake pattern did not disappear completely, and can be observed as weakly intense

signal at 130 °C, which can be clearly observed in the expanded picture of the spectra at
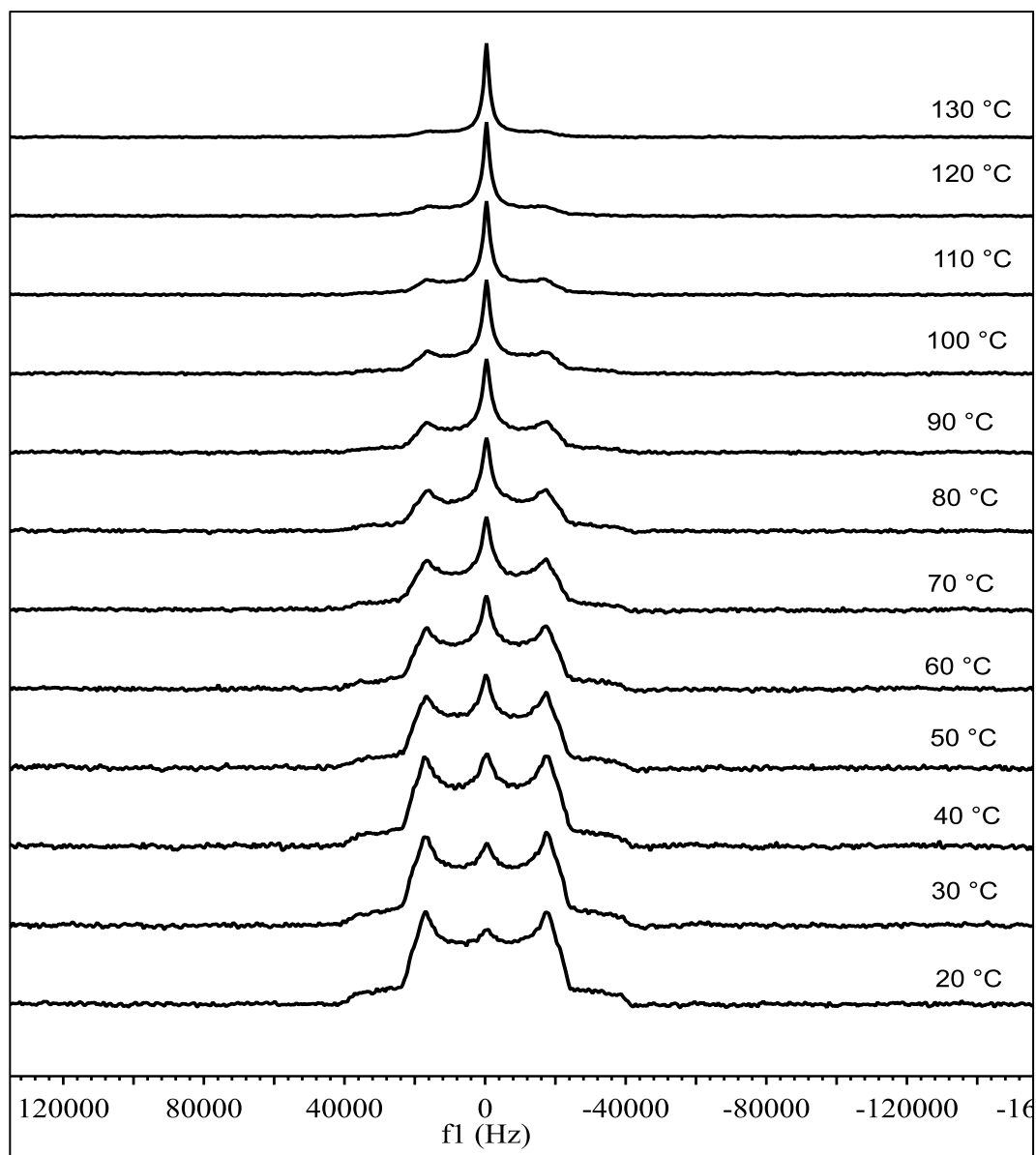
high temperatures, as shown in Figure 6.

Figure 4. ^{2}H solid-state NMR spectra of 32.4% PVAc-d_3/GO composite as a function of temperature.
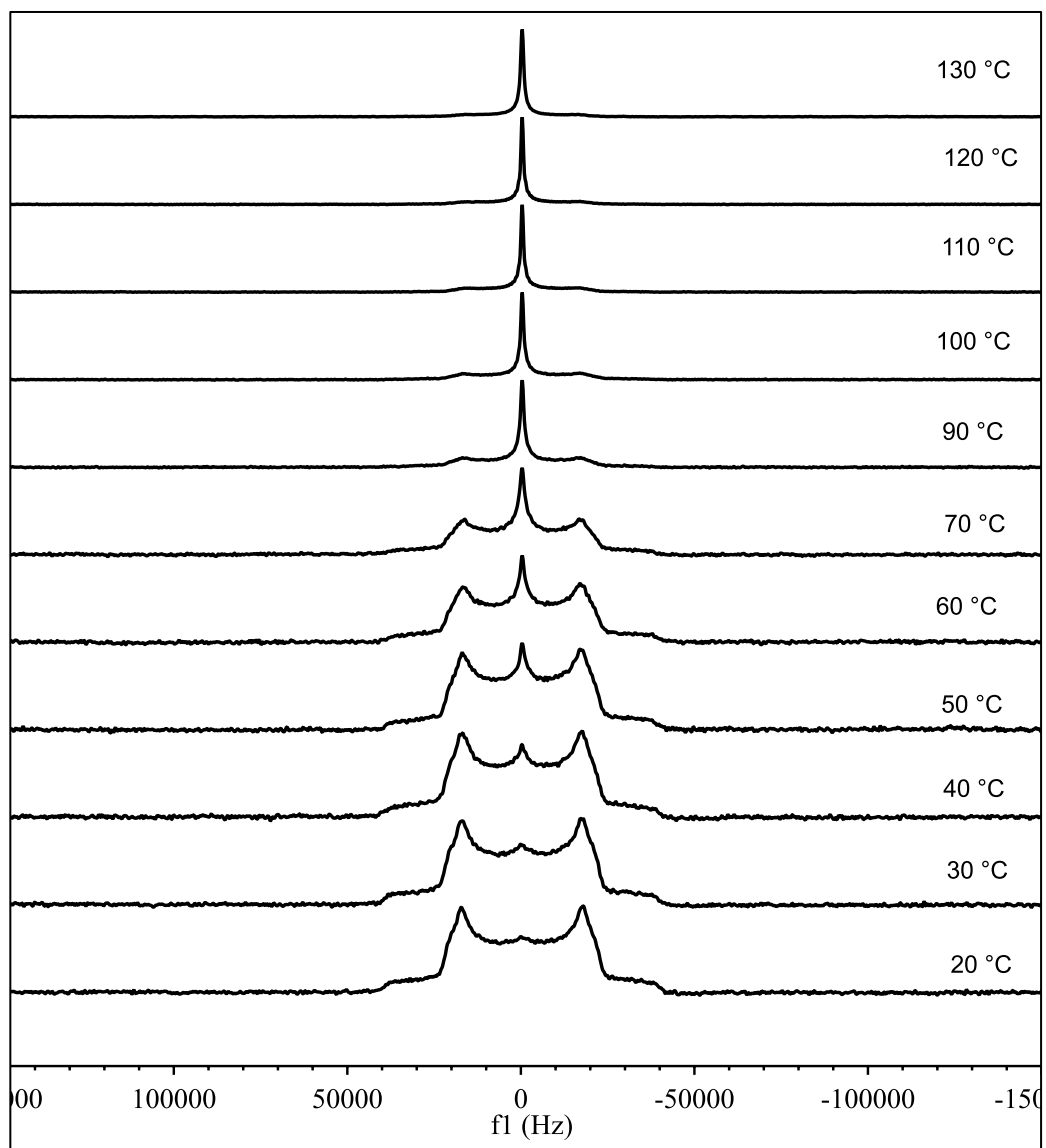
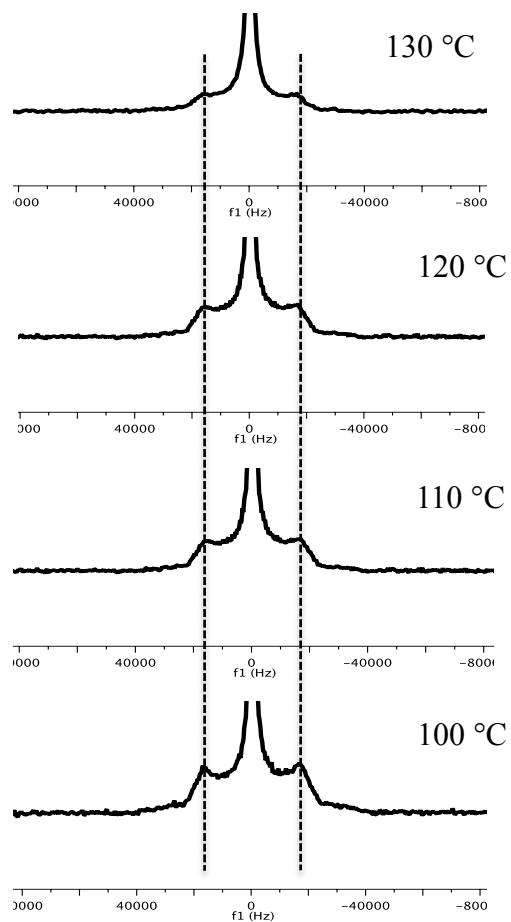Figure 5. ^{2}H solid-state NMR spectra of 50.4% PVAc-d_3/GO composite as a function of temperature.

Figure 6. Expanded view of ^{2}H NMR spectra of 50.4% of PVAc-d3/GO sample taken at higher temperatures.

For the composites with larger amounts of the polymer (70.8 and 90.7% PVAc-d_3), the spectra did not show a central component at 20 °C. For 70.8% polymer as shown in Figure 7, the middle sharp peak appeared at around 50 °C and its intensity increased with increased sample temperatures. When the temperature of the sample reached to 110 °C, the powder pattern was hard to observe resulting a narrow ("liquid-like") peak at the middle. For the 90.7% composite, there was no development of middle peak below the T_g of the bulk polymer as was observed for 70.8% and lower amounts of the polymer/GO

samples. The spectra started to become narrower and collapsed into a single peak at 100 °C. Unlike the bulk polymer, the spectra had a residual powder patterns at 80 and 90 °C, and with that at 90 °C being very weak. The changes in these spectra with increased sample temperature were similar to those of the bulk sample, although a residual Pake pattern was observed at a few degrees higher temperature for the composites with larger amounts of the polymer.
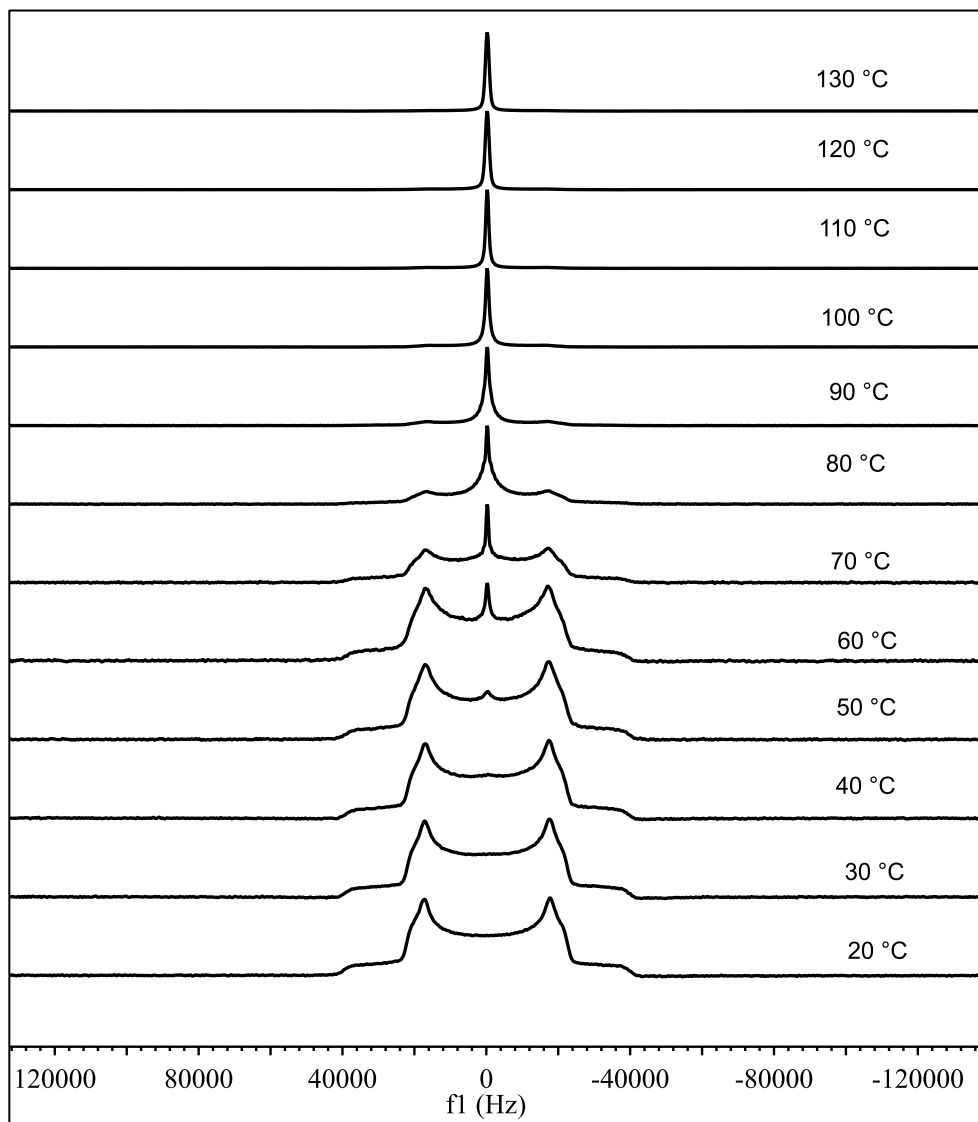

Figure 7. ^{2}H solid-state NMR spectra of 70.8% PVAc-d_3/GO composite as a function of temperature.

111
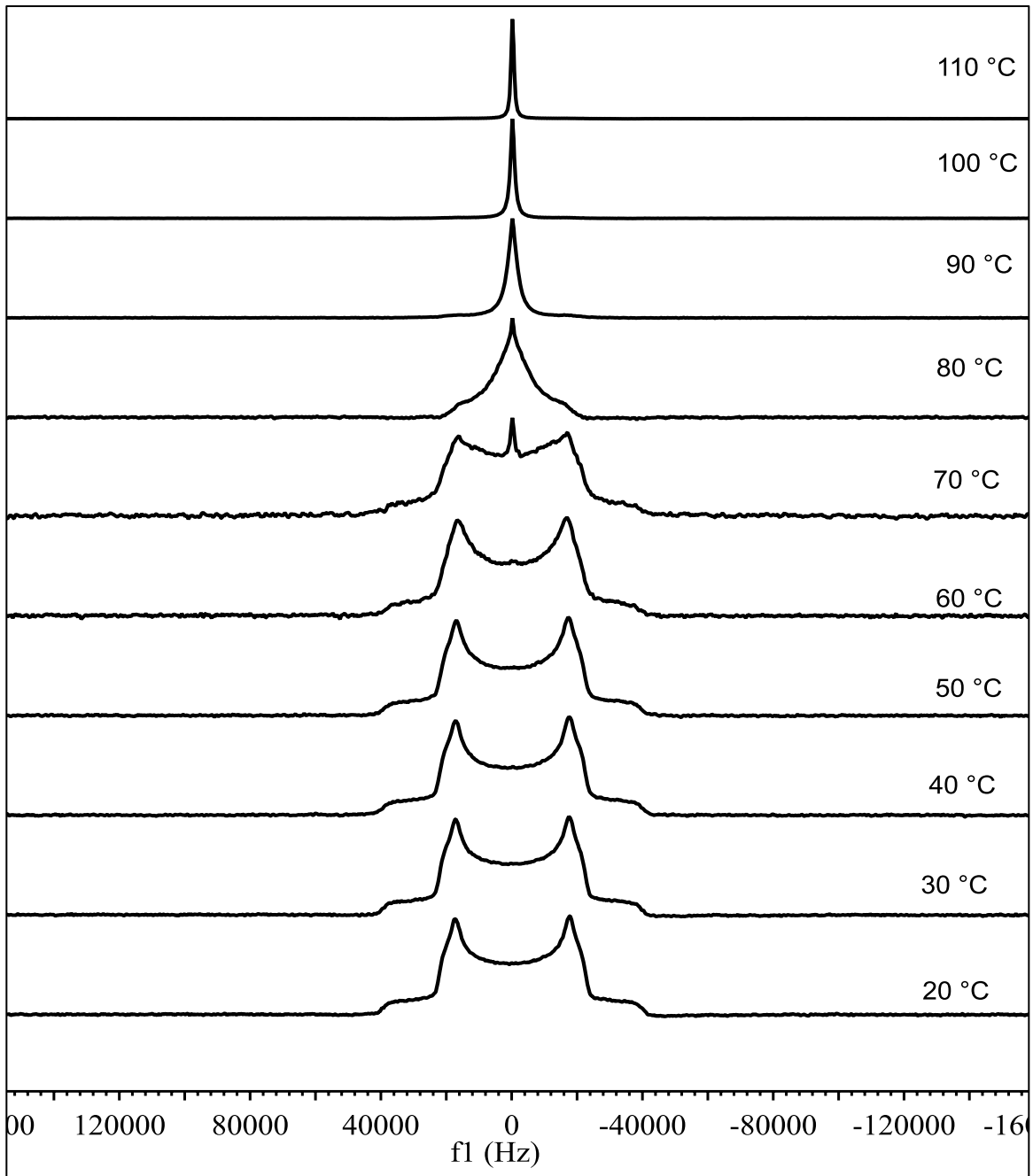
Figure 8. ^{2}H solid-state NMR spectra of 90.7% PVAc-d_3/GO composite as a function of temperature.

The ^{2}H NMR spectra of 50% PVAc-d_3 adsorbed on graphene are shown in Figure 9. The spectra resembled the bulk PVAc-d_3 below 70 °C. The horns of the powder pattern

remained intact at 80 °C, unlike the bulk polymer. The horns disappeared at 90 °C.

Above 90°C, a sharp peak was observed resembling rubbery polymer. This suggested

that the PVAc segments adsorbed on graphene had heterogeneous segmental mobility;

some polymer segments were less mobile (rigid component) than others. However, the

rigid component was not persistent at high temperatures for the PVAc-d_3/graphene
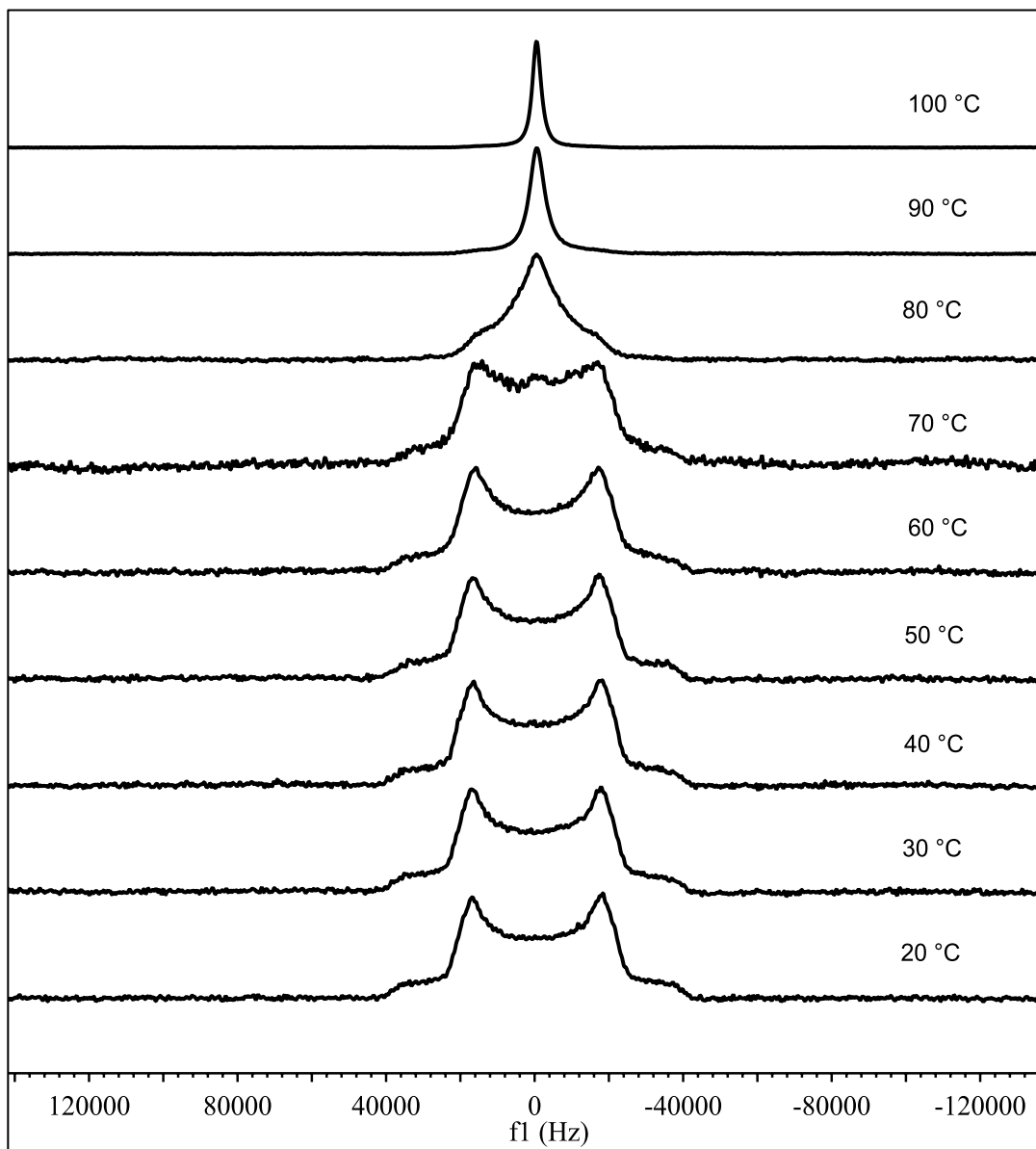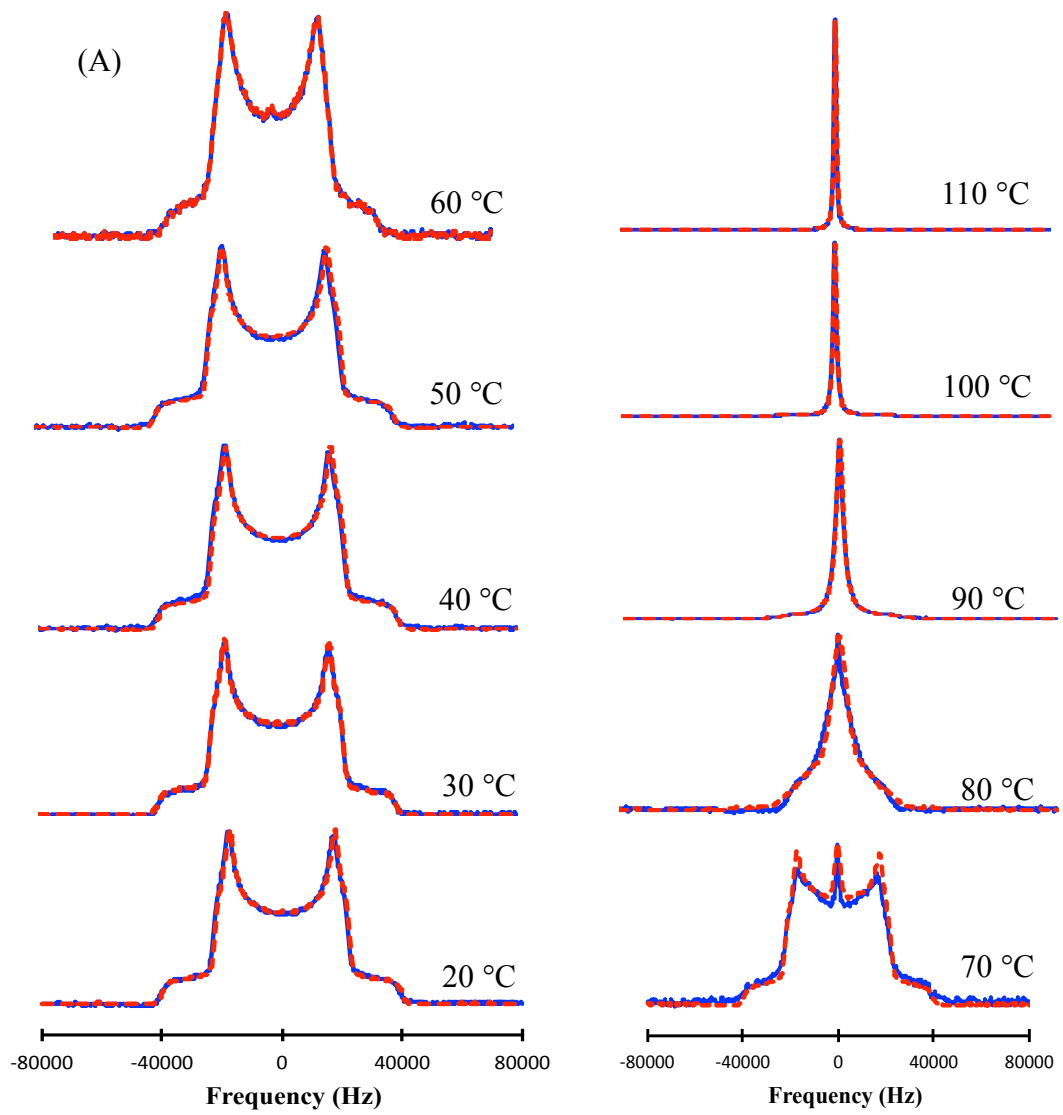
sample as observed for PVAc-d_3/GO samples.

Figure 9. ^{2}H NMR spectra of 50% PVAc-d_3/graphene sample.
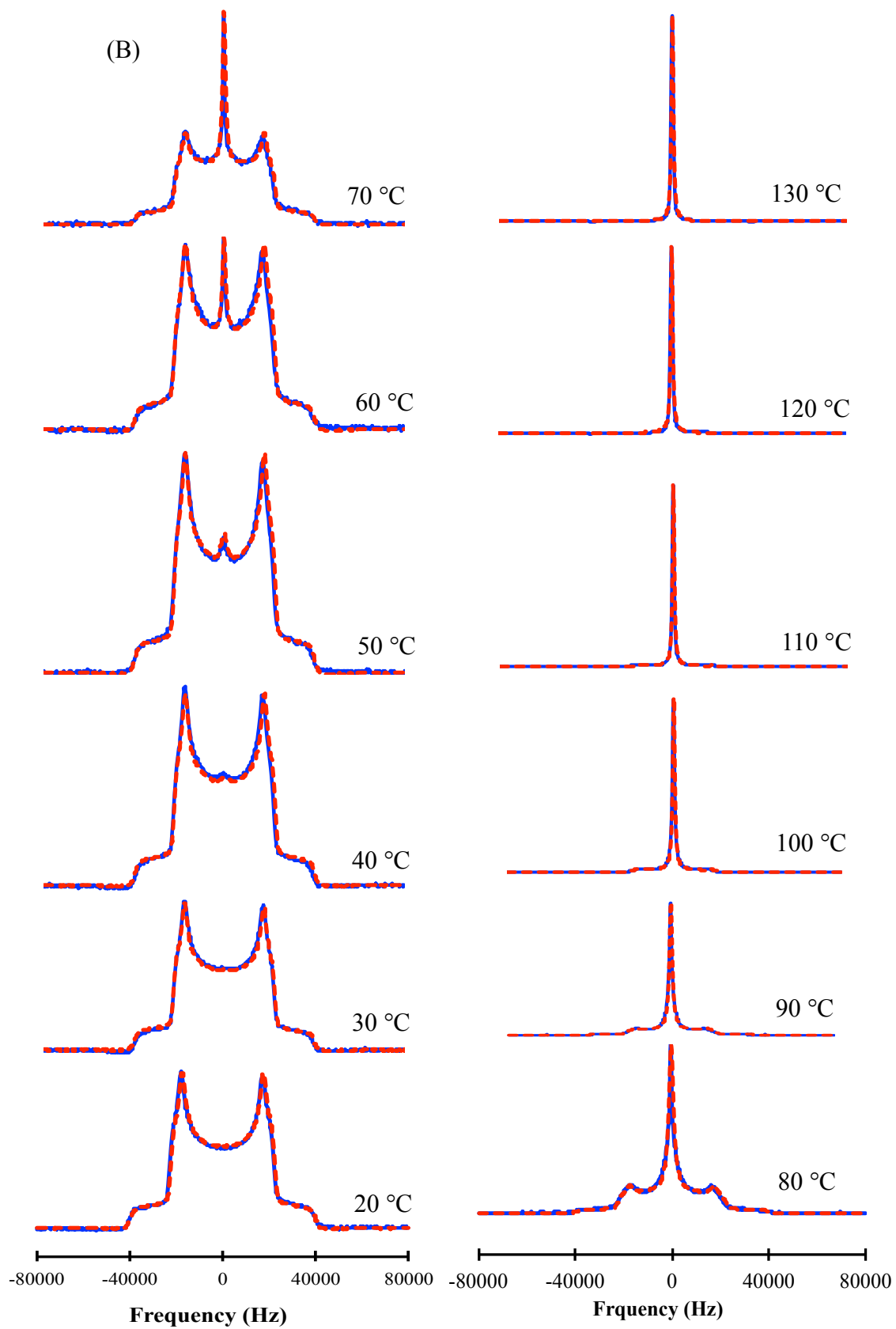
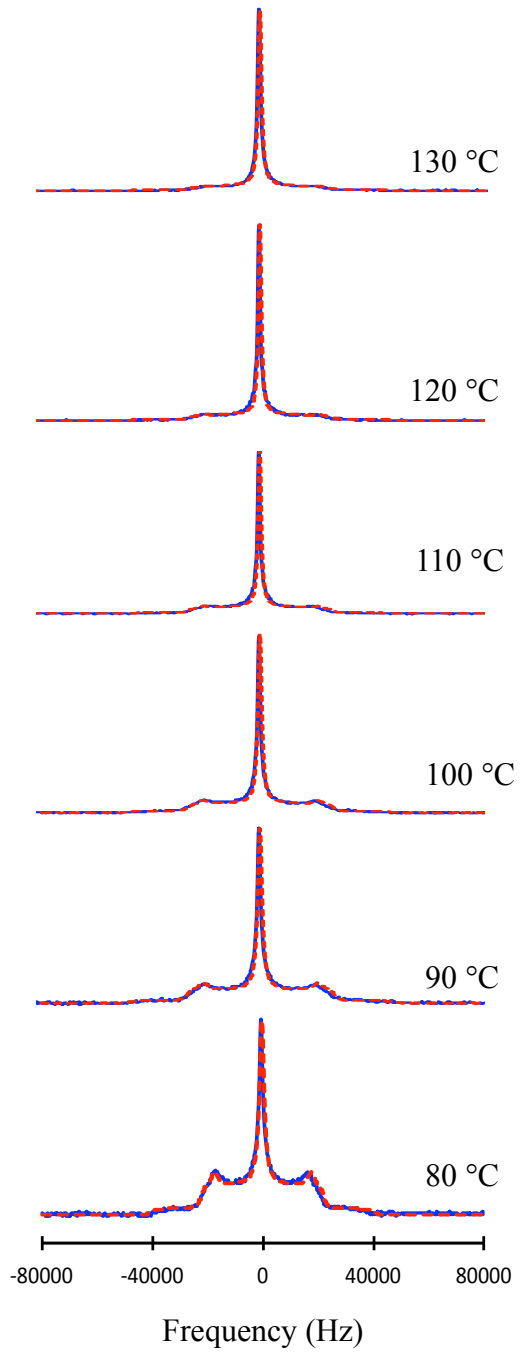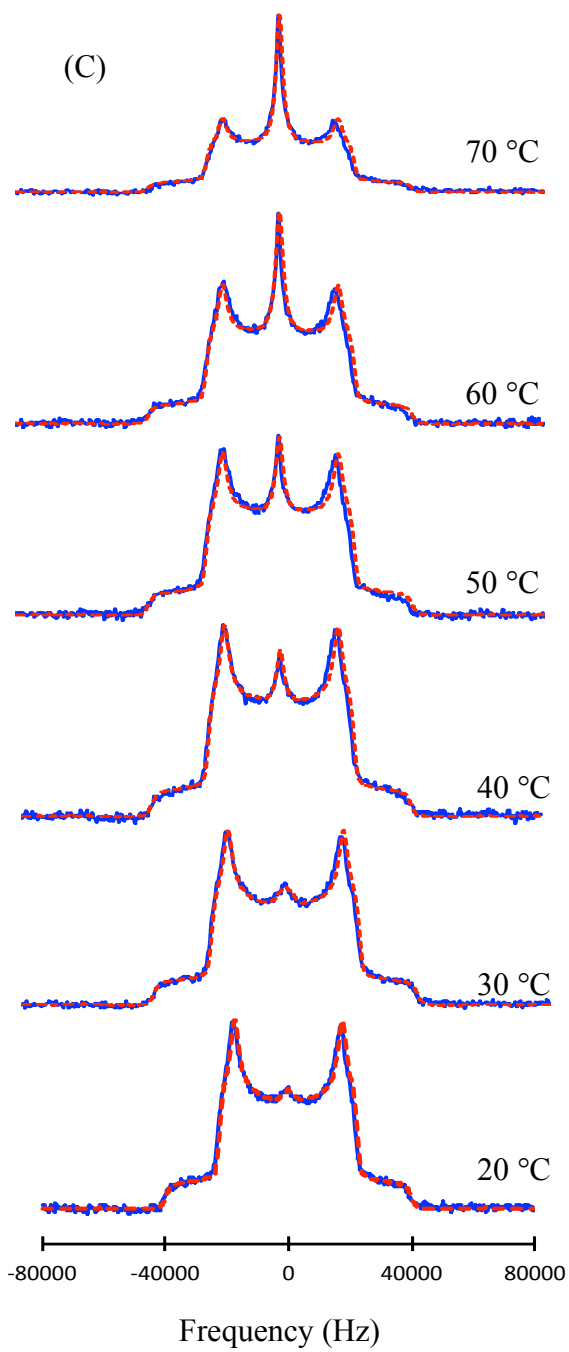### 5.4.3. Fitting of ^{2}H NMR Spectra of Adsorbed PVAc-d_3/GO Samples

As observed from the spectra of 90.7%, 70.8%, 50.4%, and 34.2% PVAc-d_3/GO samples in Figures 4 - 8, the shape of the spectra changed, the amount of mobile component increased, the amount of rigid component decreased, and the depth in between the horns got partially filled as the temperature was increased. Quantitative estimates of the fractions of rigid component, mobile component, and partially mobile component were made by fitting the experimental spectra with a model. The model was based on the combination of rigid component, partially mobile component, and mobile component and was used to fit the spectra of the PVAc-d_3/GO samples. The bulk spectrum at 20 °C was used for the rigid component. For the partially mobile component, the bulk polymer spectra at 70 °C, or combination of 60 and 70 °C were used, and for the mobile component, a Lorentzian function was used. Figure 10 shows the fitting of experimental spectra with the model. All of the spectra were shown to be well-fit with the components chosen.

The fractions of the rigid component, the partially mobile component, and the mobile components were obtained from the best-fit, based on the sum of the square of the residuals, and are shown in Figure 11. As expected, the fraction of rigid component decreased as the temperature increased. The decrease was sudden at 70 °C for 90.7 and 70.8%, and gradual for 50.4% and 34.2% of PVAc-d_3/GO samples. For the 90.7% PVAc-d_3/GO sample, around 14% of rigid component was present at 80 °C. Further increases in temperature resulted in decreased amounts of rigid component, gradually to 3% at 110 °C. Similar results were obtained for 70.8% of PVAc-d_3/GO sample, however, the decrease in the rigid component was a little more gradual. For the 50.4% and 34.2%

PVAc-d_3/GO samples, the fraction of rigid component decreased gradually to 23% and 32% at 130 °C, respectively.
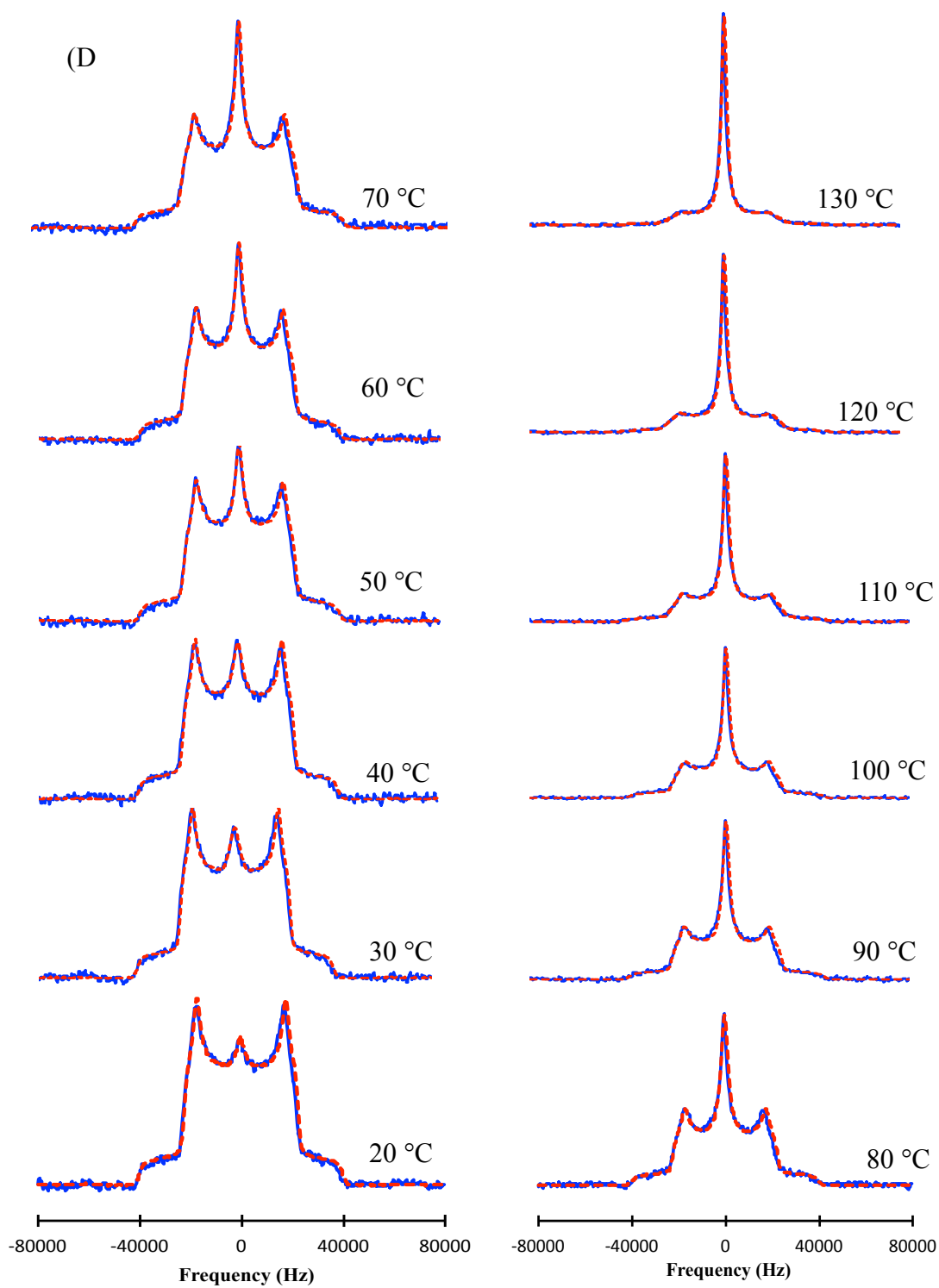

(A)

60 °C
50 °C
40 °C
30 °C
20 °C

110 °C
100 °C
90 °C
80 °C
70 °C

-80000   -40000   0   40000   80000
Frequency (Hz)

-80000   -40000   0   40000   80000
Frequency (Hz)

(B)

70 °C

60 °C

50 °C

40 °C

30 °C

20 °C

130 °C

120 °C

110 °C

100 °C

90 °C

80 °C

Frequency (Hz)

Frquency (Hz)

116

(C)

70 °C

60 °C

50 °C

40 °C

30 °C

20 °C

130 °C

120 °C

110 °C

100 °C

90 °C

80 °C

-80000   -40000   0   40000   80000

Frequency (Hz)

-80000   -40000   0   40000   80000

Frequency (Hz)

117

(D

70 °C

60 °C

50 °C

40 °C

30 °C

20 °C

130 °C

120 °C

110 °C

100 °C

90 °C

80 °C

Frequency (Hz)

Frequency (Hz)

Figure 10. Experimental (——) and simulated (- - - -) ^{2}H NMR spectra for (A) 90.7% PVAc-d_3/GO, (B) 70.8% PVAc-d_3/GO, (C) 52.4% PVAc-d_3/GO, and (D) 34.2% PVAc-d_3/GO.

The fraction of the mobile portion increased as the temperature increased. The increase was rapid at around 70 °C for the 90.7% and 70.8% of PVAc-d_3/GO samples. The fractions of mobile component reached 95% at 110 °C for 90.7% of PVAc-d_3/GO sample. For the 70.8% PVAc-d_3/GO sample, the fraction of mobile component reached 92% at 130 °C. The increment of the fraction of the mobile component was gradual for 50.4% and 34.2% of PVAc-d_3/GO samples as the temperature increased from 20 °C. However, the mobile components appeared at lower temperatures. The fractions of mobile components for the 50.4% and 34.2% of PVAc-d_3/GO samples were around 60% and 50% at 130 °C, respectively.

For adsorbed PVAc-d_3/GO samples, as the temperature of the samples increased from 20 °C, the depth in between the horns of the powder pattern got filled in due to the presence of polymer segments that are less mobile than rubbery polymer and more mobile than glassy polymer (partially mobile polymer segments). For majority of the fits, the spectra at 70 °C of the bulk polymer was used to fit the partially mobile polymer. However, for the spectra of 90.7%, 70.8%, and 34.2% of PVAc-d_3/GO samples at few temperatures, the spectrum at 60 °C in combination with the 70 °C spectrum of the bulk polymer was used. The fraction of the partially mobile component contributed from 60 °C bulk spectrum is reported in Table 1. Figure 11 (C) shows the plot of the fraction of partially mobile component as a function of temperature. For all other compositions except for 90.7% of PVAc-d_3/GO, the fraction of partially mobile component was relatively small (2.5 to 18%) as compared to the mobile and rigid component. For the 90.7%, the fraction of partially mobile component was as big as 38% and 55% at 70 and 80 °C, respectively, and was smaller at other temperatures.
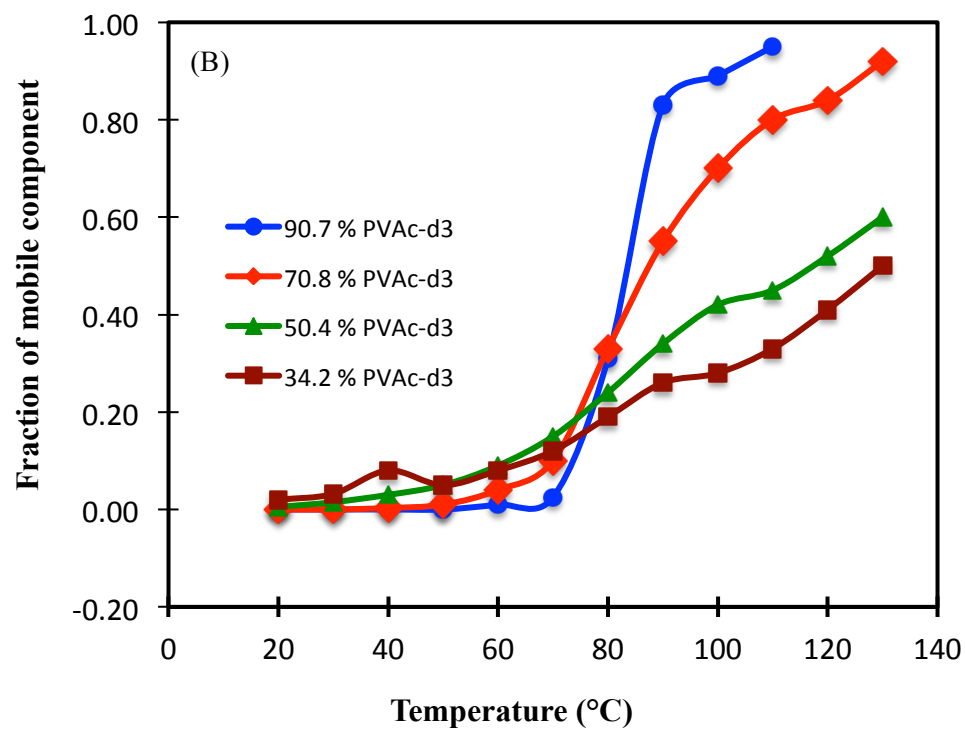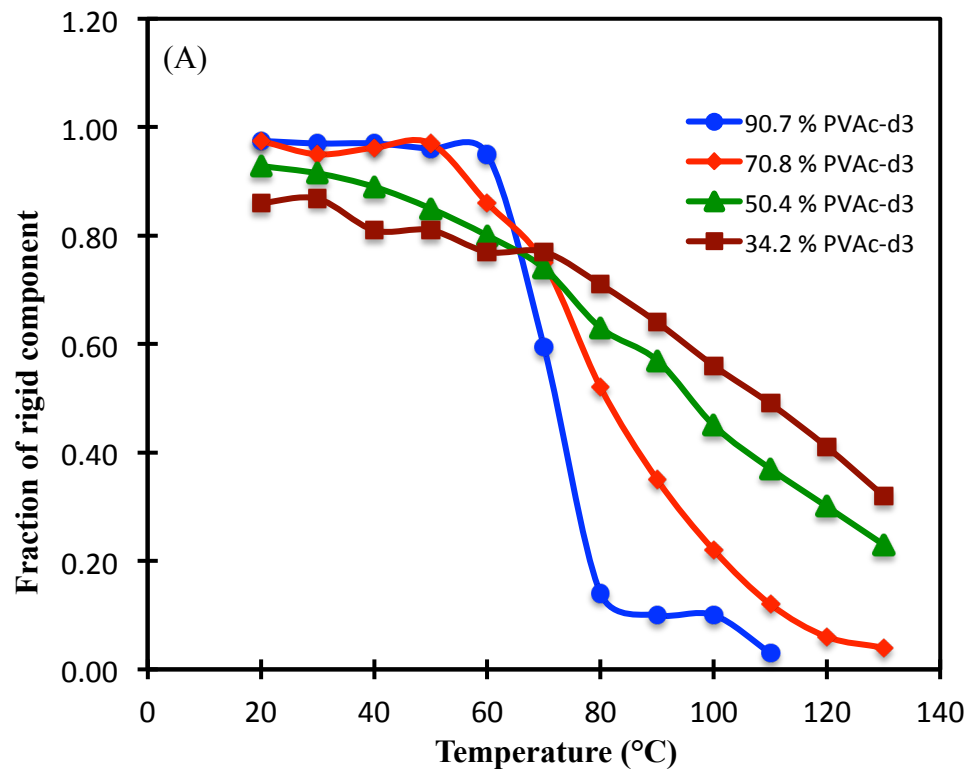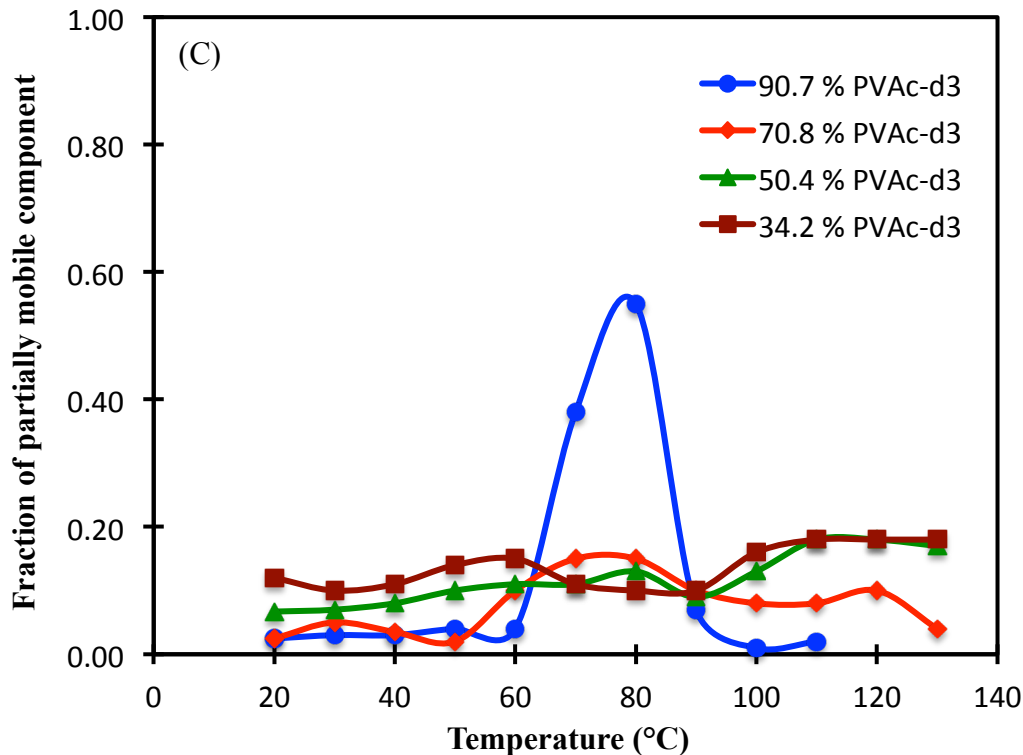
Figure 11. Fractions of (A) rigid component (bulk 20 °C spectrum), (B) partially mobile component (bulk 70 °C, or 60 °C and 70 °C spectra), and (C) mobile component ("liquid-like", Lorentzian function) of polymer segments for 90.7%, 70.8%, 50.4% and 34.2% of PVAc-d_3 adsorbed on GO at different temperatures.

Table 1. Fractions of the partially mobile components obtained using the bulk 60 °C and 70 °C spectra to fit the experimental curves. Combinations of the rigid component (bulk 20 °C spectrum), partially mobile component (bulk 60 °C and 70 °C spectra), and mobile components ("liquid-like", Lorentzian function) were used. The numbers in parentheses represent the fraction of partially mobile component obtained from the bulk 70 °C spectrum and that outside the parentheses represent the fraction of partially mobile component obtained from bulk spectrum at 60 °C. The total fraction of the partially

mobile component was obtained by adding these two fractions (fractions obtained from 60 and 70 °C).

Temperature	Amounts of PVAc-d_3 adsorbed on GO (%)			
(°C)	90.7% PVAc-d_3	70.8% PVAc-d_3	50.4% PVAc-d_3	34.2% PVAc-d_3
20 °C	0.00 (0.025)	0.00 (0.025)	0.00 (0.067)	0.03 (0.090)
30 °C	0.00 (0.030)	0.00 (0.050)	0.00 (0.070)	0.00 (0.100)
40 °C	0.00 (0.030)	0.00 (0.035)	0.00 (0.080)	0.05 (0.080)
50 °C	0.03 (0.010)	0.00 (0.020)	0.00 (0.100)	0.05 (0.090)
60 °C	0.05 (0.000)	0.10 (0.000)	0.00 (0.110)	0.06 (0.090)
70 °C	0.12 (0.260)	0.04 (0.110)	0.00 (0.110)	0.02 (0.090)
80 °C	0.00 (0.550)	0.00 (0.150)	0.00 (0.130)	0.05 (0.050)
90 °C	0.00 (0.070)	0.00 (0.100)	0.00 (0.090)	0.05 (0.050)
100 °C	0.00 (0.010)	0.00 (0.080)	0.00 (0.130)	0.06 (0.100)
110 °C	0.00 (0.020)	0.00 (0.080)	0.00 (0.180)	0.13 (0.060)
120 °C	NA	0.00 (0.100)	0.00 (0.180)	0.13 (0.060)
130 °C	NA	0.00 (0.040)	0.00 (0.170)	0.13 (0.060)

5.4.4. X-ray Diffraction (XRD) Analysis

The X-ray diffraction (XRD) analysis of graphene and graphene oxide is shown in Figure 12. As observed from the figure, graphene had a characteristic peak at two theta (2θ) of 26.4°, which corresponds to an inter-laminar thickness of 3.4 Å. This is a typical value for graphene and is consistent with other measurements.[40-42] For GO, the intensity of the scattering was significantly reduced and the peak was broader as compared to that

of the graphene. This suggested that GO was more disordered than graphene. The 2θ

value of the GO was 10.5°, which resulted to an inter-laminar spacing of 8.4 Å. This is a

typical peak for GO and is similar with the measurements by Silva et al., and Cui et

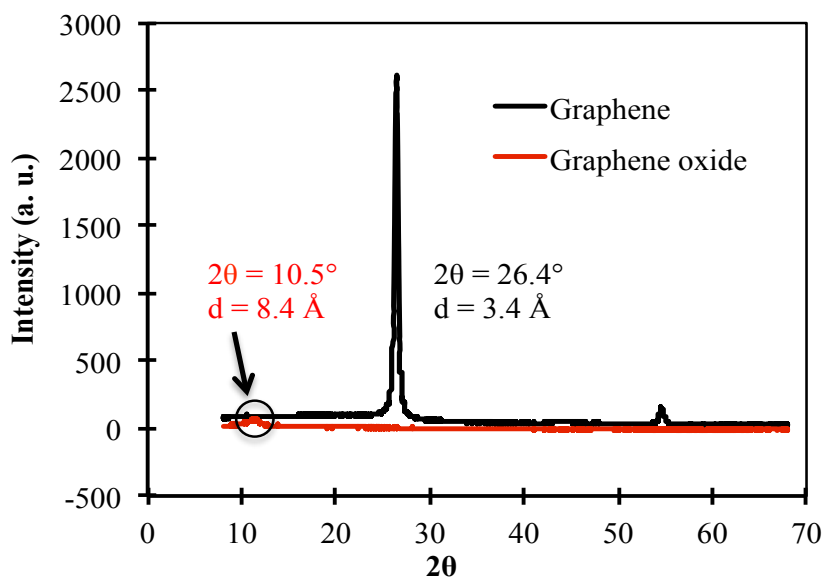al.[43,44] The oxidation of GO increased the inter-laminar spacing of graphene.

Figure 12. X-ray diffraction (XRD) analysis of graphene and GO.

The XRD pattern of bulk PVAc, PVAc adsorbed on GO (90.7%, 70.8%, 50.4%,

and 34.2% of PVAc), and bulk GO is shown in Figure 13. For the bulk GO, a relatively

sharp peak at 2θ value of 10.5° was obtained. For the bulk PVAc, two peaks at 2θ values

of 10.8° and 22.7° were observed. The peaks were broad over a wide range of 2θ values.

For amorphous polymers, it is common to observe this kind of X-ray amorphous powder

pattern. The pattern is believed to be due to the diffraction from few groups (polymer

segments) that are ordered locally over a short distance.[45,46] For the 90.7%, 70.8%, and

50.4% PVAc adsorbed on GO, peaks similar to the bulk polymer were observed. As the

amount of the polymer decreased to 34.2%, the shape of the peaks changed compared to

the bulk polymer. The peaks collapsed into a broad bump for the 34.2% PVAc sample. This might be due to the change in the structure of the polymer segments when adsorbed on GO and was clearly observed when the amount of the polymer was smaller. For the PVAc/GO samples, the peak from GO was completely disappeared, which suggested that the GO is exfoliated when polymer was adsorbed.
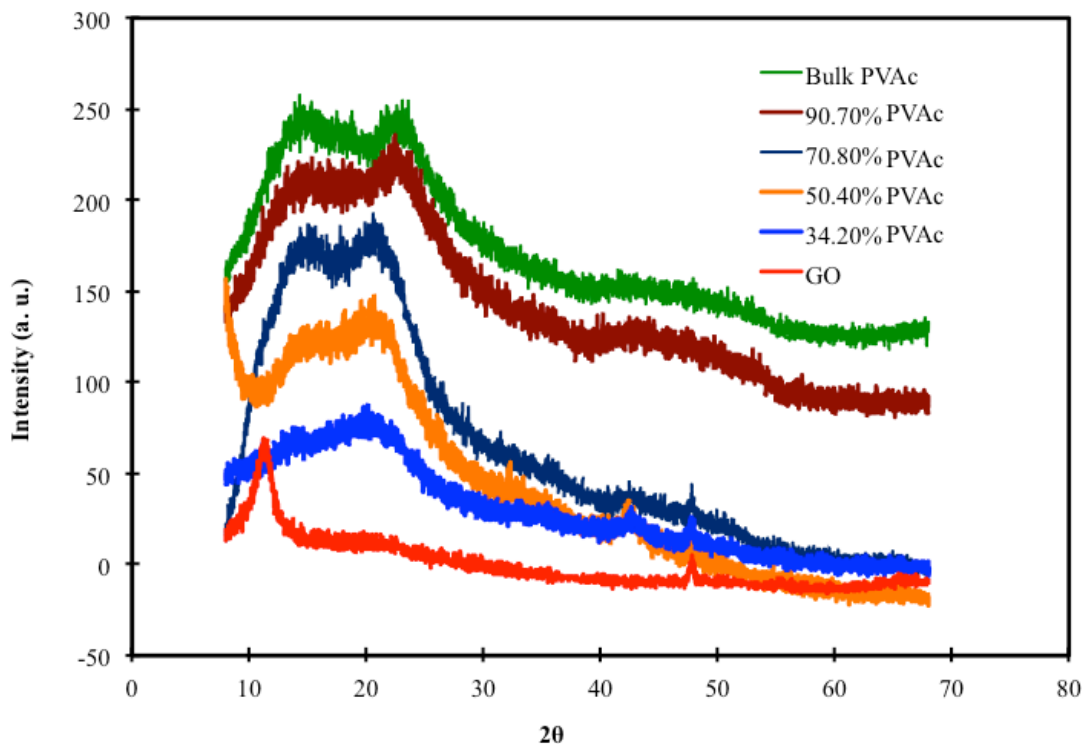

Figure 13. X-ray diffraction (XRD) analysis of bulk PVAc, 90.7%, 70.8%, 50.4%, and 34.2% of PVAc/GO, and bulk GO. The order of the legend is same with the order of the plot (in the 20 - 40° range).

Small angle X-ray scattering (SAXS) was carried out to see if the adsorption of PVAc on GO increased the inter-layer spacing of GO to the range where it could be observed for small 2θ values. Figure 14 shows the SAXS pattern of the samples that were used for the XRD analysis in Figure 13. As observed from the plot, there was no shifting

of the GO peaks to the smaller 2θ values in the range where they can be measured. The peaks, if any existed, were out of the range of 2θ values studied. This result suggests that the GO was likely exfoliated and the GO sheets were farther apart from each other such that they did not scatter X-rays detectable with SAXS.
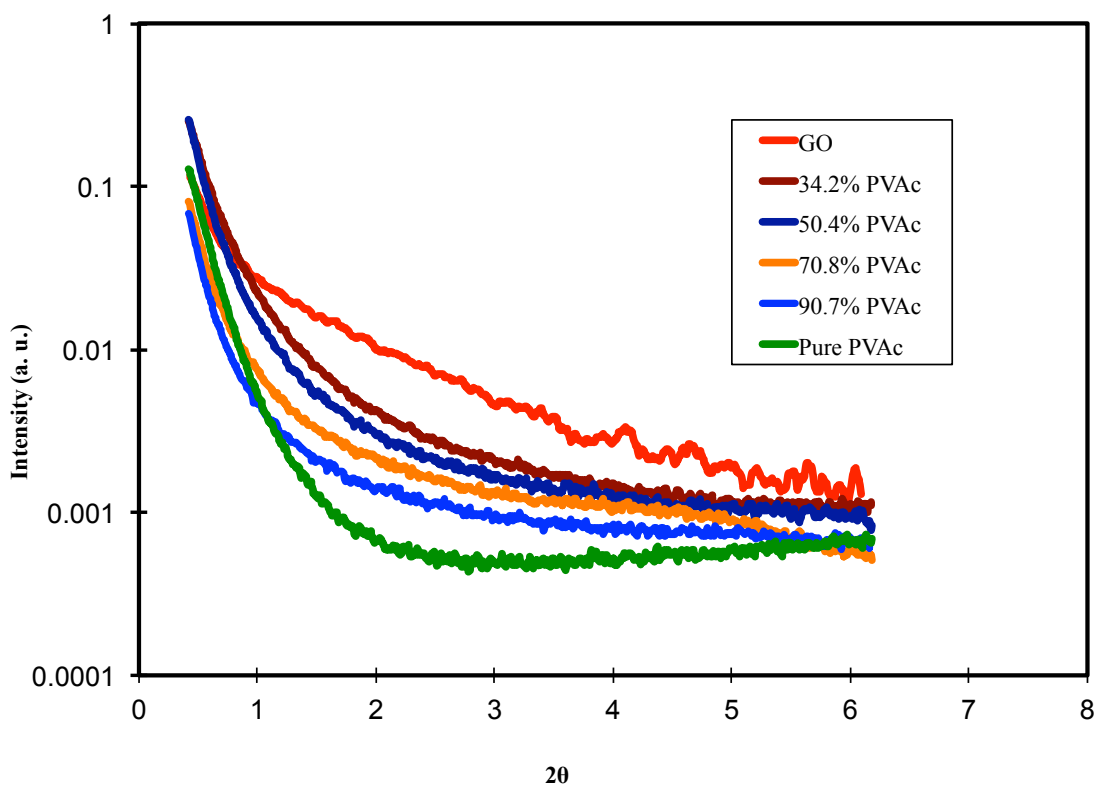

Figure 14. SAXS of bulk PVAc, 90.7%, 70.8%, 50.4%, and 34.2% of PVAc/GO, and bulk GO. The order of the legend is representative of the order of the plot (in the 2 – 4° range).

The distance between the GO sheets in PVAc/GO samples can be approximately calculated using the mass fractions of the polymer and the GO and their respective densities. The density of PVAc is well known as 1.2 g/cm^3. The density of the single layer of GO can be calculated approximately using theoretical specific surface area (SSA)

(2630 m²/g)[47,48] of graphene and thickness of the single layer of GO. The thickness (d)

of the single layer of the GO was obtained from Figure 12 and was 8.4 Å. The density of

a single layer of GO was calculated from the specific surface area (2630 m²/g) and the

thickness of the single layer (8.4 Å), (SSA/d). For GO, the calculated value was 0.45

g/cm³. Assuming that the entire polymer goes in between the sheets, a maximum repeat

distance for the sheets may be estimated by:

$$V_P = \frac{M_P / \rho_P}{M_P / \rho_P + M_{GO} / \rho_{GO}}$$

$$V_{GO} = \frac{M_{GO} / \rho_{GO}}{M_P / \rho_P + M_{GO} / \rho_{GO}}$$

(1)

where, V, M and ρ with the subscripts p and GO represent volume fractions, mass

fractions and densities of the polymer (p) and GO, respectively. For 34.2% of PVAc/GO

sample, the volume fraction of the polymer (calculated using Equation 1) was 16.3%.

Using the volume fraction of the polymer, the inter-layer spacing of the GO for 34.2% of

PVAc/GO composite was calculated and was found to be 9.8 Å, which corresponds to the

2θ value of 9°. From similar calculations, the inter-laminar spacing of GO sheets in

50.4%, 70.8%, and 90.7% of PVAc/GO samples were obtained, which were 10.8 Å, 12.4

Å, and 15.0 Å, respectively. The corresponding 2θ values were 8.1°, 7.0°, and 5.7°,

respectively. However, no peaks were observed at 2θ values of 9° and 8.1°, these peaks

should have been observed if they existed, in Figure 13. Similarly no peak corresponding

2θ value of 5.7° was observed in Figure 14. This suggests that the GO sheets might have

randomly oriented (no regular repeating sheets) when polymer was adsorbed on GO.

5.5. DISCUSSION

The Pake pattern of bulk PVAc-d_3 (at 20 °C) consists of horns separated by 44.3 kHz from each other as shown in Figure 2. This powder pattern is similar to that for a methyl group undergoing fast threefold rotational motion about the methyl group's symmetry axis, which reduces the quadrupolar coupling constant (QCC) to one third of its static analogue. The Pake powder pattern of PVAc-d_3 possesses an unusual feature in which the top of the Pake pattern is curved inwards. Similar results have been reported for the ^{2}H Pake powder pattern of the bulk PVAc-d_3.[38] ^{2}H NMR studies by Hiyama et al.[49] on thymine-d_3, and aspirin-d_3 and asprin-d_3-β-cyclodextrin by Kitchin and Halstead[50] have shown that the top of the Pake powder pattern of deuterated methyl group are curved inwards. This effect was due to the interaction of methyl deuterons with the carbonyl oxygens of these materials and the interaction between them becomes anisotropic. The deuterons close to the carbonyl oxygen can be modeled with a change in both QCC and anisotropy factor (η) compared to the two other deuterons leading to decrease in separation between the horns.[38] Another explanation was that it could be due to the interactions between deuteron and carbonyl oxygen that caused a distortion from its (methyl group) tetrahedral geometry[51] with no change in the axial symmetry of the electric field gradient. Nevertheless, these spectra are different than the spectra for a methyl group undergoing fast rotation about its symmetry axis.

For bulk PVAc-d_3, the powder pattern became narrower and collapsed into a single peak at around 70 °C, which was consistent with previous result obtained by Blum et al.[38] This temperature can be expressed as the T_g of the polymer on the NMR timescale (T_g NMR). Over a 10 °C temperature increase, the peak changed to a sharp

narrow peak, resembling "liquid-like" spectrum. The narrowing of the spectra was an indicative of polymer segments gaining additional mobility, as the polymer enters rubbery state with more mobile polymer chains. The T_g (NMR) of the polymer was about 28 °C higher than that measured by DSC (T_g DSC = 42.8 °C), which was because of the different frequencies involved in these measurements.[52] In a typical TMDSC run, the sample was heated at a ramp rate of 3 °C/min which is a few Hz or less. The collapse of the powder pattern was indicative of motion faster than the reciprocal of Pake pattern splitting (37.6 kHz). On the NMR timescale, the polymer went from a glassy state to a rubbery state (Pake pattern to a sharp "liquid-like" peak) at a higher temperature than in TMDSC.

For the polymer/GO composites, the changes in ^{2}H powder pattern with temperature were significantly different than those of the bulk polymer. The transition from a solid powder pattern to a narrower component was not distinct as for the bulk polymer. Instead, the narrower component developed at a temperature lower than bulk T_g and its intensity increased slowly with increased temperature while the horns of the powder pattern diminished in intensity, but persisted even at higher temperatures. This type of the intensity change indicated that the sample had polymers with heterogeneous mobility. Some segments of the polymer were more mobile than the bulk polymer, while some segments had reduced mobility. The heterogeneity of the sample was more evident when the amounts of polymer were smaller.

The results for PVAc-d_3/GO samples were interesting and different than those for PVAc-d_3/silica composites. For PVAc/silica composites, when the composition of PVAc was 20% or more, the ^{2}H NMR spectra resembled the bulk-like polymer. For PVAc/GO

samples, the spectra resemble that of bulk PVAc-d_3 when the composition of PVAc-d_3 was around 90%. Moreover, the start of the development of more mobile polymer was at relatively lower temperature for PVAc-d_3/GO samples (20 °C for 34.2% PVAc-d_3) as compared to the PVAc-d_3/silica samples (60 °C for 26.6% PVAc-d_3).[53] The anomalous behavior of the PVAc-d_3/GO composite was also clearly observed in the MDSC study, as shown in Figure 1. The glass transition intensity of PVAc-d_3/GO was significantly reduced when the amount of the polymer was 90.7 and 70.8%; and it was hard to distinguish (almost gone) the glass transition behavior of the composites when the amounts of the polymer were 50.4 and 34.2%. These results were different than those observed for PVAc/silica composites, in which a bulk-like glass transition behavior was observed when the amounts of the polymer was 20% or higher.[54]

The interactions of the PVAc with GO oxide layers may explain the anomalous glass transition behavior of the PVAc-d_3/GO composites. The GO has a hydrophilic surface and has a various polar functional groups such as -COOH, -OH, -COR, -COH, and epoxide, etc. Due to the presence of hydrophilic functional groups (esters) in the PVAc as well, the polymer can strongly interact with GO via H-bonding and/or dipole-dipole interactions. The polymers strongly interacting with GO were rigid and hence had restricted mobility, and these were more prominent when the amount of the polymer was less. In addition, there were some polymer segments that were more mobile than bulk polymer. There could be two possible reasons for obtaining more mobile polymer. First, it could be because some polymer segments, which were actually not interacting with the graphene sheets and were more mobile as the segments were unbound as shown in Figure 15. Second, it is possible that the basal plane of the graphene sheets may not be

completely oxidized leaving some areas of significant graphene structures. Since PVAc is a slightly hydrophilic polymer, it may not interact or weakly interact with graphene leading to non-restricted polymer with increased mobility as shown in Figure 16. Thus, it seems that GO interactions are responsible for both more mobile and less mobile behavior.
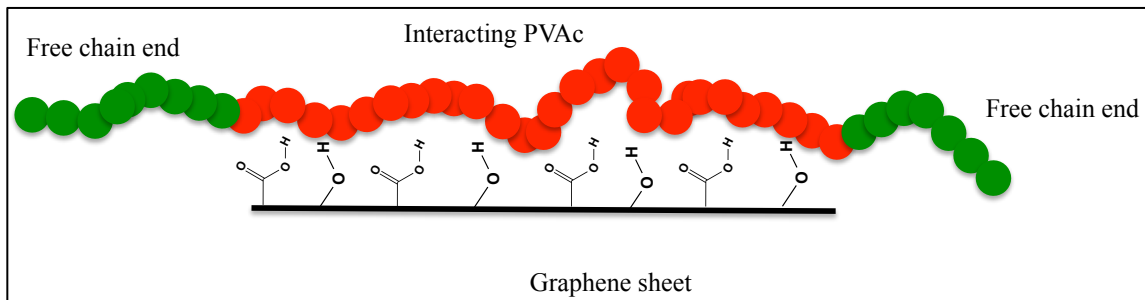

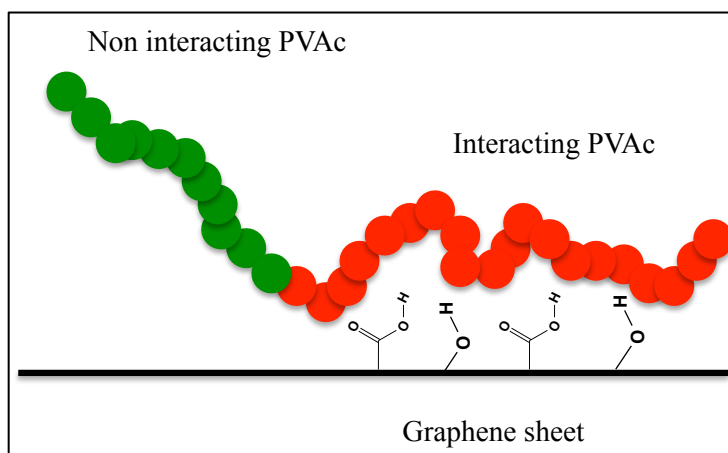Figure 15. Pictorial representation of the PVAc adsorbed on GO showing some polymer chain ends that are unbound.

Figure 16. Pictorial representation of PVAc adsorbed on partially oxidized GO. The partially oxidized GO contains some fraction of graphene surface; PVAc being a hydrophilic polymer does not bind to the hydrophobic graphene surface.

To understand the interaction of PVAc-d_3 with graphene, a PVAc-d_3/ graphene composite (50% of PVAc-d_3 w/w) was made by mixing graphene with PVAc-d_3 with tetrahydrofuran (THF) as the solvent. Prior to mixing with the polymer, the graphene was dispersed in N-methyl pyrrolidone (NMP) and re-dispersed in THF.[7] Figure 9 shows the ^{2}H NMR spectra of 50% PVAc-d_3/graphene composite. The spectra looked similar to that of the bulk polymer except that there was a small residual shoulder of Pake powder pattern at 80 °C. As the temperature was increased, the shoulder vanished, and a sharp peak was observed at 90°C resembling spectrum of a polymer in the rubbery state. This result suggested that the polymer might have not interacted with graphene or if it interacted, the interaction was very weak and did not affect the segmental motion of the polymer. XRD was carried out to understand if the polymer intercalated in-between the graphene layers (not shown). The peak for graphene ($2\theta = 26.4°$) did not change its position for 50% PVAc/graphene sample, which suggested that the polymer was not intercalated in-between the graphene layers. This also suggested that the polymer did not bind to graphene.

Various studies have been conducted to understand the effect of GO on different properties such as mechanical properties, gas barrier properties, thermal properties, and electrical properties of the polymers intercalated in GO.[18,20,21,26,27,37,55-58] Significant increases in the mechanical and gas barrier properties have been observed with incorporation of GO as low as 1-2%.[20,22,25,27,37]. However, the reason for enhancement in the properties of polymers due to incorporation of GO was not fully understood. From this study, it has been observed that the strong interactions between the polymer and the GO might have resulted in the enhancement of the properties of polymers.

5.6. CONCLUSIONS

The PVAc-d_3 segments incorporated with graphene oxide (GO) were very heterogeneous; some polymer segments were more mobile and some segments were less mobile than that of the bulk polymer. The heterogeneous behavior of the polymer segments was clearly observed from ^{2}H NMR measurements. The Pake powder pattern of the PVAc-d_3/GO composites persisted at relatively high temperatures, especially for 50.4 and 34.2% of PVAc-d_3/GO samples, due to the restriction in the mobility of the polymer segments caused by the polymer strongly interacting with the GO. The ^{2}H NMR spectra of these composites also possessed peaks from the polymer segments that are more mobile than the bulk PVAc-d_3. The presence of the polymer segments that are more mobile than that of the bulk polymer might be due to the weak interactions of the polymer with graphene surfaces that were left unoxidized while preparing GO. However, such heterogeneous behavior of the polymer segments was not clearly observed from DSC measurements. It might be due to the different level of sensitivity of the instruments used, DSC being less sensitive than NMR.

5.7. REFERENCES

(1) Khan, U.; Porwal, H.; O'Neill, A.; Nawaz, K.; May, P.; Coleman, J. N. *Langmuir* **2011**, *27*, 9077-9082.

(2) Hernandez, Y.; Nicolosi, V.; Lotya, M.; Blighe, F. M.; Sun, Z.; De, S.; McGovern, I. T.; Holland, B.; Byrne, M.; Gun'Ko, Y. K.; Boland, J. J.; Niraj, P.; Duesberg, G.; Krishnamurthy, S.; Goodhue, R.; Hutchison, J.; Scardaci, V.; Ferrari, A. C.; Coleman, J. N. *Nat. Nanotechnol.* **2008**, *3*, 563-568.

(3) Lotya, M.; Hernandez, Y.; King, P. J.; Smith, R. J.; Nicolosi, V.; Karlsson, L. S.; Blighe, F. M.; De, S.; Wang, Z.; McGovern, I. T.; Duesberg, G. S.; Coleman, J. N. *J. Am. Chem. Soc.* **2009**, *131*, 3611-3620.

(4) Vadukumpully, S.; Paul, J.; Mahanta, N.; Valiyaveettil, S. *Carbon* **2011**, *49*, 198-205.

(5) Lee, H. B.; Raghu, A. V.; Yoon, K. S.; Jeong, H. M. *J. Macromol. Sci. Phys.* **2010**, *49*, 802-809.

(6) Wang, J.; Shi, Z.; Ge, Y.; Wang, Y.; Fan, J.; Yin, J. *Mater. Chem. Phys.* **2012**, *136*, 43-50.

(7) Khan, U.; May, P.; Porwal, H.; Nawaz, K.; Coleman, J. N. *ACS Appl. Mater. Inter.* **2013**, *5*, 1423-1428.

(8) Zheng, W.; Wong, S.-C. *Compos. Sci. Technol.* **2003**, *63*, 225-235.

(9) Wajid, A. S.; Das, S.; Irin, F.; Ahmed, H. S. T.; Shelburne, J. L.; Parviz, D.; Fullerton, R. J.; Jankowski, A. F.; Hedden, R. C.; Green, M. J. *Carbon* **2012**, *50*, 526-534.

(10) Potts, J. R.; Lee, S. H.; Alam, T. M.; An, J.; Stoller, M. D.; Piner, R. D.; Ruoff, R. S. *Carbon* **2011**, *49*, 2615-2623.

(11) Hummers, W. S.; Offeman, R. E. *J. Am. Chem. Soc.* **1958**, *80*, 1339-1339.

(12) Wang, S.; Tambraparni, M.; Qiu, J.; Tipton, J.; Dean, D. *Macromolecules* **2009**, *42*, 5251-5255.

(13) Chakraborty, S.; Guo, W.; Hauge, R. H.; Billups, W. E. *Chem. Mater.* **2008**, *20*, 3134-3136.

(14) Lomeda, J. R.; Doyle, C. D.; Kosynkin, D. V.; Hwang, W.-F.; Tour, J. M. *J. Am. Chem. Soc.* **2008**, *130*, 16201-16206.

(15) Liu, N.; Luo, F.; Wu, H.; Liu, Y.; Zhang, C.; Chen, J. *Adv. Funct. Mater.* **2008**, *18*, 1518-1525.

(16) Stankovich, S.; Dikin, D. A.; Dommett, G. H. B.; Kohlhaas, K. M.; Zimney, E. J.; Stach, E. A.; Piner, R. D.; Nguyen, S. T.; Ruoff, R. S. *Nature* **2006**, *442*, 282-286.

(17) Gilje, S.; Han, S.; Wang, M.; Wang, K. L.; Kaner, R. B. *Nano Lett.* **2007**, *7*, 3394-3398.

(18) Vuluga, D.; Thomassin, J.-M.; Molenberg, I.; Huynen, I.; Gilbert, B.; Jerome, C.; Alexandre, M.; Detrembleur, C. *Chem. Commun.* **2011**, *47*, 2544-2546.

(19) Dreyer, D. R.; Park, S.; Bielawski, C. W.; Ruoff, R. S. *Chem. Soc. Rev.* **2010**, *39*, 228-240.

(20) Ma, H.-L.; Zhang, Y.; Hu, Q.-H.; He, S.; Li, X.; Zhai, M.; Yu, Z.-Z. *Mater. Lett.* **2013**, *102–103*, 15-18.

(21) Tripathi, S.; Saini, P.; Gupta, D.; Choudhary, V. *J. Mater. Sci.* **2013**, *48*, 6223-6232.

(22) Liang, J.; Huang, Y.; Zhang, L.; Wang, Y.; Ma, Y.; Guo, T.; Chen, Y. *Adv. Funct. Mater.* **2009**, *19*, 2297-2302.

(23) Cano, M.; Khan, U.; Sainsbury, T.; O'Neill, A.; Wang, Z.; McGovern, I. T.; Maser, W. K.; Benito, A. M.; Coleman, J. N. *Carbon* **2013**, *52*, 363-371.

(24) Pinto, A. M.; Martins, J.; Moreira, J. A.; Mendes, A. M.; Magalhães, F. D. *Polym. Int.* **2013**, *62*, 928-935.

(25) Huang, H.-D.; Ren, P.-G.; Chen, J.; Zhang, W.-Q.; Ji, X.; Li, Z.-M. *J. Membr. Sci.* **2012**, *409–410*, 156-163.

(26) Kim, H. M.; Lee, J. K.; Lee, H. S. *Thin Solid Films* **2011**, *519*, 7766-7771.

(27) Yoo, B. M.; Shin, H. J.; Yoon, H. W.; Park, H. B. *J. Appl. Polym. Sci.* **2014**, *131*, 1-23.

(28) Villar-Rodil, S.; Paredes, J. I.; Martinez-Alonso, A.; Tascon, J. M. D. *J. Mater. Chem.* **2009**, *19*, 3591-3593.

(29) Gao, J.; Liu, F.; Liu, Y.; Ma, N.; Wang, Z.; Zhang, X. *Chem. Mater.* **2010**, *22*, 2213-2218.

(30) Zeng, X.; Yang, J.; Yuan, W. *Eur. Polym. J.* **2012**, *48*, 1674-1682.

(31) Heo, S.; Cho, S. Y.; Kim, D. H.; Choi, Y.; Park, H. H.; Jin, H.-J. *J. Nanosci. Nanotechnol.* **2012**, *12*, 5990-5994.

(32) Kuila, T.; Bose, S.; Khanra, P.; Kim, N. H.; Rhee, K. Y.; Lee, J. H. *Composites Part A* **2011**, *42*, 1856-1861.

(33) Liu, P.; Gong, K.; Xiao, P.; Xiao, M. *J. Mater. Chem.* **2000**, *10*, 933-935.

(34) Zhang, B.; Zhang, Y.; Peng, C.; Yu, M.; Li, L.; Deng, B.; Hu, P.; Fan, C.; Li, J.; Huang, Q. *Nanoscale* **2012**, *4*, 1742-1748.

(35) Yang, X.; Li, L.; Shang, S.; Tao, X.-m. *Polymer* **2010**, *51*, 3431-3435.

(36) Barroso-Bujans, F.; Alegría, A.; Pomposo, J. A.; Colmenero, J. *Macromolecules* **2013**, *46*, 1890-1898.

(37) Zhang, B.; Xu, S.; Tang, H.; Wu, P. *RSC Adv.* **2013**, *3*, 8372-8379.

(38) Blum, F. D.; Xu, G.; Liang, M.; Wade, C. G. *Macromolecules* **1996**, *29*, 8740-8745.

(39) Marcano, D. C.; Kosynkin, D. V.; Berlin, J. M.; Sinitskii, A.; Sun, Z.; Slesarev, A.; Alemany, L. B.; Lu, W.; Tour, J. M. *ACS Nano* **2010**, *4*, 4806-4814.

(40) Mhamane, D.; Ramadan, W.; Fawzy, M.; Rana, A.; Dubey, M.; Rode, C.; Lefez, B.; Hannoyer, B.; Ogale, S. *Green Chemistry* **2011**, *13*, 1990-1996.

(41) Fang, M.; Wang, K.; Lu, H.; Yang, Y.; Nutt, S. *J. Mater. Chem.* **2009**, *19*, 7098-7105.

(42) Bo, Z.; Shuai, X.; Mao, S.; Yang, H.; Qian, J.; Chen, J.; Yan, J.; Cen, K. *Sci. Rep.* **2014**, *4*, 1-8.

(43) De Silva, K. S. B.; Gambhir, S.; Wang, X. L.; Xu, X.; Li, W. X.; Officer, D. L.; Wexler, D.; Wallace, G. G.; Dou, S. X. *J. Mater. Chem.* **2012**, *22*, 13941-13946.

(44) Cui, P.; Lee, J.; Hwang, E.; Lee, H. *Chem. Commun.* **2011**, *47*, 12370-12372.

(45) Kanaze, F. I.; Kokkalou, E.; Niopas, I.; Georgarakis, M.; Stergiou, A.; Bikiaris, D. *J. Appl. Polym. Sci.* **2006**, *102*, 460-471.

(46) Ulaganathan, M.; Nithya, R.; Rajendran, S. *Surface Analysis Studies on Polymer Electrolyte Membranes Using Scanning Electron Microscope and Atomic Force Microscope;* **2012**.

(47) Li, Z.-F.; Zhang, H.; Liu, Q.; Sun, L.; Stanciu, L.; Xie, J. *ACS Applied Materials & Interfaces* **2013**, *5*, 2685-2691.

(48) Zhu, Y.; Murali, S.; Cai, W.; Li, X.; Suk, J. W.; Potts, J. R.; Ruoff, R. S. *Adv. Mater.* **2010**, *22*, 3906-3924.

(49) Hiyama, Y.; Roy, S.; Guo, K.; Butler, L. G.; Torchia, D. A. *J. Am. Chem. Soc.* **1987**, *109*, 2525-2526.

(50) Kitchin, S. J.; Halstead, T. K. *Appl. Magn. Reson.* **1999**, *17*, 283-300.

(51) Wann, M. H.; Harbison, G. S. *J. Chem. Phys.* **1994**, *101*, 231-237.

(52) McCall, D. W. *Acc. Chem. Res.* **1971**, *4*, 223-232.

(53) Nambiar, R. R.; Blum, F. D. *Macromolecules* **2009**, *42*, 8998-9007.

(54) Hetayothin, B.; Blum, F. D. Effect of Structure and Plasticizer on the Glass Transition of Adsorbed Polymer. Ph.D. Thesis, Missouri University of Science and Technology, **2010**.

(55) Potts, J. R.; Dreyer, D. R.; Bielawski, C. W.; Ruoff, R. S. *Polymer* **2011**, *52*, 5-25.

(56) Sham, A. Y. W.; Notley, S. M. *Soft Matter* **2013**, *9*, 6645-6653.

(57) Hsu, F.-H.; Wu, T.-M. *Synth. Met.* **2012**, *162*, 682-687.

(58) Sawangphruk, M.; Suksomboon, M.; Kongsupornsak, K.; Khuntilo, J.; Srimuk, P.; Sanguansak, Y.; Klunbud, P.; Suktha, P.; Chiochan, P. *J. Mater. Chem. A* **2013**, *1*, 9630-9636.

(59) Blanton, T. N.; Majumdar, D. *Powder Diffr.* **2012**, *27*, 104-107.

APPENDICES

APPENDIX A.

TEMPERATURE MODULATED DIFFERENTIAL SCANNING CALORIMETRY TO

DETERMINE THE GLASS TRANSITION TEMPERATURE (T_g) OF POLYMERS

This appendix describes the benefits of using temperature-modulated differential

scanning calorimetry (TMDSC) to determine the glass transition behavior of polymers.

The TMDSC measurements can be separated into two components (reversing and non-

reversing). These two components (heat flow curves) contain different information about

the materials.

As can be observed from Figure A1 for the bulk PMMA, reversible heat flow

curves (represented by dashed lines) are clearer in describing glass transition behavior of

the polymer, especially in the derivative mode as in Figure A1 (ii). Reversing heat flow

curves can be used to describe the heat capacity of a material, while non-reversing heat

flow describes kinetic events (such as enthalpy relaxation, evaporation of residual

solvent) of the sample. Since, the glass transition is a reversing event, it is generally

better to use the reversing heat flow curve to study the glass transition behavior of a

material. Then one can eliminate some of the effects of kinetic events in the plot, such as

relaxation of a polymer, solvent evaporation.

Figure A1. A comparison between reversing and non-reversing heat flow curves to determine the T_g of a polymer, obtained from modulated heat flow curves. Figures (i) and (ii) are the heat flows (reversing, non-reversing, and total) for the bulk PMMA in normal and derivative mode (with respect to temperature), respectively.

APPENDIX B

EFFECT OF SHAPE FACTOR (M) ON THE SHAPE OF GAUSSIAN-LORENTZIAN

MIXED FUNCTION AND THEIR BEST FITS FOR PMMA/SILICA DERIVATIVE

HEAT FLOW CURVES

This appendix describes the shape and best fit of the Gaussian-Lorentzian mixed function for MDSC thermograms of PMMA/silica composites when the mixing parameter ($0 <= M <= 1$) is changed keeping the other parameters (width (w), amplitude (a) and center of the peak (x_0)) fixed. The functional form for the Gaussian-Lorentzian mixed function was given by,[1]

$$f(x) = \frac{a}{[1 + \frac{4M(x - x_0)^2}{w^2}]\exp[\frac{4\ln 2(1 - M)(x - x_0)^2}{w^2}]}$$

(B1)

A plot showing how the shape of the Gaussian-Lorentzian mixed function changes with change in mixing ratio, M is shown in Figure B1. When the value of $M = 1$, the function takes the form of pure Lorentzian function as shown in figure with black curve at the top of Figure B1.
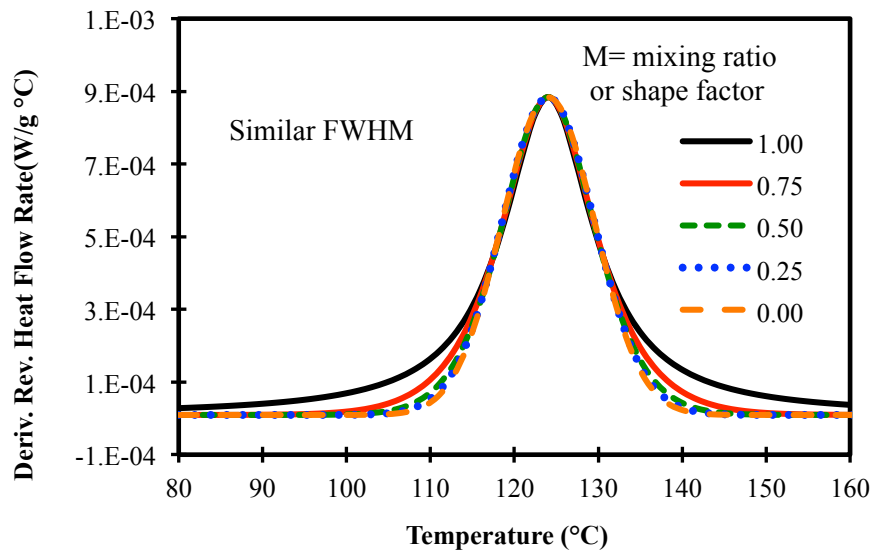
Figure B1. Shape of Gaussian-Lorentzian mixed function with different value of mixing ratios (M = 0, pure Gaussian function, M=1, pure Lorentzian function, and 0 < M < 1, Gaussian-Lorentzian mixed function).

The Lorentzian function has a shape similar to the Gaussian function, but has longer tails. As the value of M decreases from 1 towards 0, the shape of the distribution changes from pure Lorentzian towards the Gaussian shape. When the value of M = 0, the function takes a form of pure Gaussian function as shown with orange dotted lines at the bottom of the Figure B1. The Gaussian function is a narrower distribution when the intensity is smaller than the Lorentzian function.

Figure B2 shows the fitting of the MDSC heat flow curve of 3.28 mg/m^2 of PMMA adsorbed on silica surface with Gausian-Lorentzian mixed function for both loosely and tightly bound glass transition peaks. Figure B2 (i) shows the fitting of Gaussian-Lorentzian mixed function when the value of M is zero, which is basically pure Gaussian function. Even though the fits look good, the R^2-value (goodness of fit) of the fit was minimum. Figure B2 (ii, iii, iv, and v) shows the fittings of the curve with

increasing the value of M (0.25, 0.5, 0.75, 1) for both loosely and tightly bound peaks. For none of the above values of M, the best fit for the curve was obtained. As can be observed from different fittings obtained with changing the value of M, the best fitting was obtained when the value of M was 0.995 and 0.797 for loosely bound and tightly bound polymers, respectively. The best fit of the curves was based on the R^2-value of the fit, which becomes close to 1. These peaks seem to generally be more closely described by Gaussian rather than Lorentzian functions.

(iv)

M = 0.75

(v)

M = 1
Pure lorentzian
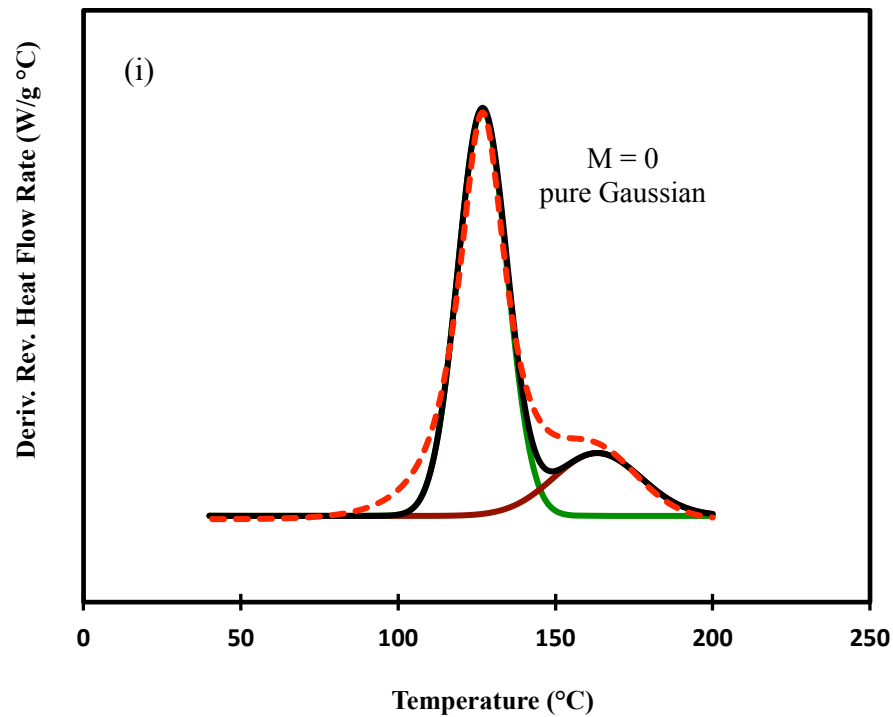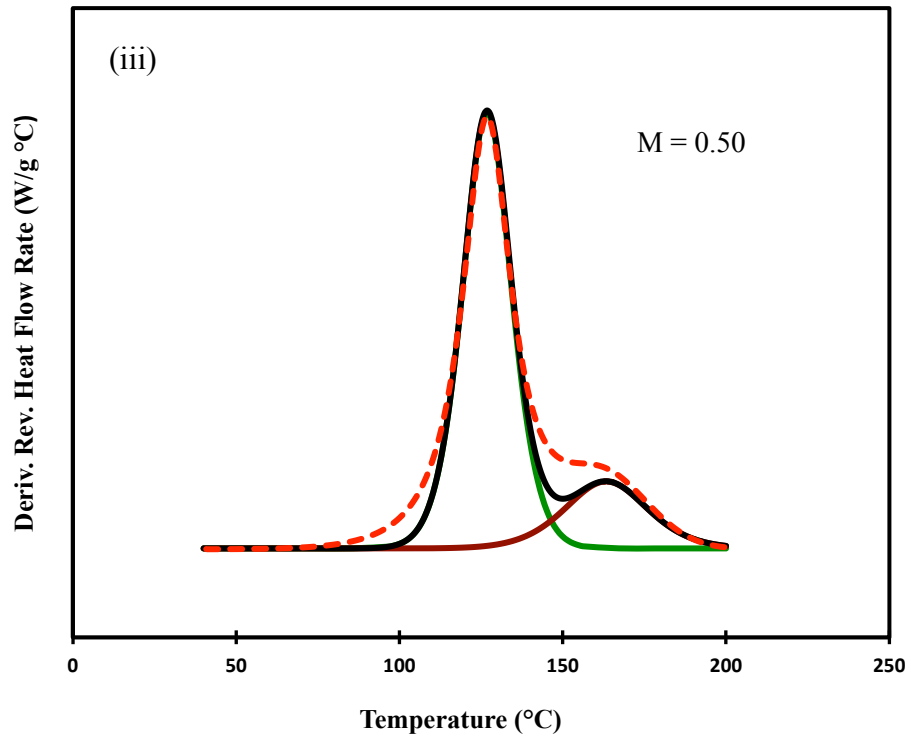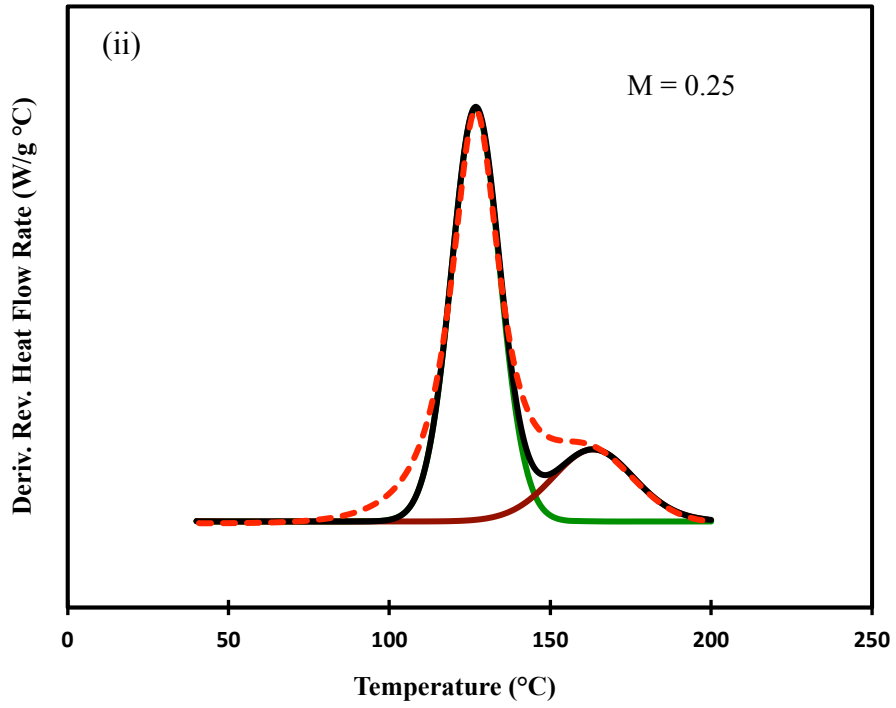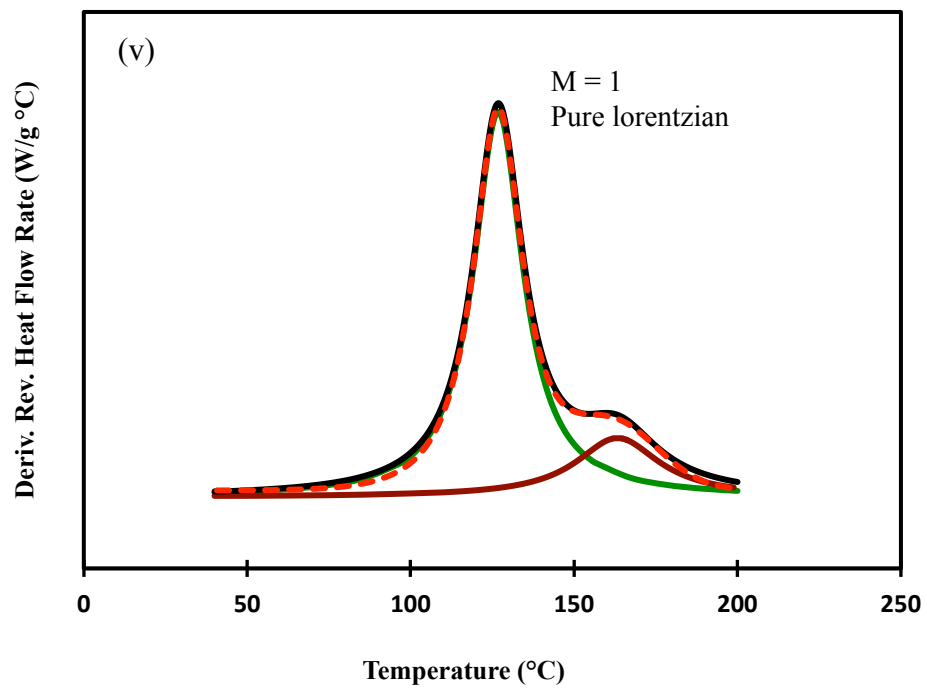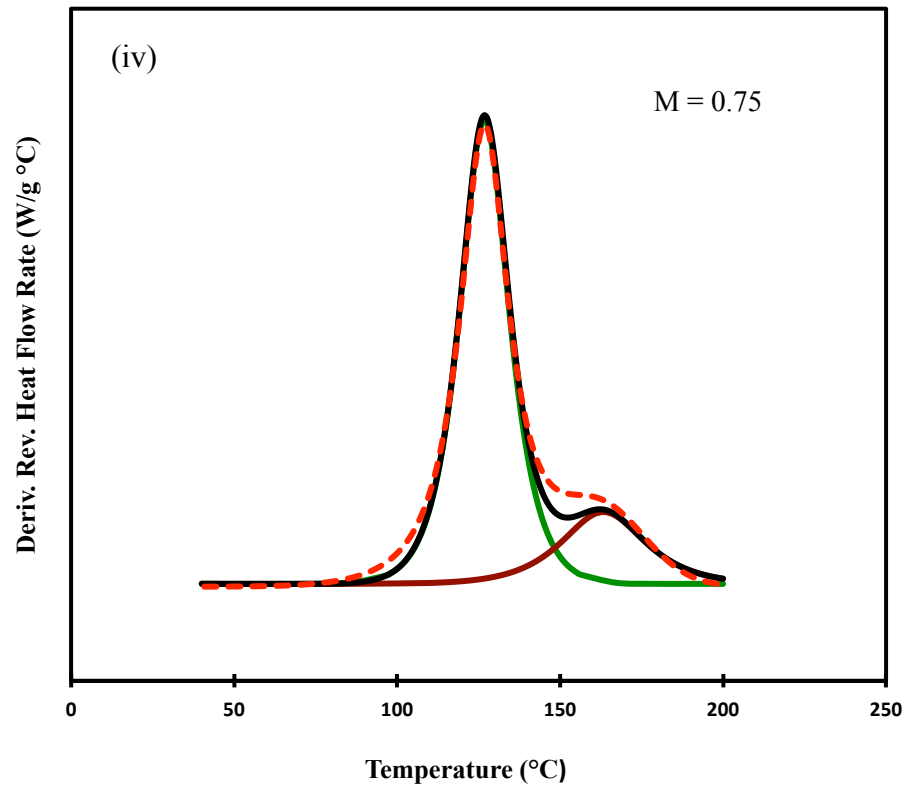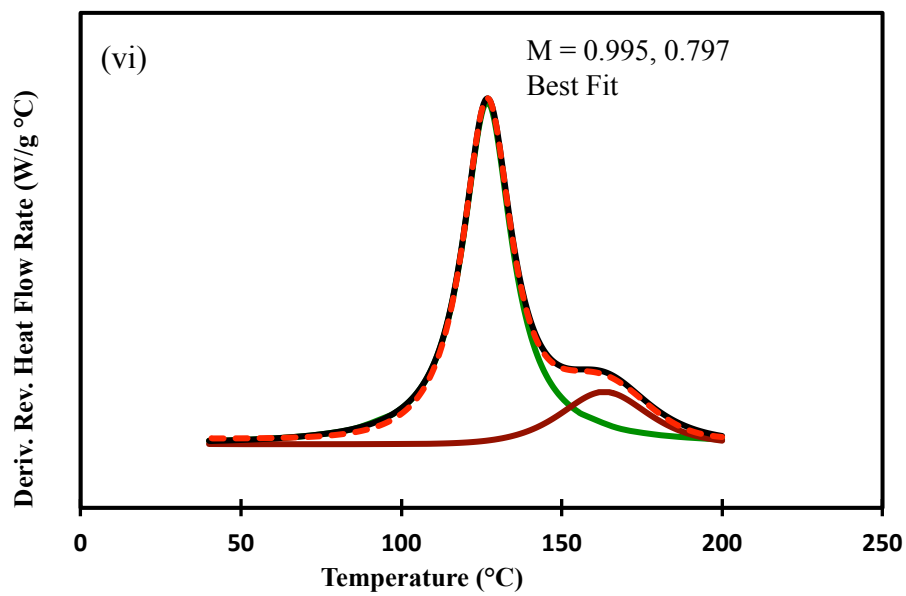
Figure B2. The shape of the Gaussian-Lorentzian mixed function with different values of the shape factor, M, i) M = 0, ii) M = 0.25, iii) M = 0.5, iv) M = 0.75, v) M = 1, and vi) the best fit (M = 0.995 for the loosely bound component, and 0.797 for the tightly-bound component) to the experimental thermogram for 3.28 mg/m^2 PMMA/silica sample.

APPENDIX C

COMPARISION OF HEATING VERSUS COOLING CYCLE IN MDSC

MEASUREMENTS OF PMMA/SILICA SYSTEM

This appendix compares the nature of MDSC curves and the measurement of glass transition temperatures (T_g) of bulk and adsorbed PMMA on silica surfaces from heating versus cooling cycles. Figures C1 and C2 show the plots of reversing heat flow at different temperatures for bulk and adsorbed PMMA obtained from the second heating cycle and first cooling cycle, respectively. The derivative heat flow curves for both heating and cooling cycles look very similar. However, the width (full width at half maximum) of the first peak (Peak A) and of the bulk polymer was about 35 - 41% wider in the cooling than the heating cycle.
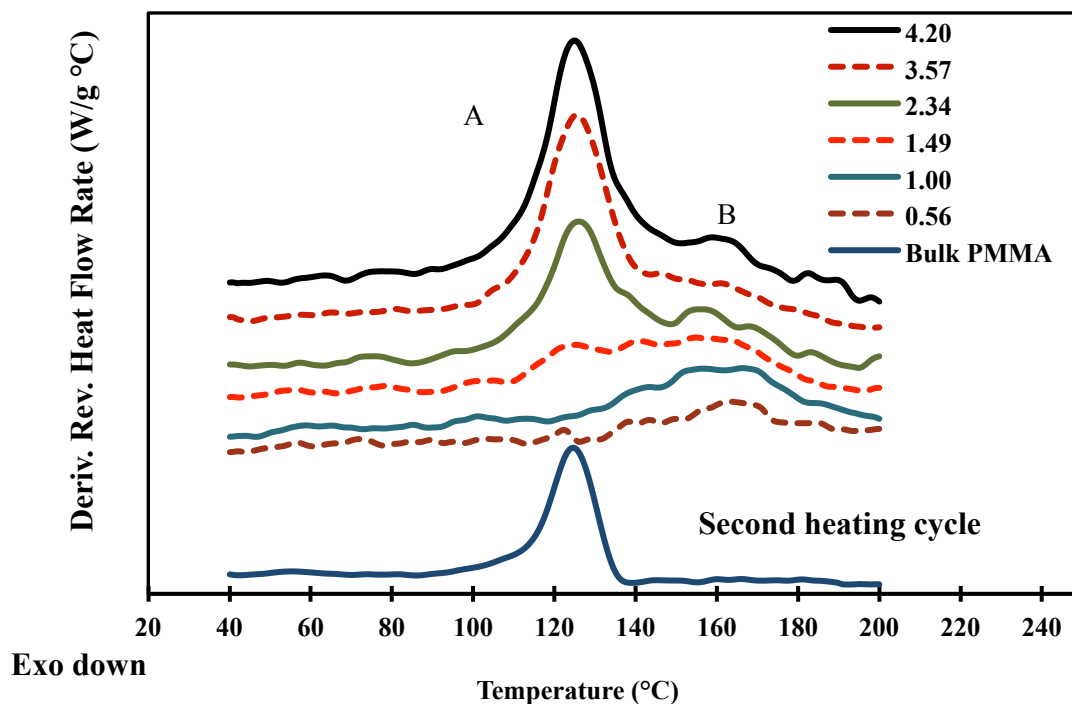
Figure C1. Derivative reversible heat flow curves at different temperatures obtained from second heating cycles for bulk and adsorbed PMMA on silica samples. The curves are separated (curves are moved upwards) manually to make them clear to observe. The intensity of bulk polymer was reduced to fit with curves for adsorbed samples.

The glass transition temperature was determined from the temperature at which the heat flow is maximum (peak of the heat flow curve). From the measurements of T_g, it was observed that there was no difference in T_g from the heating versus cooling cycles for the different samples.
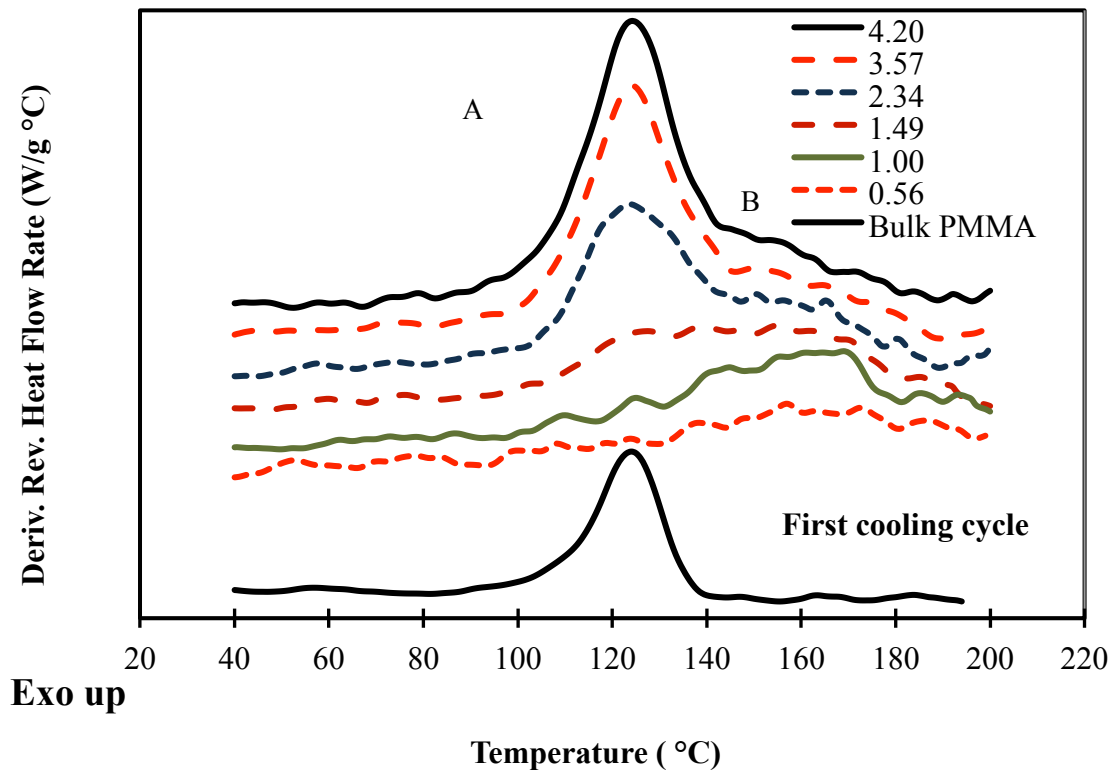
Figure C2. Derivative reversible heat flow curves with different temperatures obtained from first cooling cycles for bulk and adsorbed PMMA on silica surfaces. Curves are separated (curves are moved upwards) manually to make them clear to observe. The intensity of bulk polymer was reduced to fit with curves for adsorbed samples.

APPENDIX D

QUASI-ISOTHERMAL HEAT CAPACITY MEASUREMENTS OF BULK AND
ADSORBED PMMA ON SILICA

Heat capacity measurements of bulk and adsorbed PMMA on silica were carried

out using quasi-isothermal method, in which the samples were heated in 10 °C

increments and kept at the targeted temperature for 10 minutes. The heat capacity was

measured by heating and cooling the sample with the same rate (with +/- 1 °C/120

second) so that the temperature of the sample changed only by a small amount, hence the

term quasi-isothermal. The heat flow from the heating and cooling of the sample was

used to calculate the heat capacity.

As observed in Figure D.1, the sample was kept at a temperature for 10 min and a

sinusoidal modulation of +/- 1 °C/120 second was applied at this condition. The overall

temperature of the sample only varied a small amount (typically +/- 1 °C). As observed,

five complete cycles were made when the sample was kept at the target temperature for

10 minutes and a modulation of +/- 1 °C/120 second was used.

The procedure for quasi-isothermal heat capacity measurement is,

(1) Ramp 10 °C/min to 140 °C

(2) Isothermal for 10 minutes

(3) Data storage off

(4) Equilibrate at 25 °C

(5) Modulate +/- 1 °C/ 120 second

(6) Isothermal for 5 minutes

(7) Data storage on

(8) Isothermal for 10 minutes

(9) Data storage off

(10) Increment by 10 °C

(11) Repeat segment (6) for 15 times

(12) Event off

The step (1) and (2) eliminates the thermal history of the material.
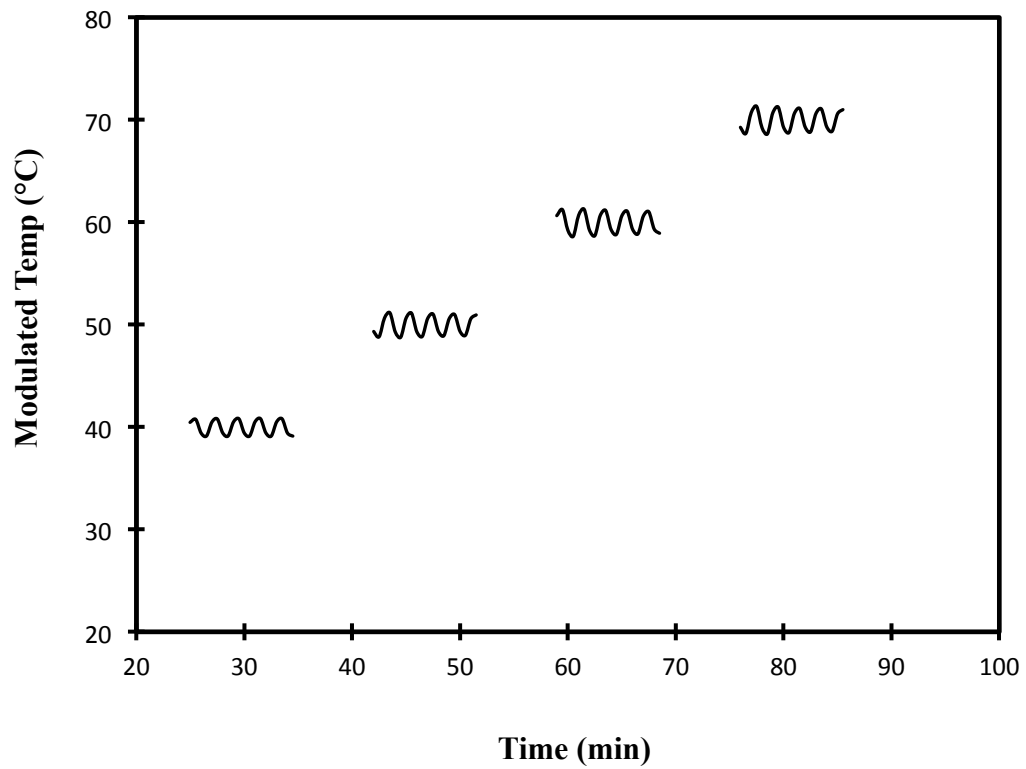
Figure D1. Quasi-isothermal method of heat capacity determination for bulk PMMA sample. The sample was heated to a certain temperature (for instance, if the heat capacity measurement was desired at 25 °C, then the sample was heated to 25 °C), wait 10 minutes at this temperature, and a sinusoidal modulation of +/- 1 °C/120 second was applied on the top of this temperature. The average temperature of the sample does not change.

APPENDIX E

FITTING HEAT CAPACITIES OF PMMA ADSORBED ON SILICA

The fitting of the heat capacities of the polymers alone adsorbed on silica with the bound segment model and transitional model at a few temperatures below bulk glass transition temperature (T_g), from 40 to 100 °C, are shown in Figure E1. The heat capacities of adsorbed polymers were compared with the bulk heat capacity, which is represented by dot-dashed line on the top of the figures. In the chapter 4, the fitting of the heat capacities of polymers adsorbed on surface at 50 °C has been described, as a representative of fitting well below bulk glass transition, in detail. Here, the fitting for all other temperatures below the bulk T_g (40 – 100 °C) is reported.
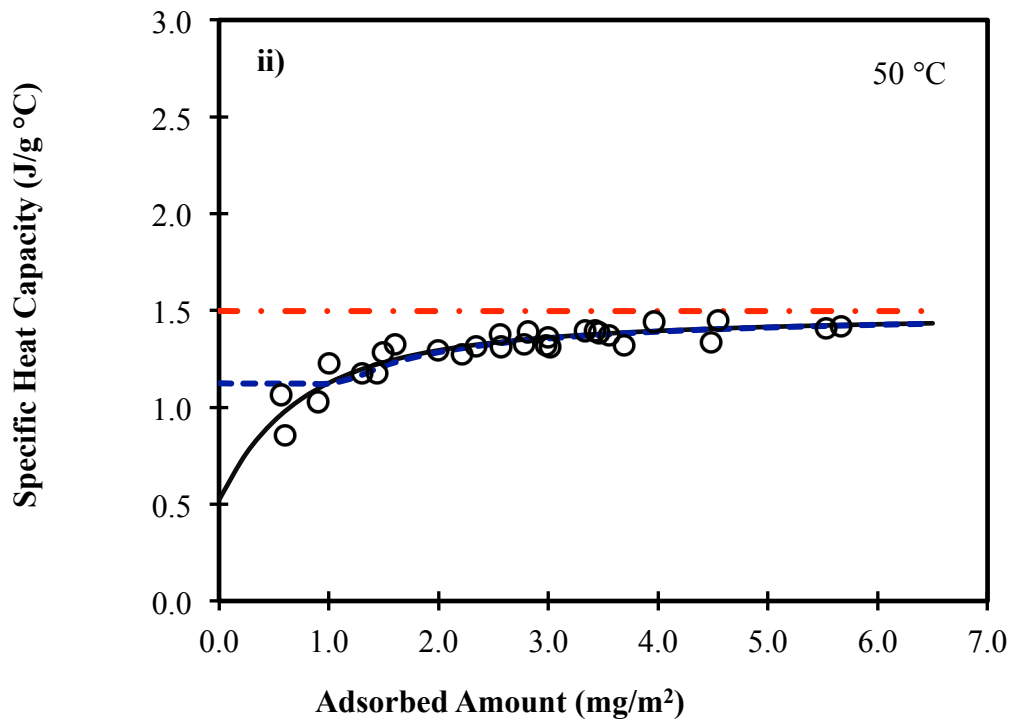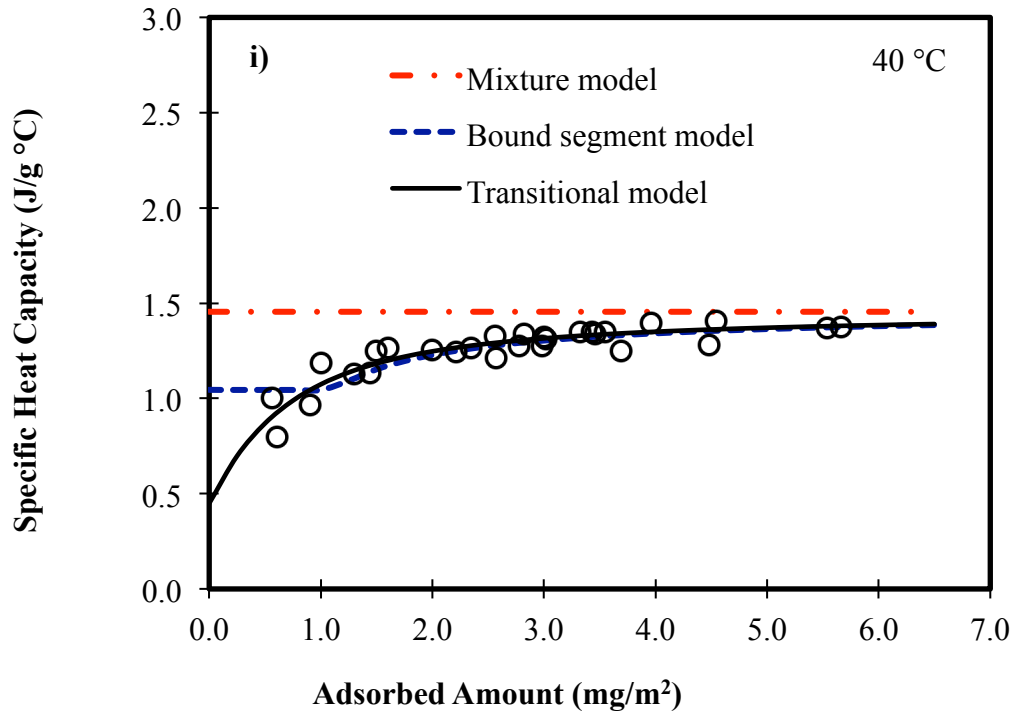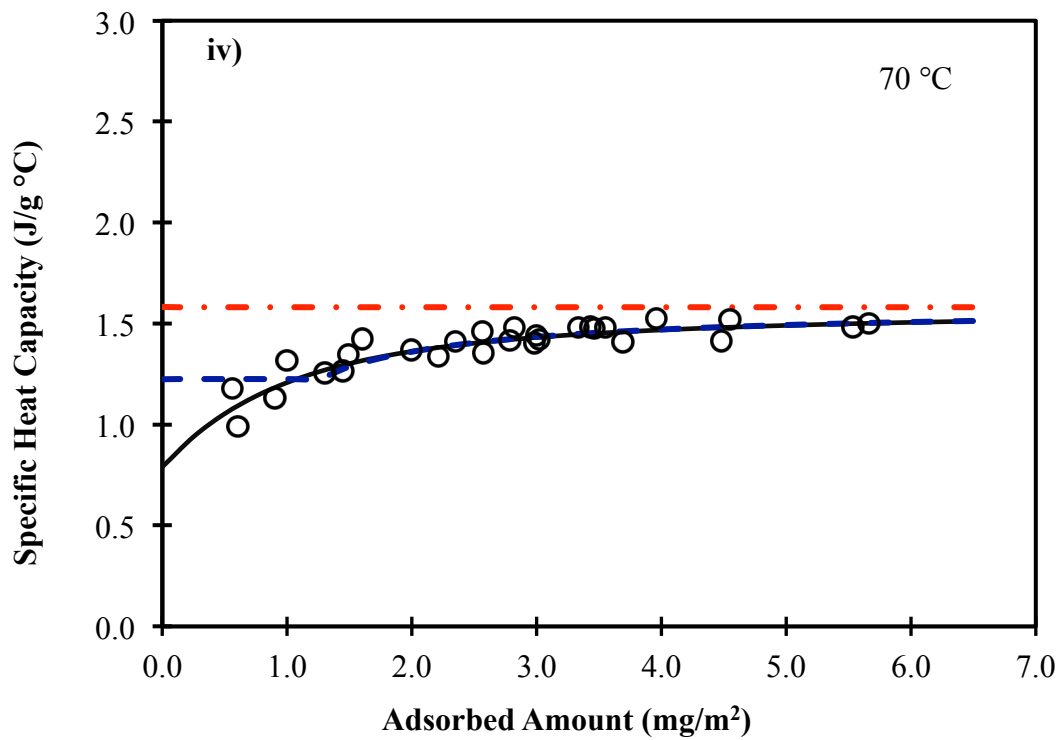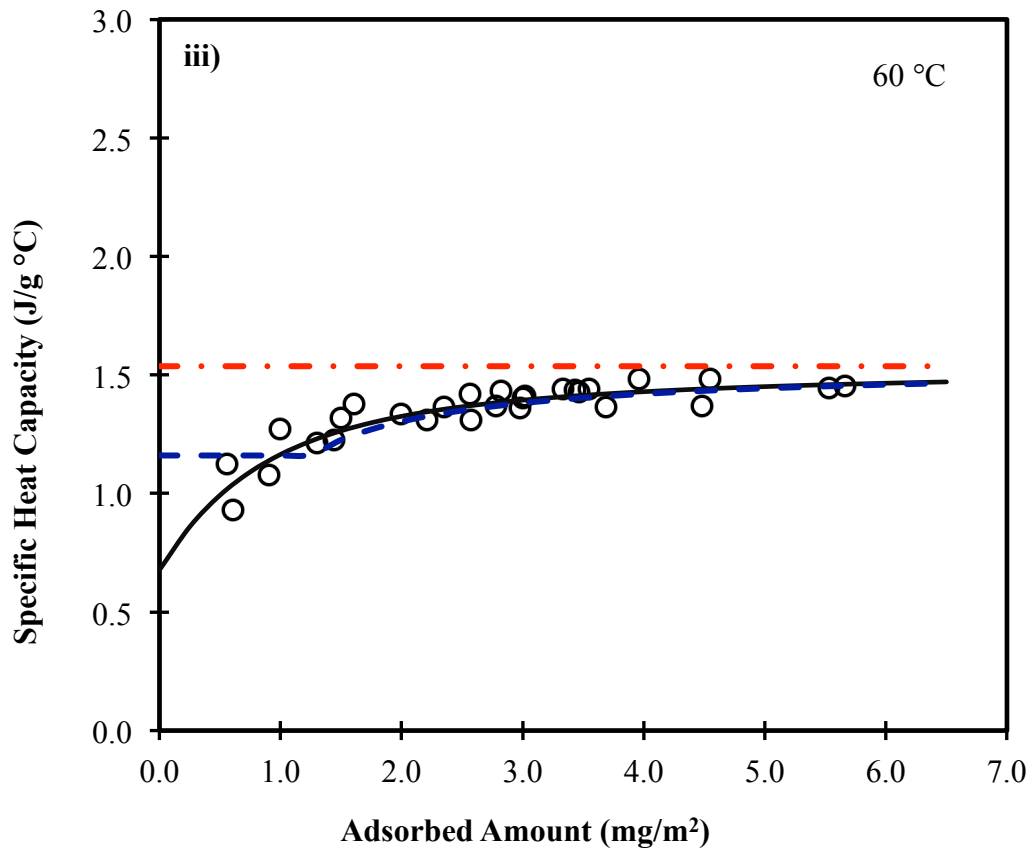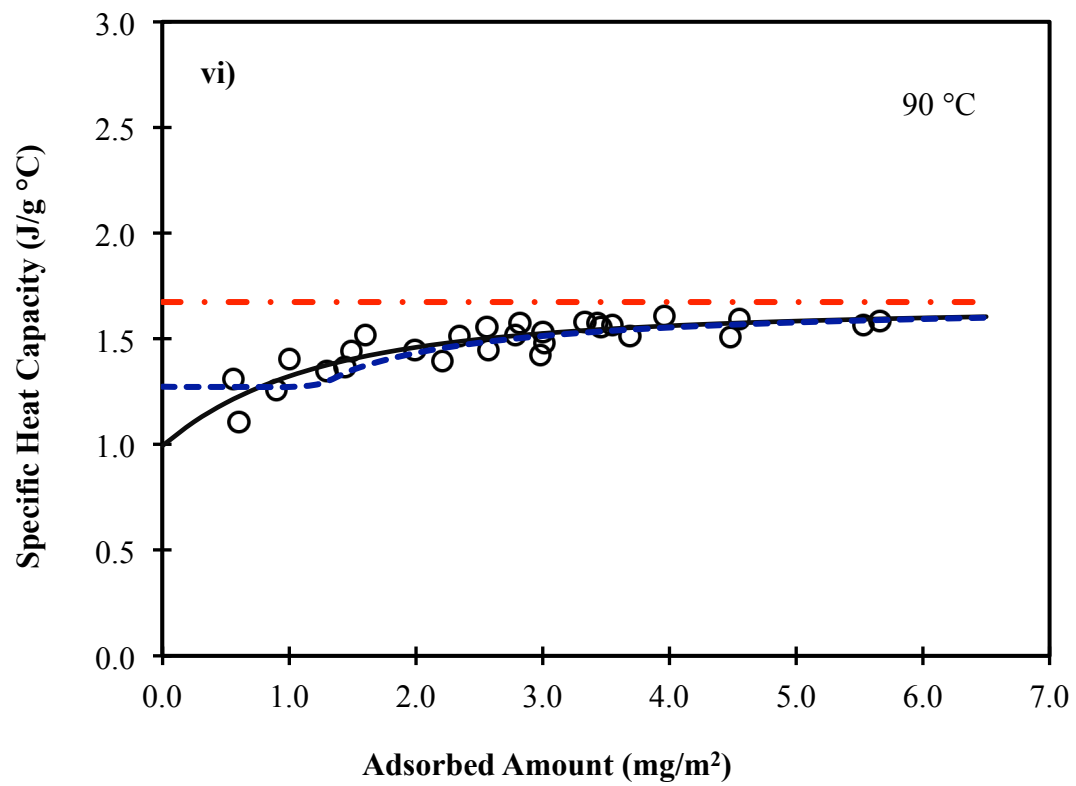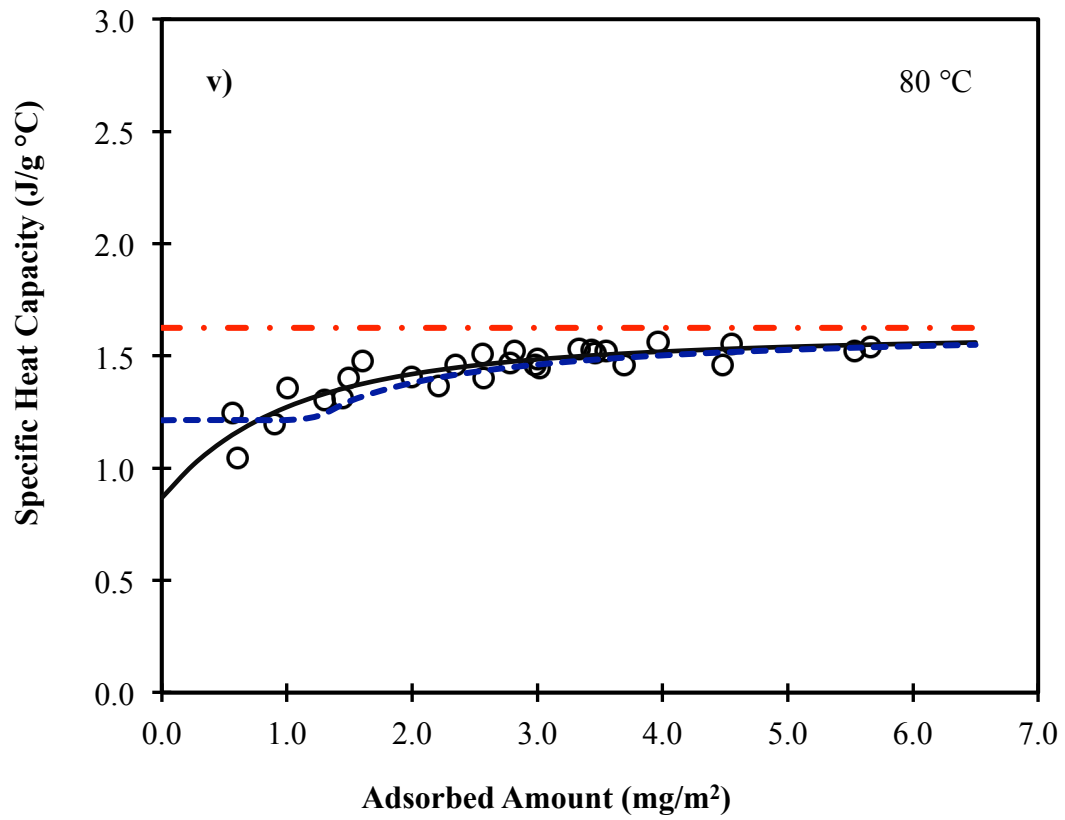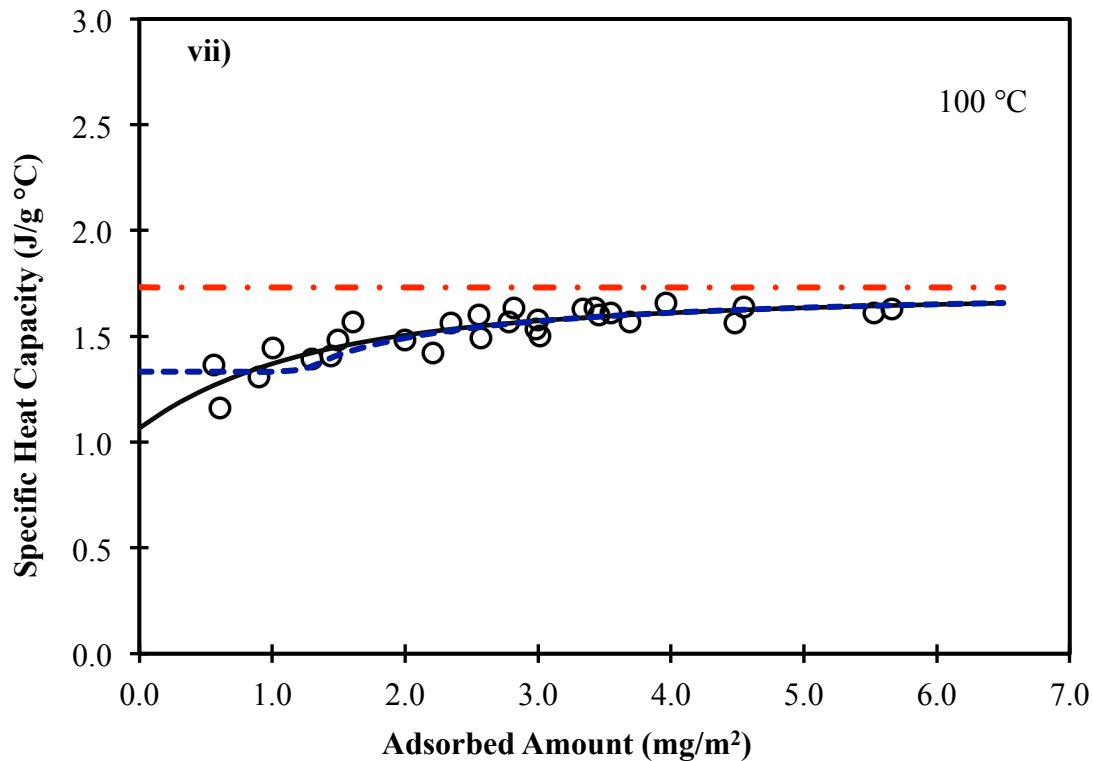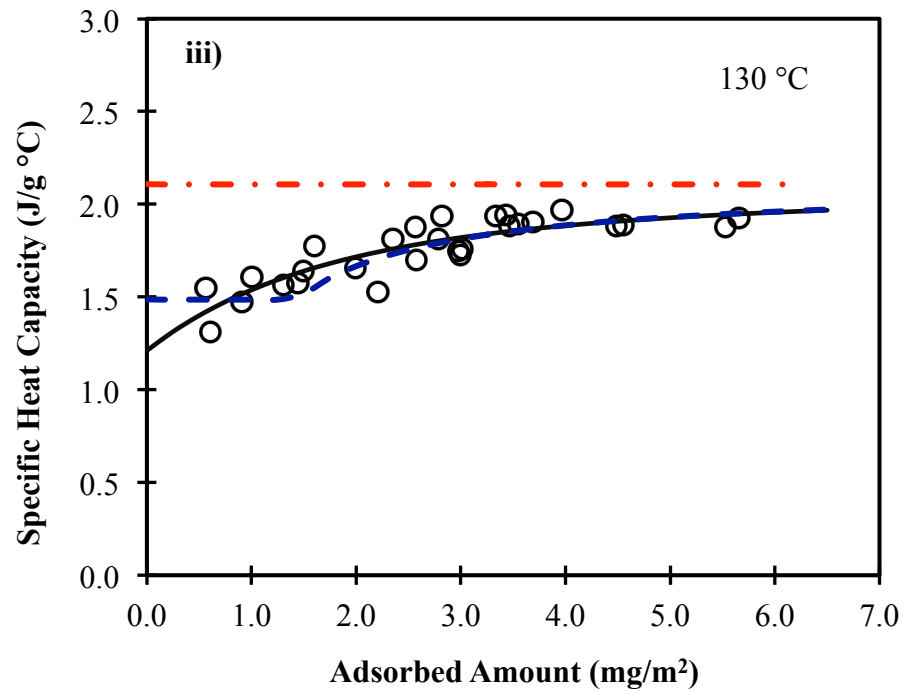
Figure E1. Heat capacity of adsorbed polymers at different adsorbed amounts showing the prediction from bound segment model and transitional model at different temperatures starting from i) 40 °C to vii) 100 °C. The dot-dashed line on the top is for heat capacity of bulk polymer to compare with adsorbed polymers.

Similar fitting at other temperatures around bulk T_g is shown in Figure E2. In the chapter 4, the fitting at 120 °C has been described in detail. The rest of the fitting from 110 – 140 °C have been provided in this section.
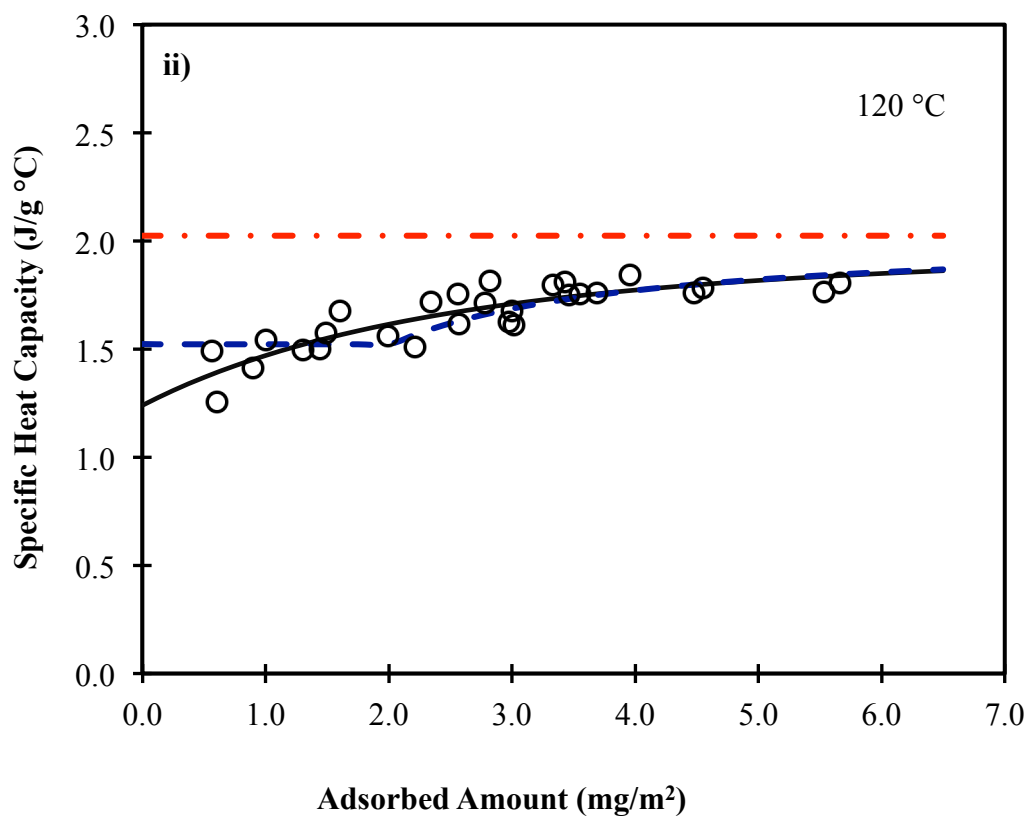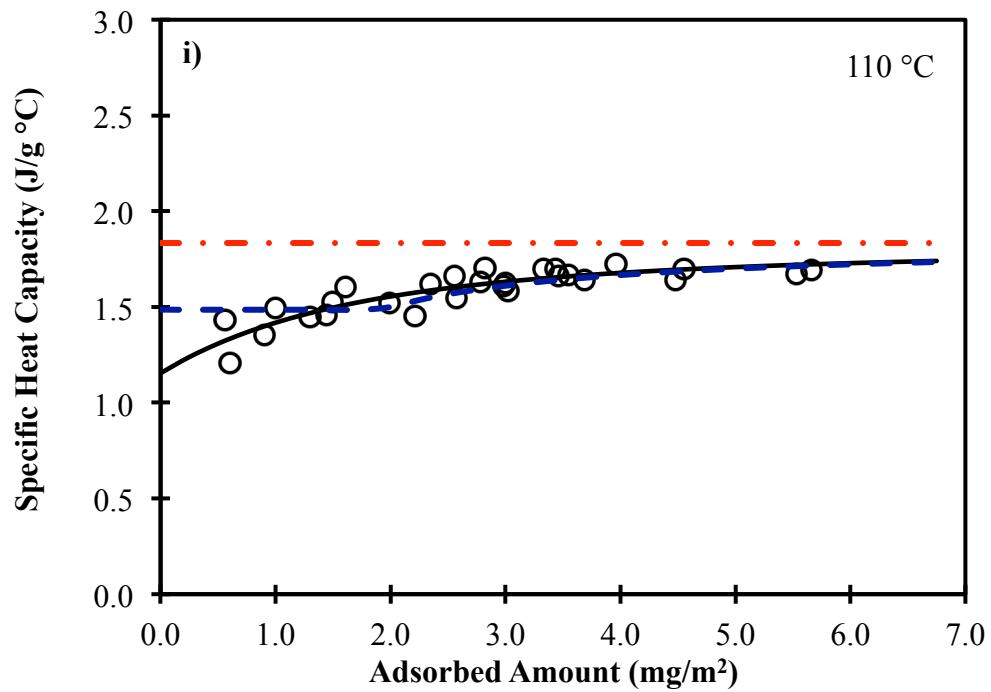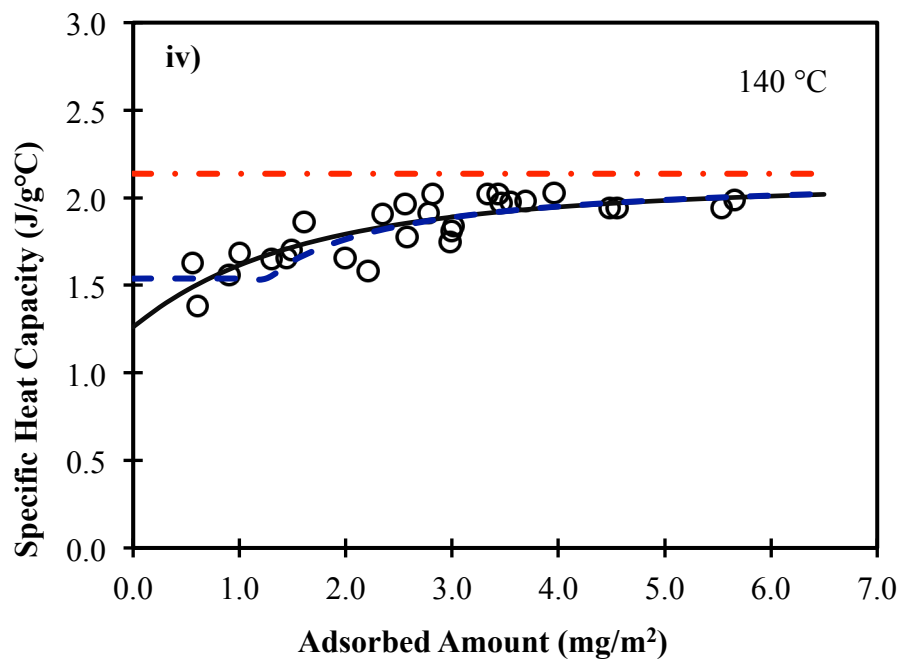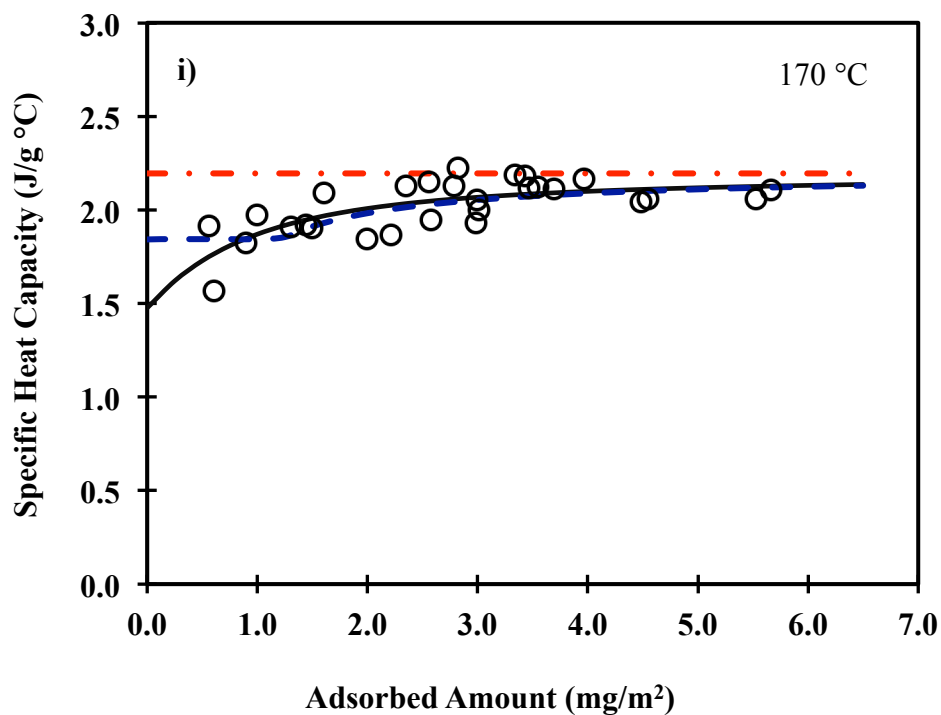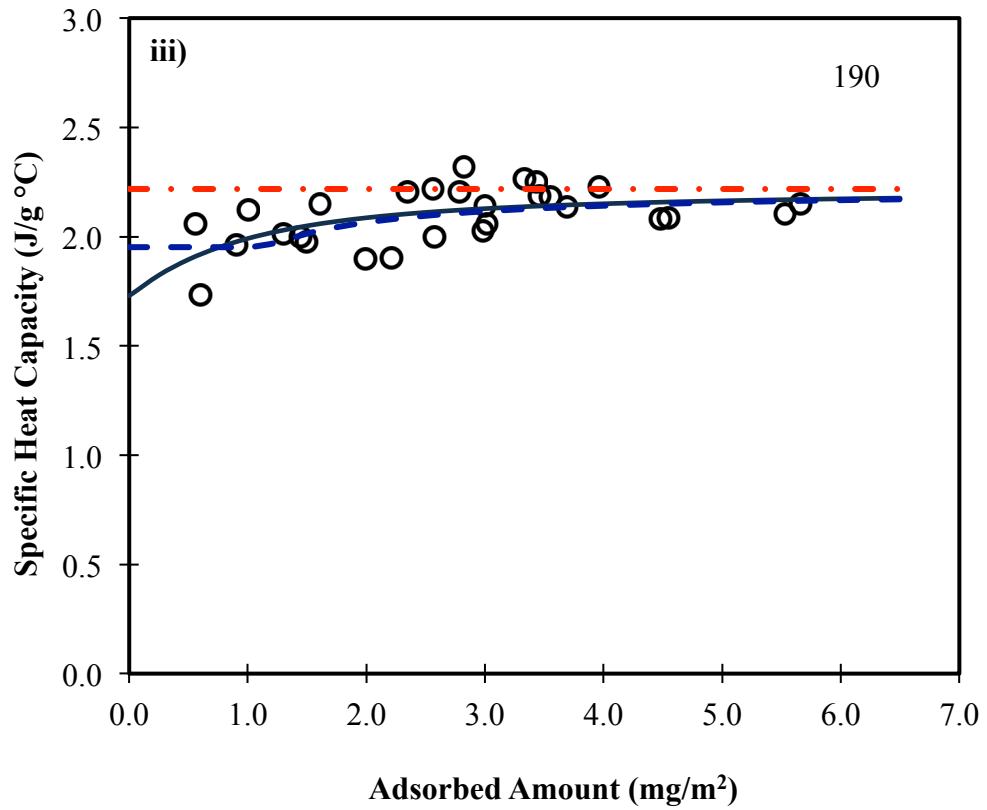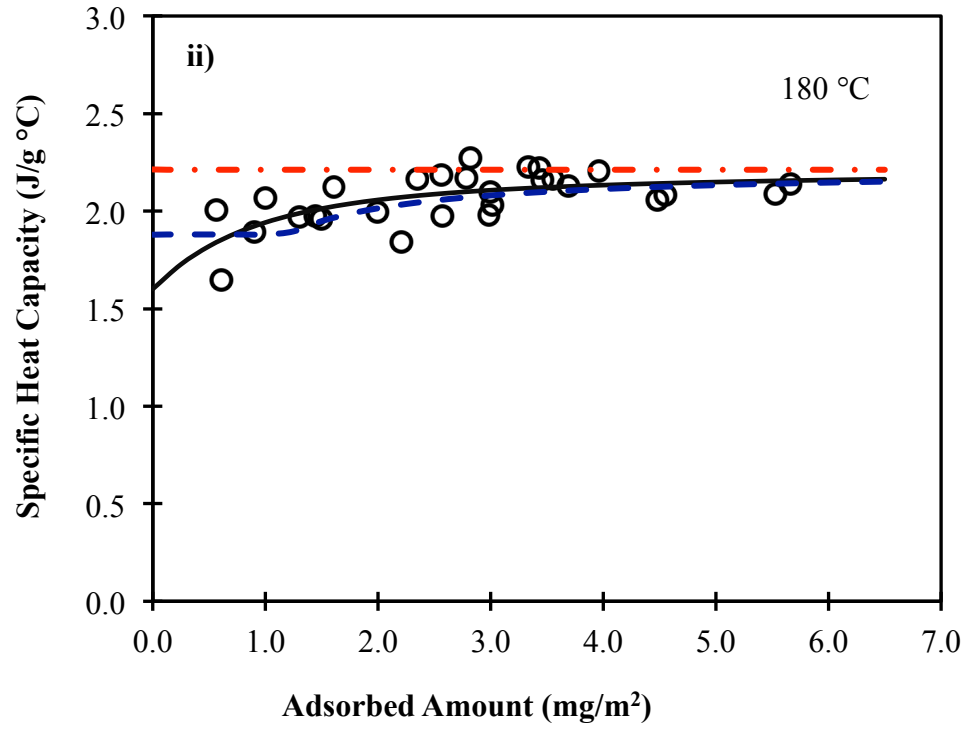
Figure E2. Heat capacity of adsorbed polymers at different adsorbed amounts showing the prediction from bound segment model and transitional model at different temperatures starting from i) 110 °C to iv) 140 °C. The dot-dashed line on the top is for heat capacity of bulk polymer to compare with adsorbed polymers.

Similar fitting at other temperatures well above bulk T_g is shown in Figure E3. In the chapter 4, the fitting at 200 °C has been described in detail. The rest of the fitting at temperatures from 170 – 200 °C have been provided in this section. At all temperatures, the heat capacity of adsorbed polymers was less than bulk heat capacity suggesting adsorption of polymer on surface altered its heat capacity. The alteration in heat capacity was significant when the amounts of adsorbed polymer were less and approached bulk for higher adsorbed amounts.
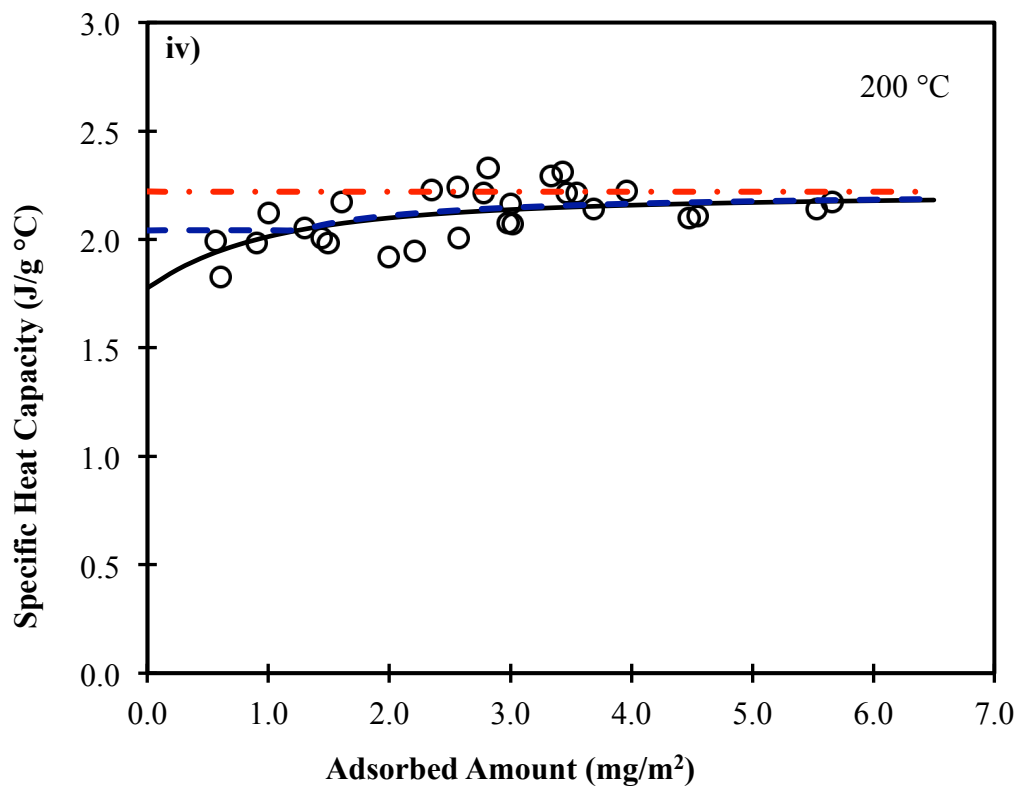
Figure E3. Heat capacity of adsorbed polymers at different adsorbed amounts showing the prediction from bound segment model and transitional model at different temperatures starting from i) 170 °C to iv) 200 °C. The dot-dashed line on the top is for heat capacity of bulk polymer to compare with adsorbed polymers.

REFERENCE

(1) Kojima, I.; Kurahashi, M. *J. Electron Spectrosc. Relat. Phenom.* **1987**, *42*, 177-181.

VITA

Bal Kumari Khatiwada

Candidate for the Degree of

Doctor of Philosophy

Thesis: INTERACTIONS OF POLYMERS WITH SURFACES

Major Field: POLYMER CHEMISTRY

Biographical:

Education:
Doctor of Philosophy, Polymer Chemistry   July 2014
Oklahoma State University, Stillwater, OK

Master of Science, Physical Chemistry   May 2009
Tribhuvan University, Kathmandu, Nepal
Bachelor of Science, Chemistry   May 2006
Tri-Chandra College, Kathmandu, Nepal

Experience:
August 2009 – July 2014
Graduate Teaching Assistant at OSU
Graduate Research Assistant at OSU

Professional Memberships:
American Chemical Society, 2011–present
Phi kappa phi, 2011-2012

Awards:
O.C. Dermer Award, Department of Chemistry, Oklahoma State University, 2012.
Best Poster Presentation Award, Northern American Thermal Analysis Society (NATAS), 2011.